Table of Contents – Chapter VI

Page

1.5 UT Modeling and Simulation 1

1.5.1 Use of UT Modeling and Simulation to Define Sizing Limits 1
1.5.2 UT Modeling and Simulation of Repair Welds 8

Tables

Table 1.5.1-1. Beam Measurements Based on Modeling Results 2

Table 1.5.2-1. Beam Cross Sections Tabulation – Saddle Position at FD 6.25, 9.375, and 12.5 mm (6.4-mm Wall Thickness), 45-, 55-, and 65-Degree Beams – Geometry 7 16

Table 1.5.2-2. Beam Cross Sections Tabulation – Crotch Position at FD 6.25, 9.375, and 12.5 mm (6.4-mm Wall Thickness), 45-, 55-, and 65-Degree Beams – Geometry 7 16

Table 1.5.2-3. Beam Cross Sections Tabulation – Saddle Position at FD 10, 15, and 20 mm (10.7-mm Wall Thickness) – Geometry 8 22

Table 1.5.2-4. Beam Cross Sections Tabulation – Crotch Position at FD 10, 15, and 20 mm (10.7-mm Wall Thickness) – Geometry 8 23

Figures

Figure 1.5.1-1. Simulation to Actual Comparison of 0.5- and 1.0-mm-Deep Notches Using SE5-60 UT Technique 3

Figure 1.5.1-2. Simulation to Actual Comparison of 1.5- and 2.0-mm-Deep Notches Using SE5-60 UT Technique 3

Figure 1.5.1-3. Simulation to Actual Comparison of 0.5- and 1.0-mm-Deep Notches Using PA7-60/17 UT Technique 4

Figure 1.5.1-4. Simulation to Actual Comparison of 1.5- and 2.0-mm-Deep Notches Using PA7-60/17 UT Technique 4

Figure 1.5.1-5. Simulation of 0.5- to 2.5-mm-Deep Notches Using SE5-60 UT Technique 5

Figure 1.5.1-6. Simulation of 0.5- to 2.5-mm-Deep Notches Using PA7-60/17 UT Technique 5

Figure 1.5.1-7. Simulation of Fatigue Portion of Flaw W3-1 6

Table of Contents – Chapter VI (Continued)

Page

Figure 1.5.1-8. Simulation of Fatigue and Brittle Fracture Combination of Flaw W3-1 6

Figure 1.5.1-9. Comparison of Experimental C-Scan and Predicted C-Scan of W3-1 Fatigue Crack Using Single-Element, 5-MHz, 60-Degree Probe 7

Figure 1.5.1-10. Comparison of Experimental C-Scan and Predicted C-Scan of W3-1 Fatigue Crack Using PA 7-MHz 60/17 Element Probe at a 60-Degree Angle 7

Figure 1.5.2-1. Branch Geometry 7 Setup 9

Figure 1.5.2-2. Branch Geometry 7 – Saddle Position Cross Section 10

Figure 1.5.2-3. Branch Geometry 7 – Crotch Position Cross Section 11

Figure 1.5.2-4. Branch Geometry 7 – 141-Degree Position Cross Section 11

Figure 1.5.2-5. Beam Cross Sections Capture – Saddle Position at FD 6.25 and 9.375 mm (6.4-mm Wall Thickness), 45-Degree Beam – Geometry 7 12

Figure 1.5.2-6. Beam Cross Sections Capture – Saddle Position at FD 6.25, 9.375, and 12.5 mm (6.4-mm Wall Thickness), 55-Degree Beam – Geometry 7 12

Figure 1.5.2-7. Beam Cross Sections Capture – Saddle Position at FD 6.25, 9.375, and 12.5 mm (6.4-mm Wall Thickness), 65-Degree Beam – Geometry 7 13

Figure 1.5.2-8. Beam Cross Sections Capture – Crotch Position at FD 6.25 and 9.375 mm (6.4-mm Wall Thickness), 45-Degree Beam – Geometry 7 13

Figure 1.5.2-9. Beam Cross Sections Capture – Crotch Position at FD 6.25, 9.375, and 12.5 mm (6.4-mm Wall Thickness), 55-Degree Beam – Geometry 7 14

Figure 1.5.2-10. Beam Cross Sections Capture – Crotch Position at FD 6.25, 9.375, and 12.5 mm (6.4-mm Wall Thickness), 65-Degree Beam – Geometry 7 14

Figure 1.5.2-11. Typical Beam Cross Section Capture 15

Figure 1.5.2-12. Branch Geometry Setup for Geometry 8 17

Figure 1.5.2-13. Branch Geometry 8 – Saddle Position Cross Section 17

Figure 1.5.2-14. Branch Geometry 8 – Crotch Position Cross Section 18

Figure 1.5.2-15. Branch Geometry 8 – 141-Degree Position Cross Section 18

Table of Contents – Chapter VI (Continued)

Page

Figure 1.5.2-16. Beam Cross Sections Capture – Saddle Position at FD 10, 15, and 20 mm (10.7-mm Wall Thickness), 45-Degree Beam – Geometry 8 19

Figure 1.5.2-17. Beam Cross Sections Capture – Saddle Position at FD 10, 15, and 20 mm (10.7-mm Wall Thickness), 55-Degree Beam – Geometry 8 20

Figure 1.5.2-18. Beam Cross Sections Capture – Saddle Position at FD 10, 15, and 20 mm (10.7-mm Wall Thickness), 65-Degree Beam – Geometry 8 20

Figure 1.5.2-19. Beam Cross Sections Capture – Crotch Position at FD 10, 15, and 20 mm (10.7-mm Wall Thickness), 45-Degree Beam – Geometry 8 21

Figure 1.5.2-20. Beam Cross Sections Capture – Crotch Position at FD 10, 15, and 20 mm (10.7-mm Wall Thickness), 55-Degree Beam – Geometry 8 21

Figure 1.5.2-21. Beam Cross Sections Tabulation – Crotch Position at FD 10, 15, and 20 mm (10.7-mm Wall Thickness), 65-Degree Beam – Geometry 8 22

Figure 1.5.2-22. Typical Toe Crack Interaction Setup 24

Figure 1.5.2-23. Typical Root Crack Interaction Setup 24

Figure 1.5.2-24. Modal Analysis Capture – Shows the Color Coding of the Different Flaw Interaction Modes to Analyze the Source of the Reflection, e.g., Tip Reflection or Corner Trap Reflection 26

Figure 1.5.2-25. Interaction Calculations Capture – 1-mm Crack Height at Saddle Position, 45-Degree Beam (Toe Crack – Left, Root Crack – Right) – Geometry 7 28

Figure 1.5.2-26. Interaction Calculations Capture – 1-mm Crack Height at Saddle Position, 55-Degree Beam (Toe Crack – Left, Root Crack – Right) – Geometry 7 28

Figure 1.5.2-27. Interaction Calculations Capture – 1-mm Crack Height at Saddle Position, 65-Degree Beam (Toe Crack – Left, Root Crack – Right) –Geometry 7 29

Figure 1.5.2-28. (dB) Interaction Calculations Plot – 1-mm Crack Height at Saddle Position, 45-, 55-, and 65-Degree Beam (Toe Crack – Left, Root Crack – Right) – Geometry 7 30

Figure 1.5.2-29. Interaction Calculations Capture – 1-mm Crack Height at Crotch Position, 45-Degree Beam (Toe Crack – Left, Root Crack – Right) – Geometry 7 32

Figure 1.5.2-30. Interaction Calculations Capture – 1-mm Crack Height at Crotch Position, 55-Degree Beam (Toe Crack – Left, Root Crack – Right) – Geometry 7 32

Table of Contents – Chapter VI (Continued)

Page

Figure 1.5.2-31. Interaction Calculations Capture – 1-mm Crack Height at Crotch Position, 65-Degree Beam (Toe Crack – Left, Root Crack – Right) – Geometry 7 33

Figure 1.5.2-32. (dB) Interaction Calculations Plot – 1-mm Crack Height at Crotch Position, 45-, 55-, and 65-Degree Beam (Toe Crack – Left, Root Crack – Right) – Geometry 7 33

Figure 1.5.2-33. Interaction Calculations Capture – 1-mm Crack Height at 141-Degree Position, 45-Degree Beam (Toe Crack – Left, Root Crack – Right) – Geometry 7 35

Figure 1.5.2-34. Interaction Calculations Capture – 1-mm Crack Height at 141-Degree Position, 55-Degree Beam (Toe Crack – Left, Root Crack – Right) – Geometry 7 35

Figure 1.5.2-35. Interaction Calculations Capture – 1-mm Crack Height at 141-Degree Position, 65-Degree Beam (Toe Crack – Left, Root Crack – Right) – Geometry 7 36

Figure 1.5.2-36. (dB) Interaction Calculations Plot – 1-mm Crack Height at 141-Degree Position, 45-, 55-, and 65-Degree Beam (Toe Crack – Left, Root Crack – Right) – Geometry 7 36

Figure 1.5.2-37. Modal Analysis – Toe Flaw on Saddle, 65-Degree Beam; -60-Degree Flaw Tilt – Geometry 7 38

Figure 1.5.2-38. Modal Analysis – Toe Flaw on Saddle, 65-Degree Beam; -50-Degree Flaw Tilt – Geometry 7 38

Figure 1.5.2-39. Modal Analysis – Toe Flaw on Saddle, 65-Degree Beam -40-Degree Flaw Tilt – Geometry 7 39

Figure 1.5.2-40. Modal Analysis – Toe Flaw on Saddle, 65-Degree Beam; -30-Degree Flaw Tilt – Geometry 7 39

Figure 1.5.2-41. Modal Analysis – Toe Flaw on Saddle, 65-Degree Beam; -20-Degree Flaw Tilt – Geometry 7 40

Figure 1.5.2-42. Modal Analysis – Toe Flaw on Saddle, 65-Degree Beam; -10-Degree Flaw Tilt – Geometry 7 40

Figure 1.5.2-43. Modal Analysis – Toe Flaw on Saddle, 65-Degree Beam; 0-Degree Flaw Tilt – Geometry 7 41

Figure 1.5.2-44. Modal Analysis – Toe Flaw on Saddle, 65-Degree Beam; 10-Degree Flaw Tilt – Geometry 7 41

Table of Contents – Chapter VI (Continued)

Page

Figure 1.5.2-45. Modal Analysis – Toe Flaw on Saddle, 65-Degree Beam; 20-Degree Flaw Tilt – Geometry 7 42

Figure 1.5.2-46. Modal Analysis – Toe Flaw on Saddle, 65-Degree Beam; 30-Degree Flaw Tilt – Geometry 7 42

Figure 1.5.2-47. Modal Analysis – Toe Flaw on Saddle, 65-Degree Beam; 40-Degree Flaw Tilt – Geometry 7 43

Figure 1.5.2-48. Modal Analysis – Toe Flaw on Saddle, 65-Degree Beam; 50-Degree Flaw Tilt – Geometry 7 43

Figure 1.5.2-49. Modal Analysis – Toe Flaw on Saddle, 65-Degree Beam; 60-Degree Flaw Tilt – Geometry 7 44

Figure 1.5.2-50. Modal Analysis – Root Flaw on Saddle, 65-Degree Beam; -60-Degree Flaw Tilt – Geometry 7 44

Figure 1.5.2-51. Modal Analysis – Root Flaw on Saddle, 65-Degree Beam; -30-Degree Flaw Tilt – Geometry 7 45

Figure 1.5.2-52. Modal Analysis – Root Flaw on Saddle, 65-Degree Beam; 0-Degree Flaw Tilt – Geometry 7 45

Figure 1.5.2-53. Modal Analysis – Root Flaw on Saddle, 65-Degree Beam; 30-Degree Flaw Tilt – Geometry 7 46

Figure 1.5.2-54. Modal Analysis – Root Flaw on Saddle, 65-Degree Beam; 60-Degree Flaw Tilt – Geometry 7 46

Figure 1.5.2-55. Interaction Calculations Capture – 1-mm Crack Height at Saddle Position, 45-Degree Beam (Toe Crack – Left, Root Crack – Right) – Geometry 8 48

Figure 1.5.2-56. Interaction Calculations Capture – 1-mm Crack Height at Saddle Position, 55-Degree Beam (Toe Crack – Left, Root Crack – Right) – Geometry 8 48

Figure 1.5.2-57. Interaction Calculations Capture – 1-mm Crack Height at Saddle Position, 65-Degree Beam (Toe Crack – Left, Root Crack – Right) – Geometry 8 49

Figure 1.5.2-58. (dB) Interaction Calculations Plot – 1-mm Crack Height at Saddle Position, 45-, 55-, and 65-Degree Beam (Toe Crack – Left, Root Crack – Right) – Geometry 8 49

Figure 1.5.2-59. Interaction Calculations Capture – 1-mm Crack Height at Crotch Position, 45-Degree Beam (Toe Crack – Left, Root Crack – Right) – Geometry 8 51

Table of Contents – Chapter VI (Continued)

Page

Figure 1.5.2-60. Interaction Calculations Capture – 1-mm Crack Height at Crotch Position, 55-Degree Beam (Toe Crack – Left, Root Crack – Right) – Geometry 8 51

Figure 1.5.2-61. Interaction Calculations Capture – 1-mm Crack Height at Crotch Position, 65-Degree Beam (Toe Crack – Left, Root Crack – Right) – Geometry 8 52

Figure 1.5.2-62. (dB) Interaction Calculations Plot – 1-mm Crack Height at Crotch Position, 45-, 55-, and 65-Degree Beam (Toe Crack – Left, Root Crack – Right) – Geometry 8 52

Figure 1.5.2-63. Interaction Calculations Capture – 1-mm Crack Height at 141-Degree Position, 45-Degree Beam (Toe Crack – Left, Root Crack – Right) – Geometry 8 54

Figure 1.5.2-64. Interaction Calculations Capture – 1-mm Crack Height at 141-Degree Position, 55-Degree Beam (Toe Crack – Left, Root Crack – Right) – Geometry 8 54

Figure 1.5.2-65. Interaction Calculations Capture – 1-mm Crack Height at 141-Degree Position, 65-Degree Beam (Toe Crack – Left, Root Crack – Right) – Geometry 8 55

Figure 1.5.2-66. (dB) Interaction Calculations Plot – 1-mm Crack Height at 141-Degree Position, 45-, 55-, and 65-Degree Beam (Toe Crack – Left, Root Crack – Right) – Geometry 8 55

Figure 1.5.2-67. Modal Analysis – Toe Flaw on Saddle, 45-Degree Beam; -60-Degree Flaw Tilt – Geometry 8 57

Figure 1.5.2-68. Modal Analysis – Toe Flaw on Saddle, 45-Degree Beam; -50-Degree Flaw Tilt – Geometry 8 57

Figure 1.5.2-69. Modal Analysis – Toe Flaw on Saddle, 4-Degree Beam; -40-Degree Flaw Tilt – Geometry 8 58

Figure 1.5.2-70. Modal Analysis – Toe Flaw on Saddle, 45-Degree Beam; -30-Degree Flaw Tilt – Geometry 8 58

Figure 1.5.2-71. Modal Analysis – Toe Flaw on Saddle, 45-Degree Beam; -20-Degree Flaw Tilt – Geometry 8 59

Figure 1.5.2-72. Modal Analysis – Toe Flaw on Saddle, 45-Degree Beam; -10-Degree Flaw Tilt – Geometry 8 59

Figure 1.5.2-73. Modal Analysis – Toe Flaw on Saddle, 45-Degree Beam; 0-Degree Flaw Tilt –Geometry 8 60

Table of Contents – Chapter VI (Continued)

Page

Figure 1.5.2-74. Modal Analysis – Toe Flaw on Saddle, 45-Degree Beam; 10-Degree Flaw Tilt – Geometry 8 60

Figure 1.5.2-75. Modal Analysis – Toe Flaw on Saddle, 45-Degree Beam; 20-Degree Flaw Tilt – Geometry 8 61

Figure 1.5.2-76. Modal Analysis – Toe Flaw on Saddle, 45-Degree Beam; 30-Degree Flaw Tilt – Geometry 8 61

Figure 1.5.2-77. Modal Analysis – Toe Flaw on Saddle, 45-Degree Beam; 40-Degree Flaw Tilt – Geometry 8 62

Figure 1.5.2-78. Modal Analysis – Toe Flaw on Saddle, 45-Degree Beam; 50-Degree Flaw Tilt – Geometry 8 62

Figure 1.5.2-79. Modal Analysis – Toe Flaw on Saddle, 45-Degree Beam; 60-Degree Flaw Tilt – Geometry 8 63

Figure 1.5.2-80. Modal Analysis – Root Flaw on Saddle, 45-Degree Beam; -60-Degree Flaw Tilt – Geometry 8 63

Figure 1.5.2-81. Modal Analysis – Root Flaw on Saddle, 45-Degree Beam; -30-Degree Flaw Tilt – Geometry 8 64

Figure 1.5.2-82. Modal Analysis – Root Flaw on Saddle, 45-Degree Beam; 0-Degree Flaw Tilt – Geometry 8 64

Figure 1.5.2-83. Modal Analysis – Root Flaw on Saddle, 45-Degree Beam; 30-Degree Flaw Tilt – Geometry 8 65

Figure 1.5.2-84. Modal Analysis – Root Flaw on Saddle, 45-Degree Beam; 60-Degree Flaw Tilt – Geometry 8 65

Figure 1.5.2-85. Interaction Calculations Capture – 3-mm Crack Height at Saddle Position, 45-Degree Beam (Toe Crack – Left, Root Crack – Right) – Geometry 8 66

Figure 1.5.2-86 (dB) Interaction Calculations Plot – 3-mm High Toe and Root Cracks at Saddle Position; Geometry 8; 4-MHz, 45-Degree Beam 66

1.5 UT Modeling and Simulation

One other important aspect of this project was the simulation of ultrasonic techniques to evaluate the benefits and limitations of each AUT technique. During the three previous EWI projects modeling and simulations were performed to optimize UT inspection of thin-walled pipe welds (see References 1.2-5 through 1.2-7 in Chapter III) to predict the performance of PA UT techniques for inspection of one hot tab and one repair sleeve configuration (see References 1.2-8 and 1.2-9 in Chapter III), and to analyze over- and undersized results from the EWI and Advantica AUT sizing trials (see Reference 1.2-10 in Chapter III). Details about UT semi-analytical modeling theory, software tools, and simulation steps are described elsewhere (see References 1.2-5 through 1.2-10 in Chapter III). During this project UT simulations were performed and compared to those from the actual scan data to determine sizing limits of the proposed time-based PA technique and develop optimized PA techniques for two additional hot tab configurations. The modeled beams were interacted with simulated flaws to assess the ability to detect and size flaws of different sizes, types, and orientations. The modeling results showed good correlation between predicted results and actual results. Based on these findings, it was confirmed that modeling and simulation is a good tool for UT technique development, optimization, and validation purposes.

1.5.1 Use of UT Modeling and Simulation to Define Sizing Limits

Models of ultrasonic beams for each UT technique were produced in order to determine the relative intensity of the sound energy along the path of beam propagation. In addition, the models allowed the beam spot size to be determined at selected locations perpendicular to the direction of propagation. Appendix A1.5.1 contains results of the sound beam models for the different UT techniques. These beam models were helpful when comparing differences in experimental scan results from one technique to another on scans of the same flaw.
Table 1.5.1-1 gives the beam dimensions for each technique based on the modeling results.

Table 1.5.1-1. Beam Measurements Based on Modeling Results

Transducer Parameters	6 dB Spread [1]		12 dB Spread [1]		Comments
	[2] Z (mm)	[2] Y (mm)	[2] Z (mm)	[2] Y (mm)	
SE4F-45	3.0	2.4	4.3	3.6	75 mm radius element
SE4F-60	5.3	3.1	7.5	4.6	75 mm radius element
SE5-45	3.3	3.3	5.8	7.7	Flat element
SE5-60	5.0	4.4	7.0	7.2	Flat element
PA4-24/24	3.5	6.2	5.0	8.7	Beam angle of 60 degrees & focal depth of 20 mm
DPA4-24/24	4.3	6.2	6.0	9.1	Beam angle of 53 degrees & focal depth of 20 mm
PA4-32/64	2.5	7.5	3.8	12.5	Beam angle of 60 degrees & focal depth of 20 mm
PA5-16/16	3.5	4.4	5.0	7.0	Beam angle of 60 degrees & focal depth of 20 mm
PA5-32/32	2.3	4.9	3.3	7.8	Beam angle of 60 degrees & focal depth of 20 mm
PA7-17/60	2.8	4.5	4.0	6.8	Beam angle of 60 degrees & focal depth of 20 mm

Notes:

1. Beam spread at a depth of 24 mm
2. "Z" is beam spread in through wall direction; "Y" is beam spread along weld

After calculating the ultrasonic beams for the different techniques, calculated beam models were then interacted with simulated calibration reference reflectors and simulated flaws. The first step was to perform a comparison of simulated UT scans of the notches in the calibration reference sample shown in Figure 1.4.3-1 to actual scans of the same notches. For comparison purposes, the SE5-60 single-element technique and the PA7-60/17 PA technique were selected. The A-scan results in Figures 1.5.1-1 through 1.5.1-4 show that the simulations agreed well with the actual UT data. Further, the results showed that the a tip signal from the notch was not resolved until the notch depth was about 1.5 to 2.0 mm (0.06 to 0.08 in.) for the single-element probe and about 1.0 to 1.5 mm (0.04 to 0.06 in.) for the PA probe. The full-wave A-scan simulation results in Figures 1.5.1-5 and 1.5.1-6 also confirm the notch depth needed to resolve a tip signal for the two techniques.

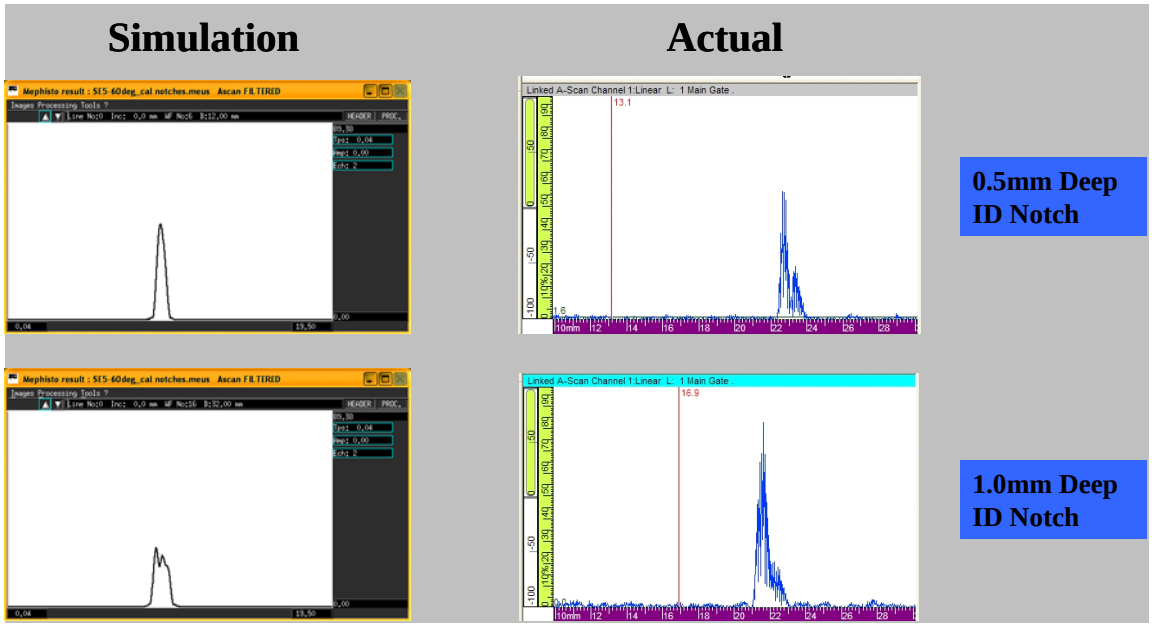

Figure 1.5.1-1. **Simulation to Actual Comparison of 0.5- and 1.0-mm-Deep Notches Using SE5-60 UT Technique**

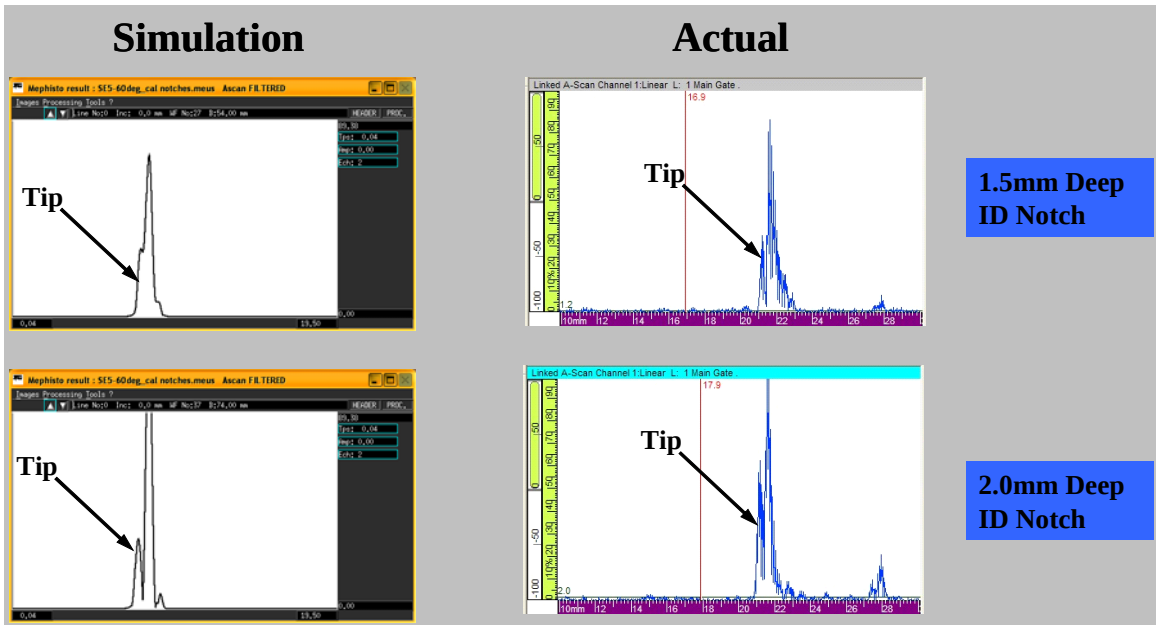

Figure 1.5.1-2. **Simulation to Actual Comparison of 1.5- and 2.0-mm-Deep Notches Using SE5-60 UT Technique**

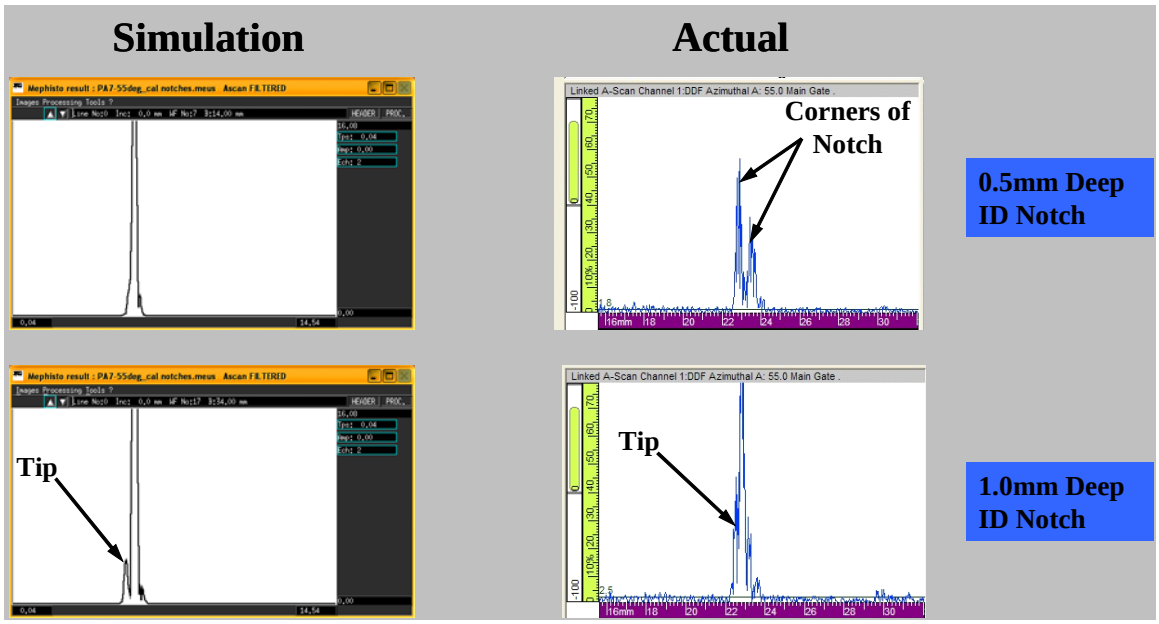

Figure 1.5.1-3. **Simulation to Actual Comparison of 0.5- and 1.0-mm-Deep Notches Using PA7-60/17 UT Technique**

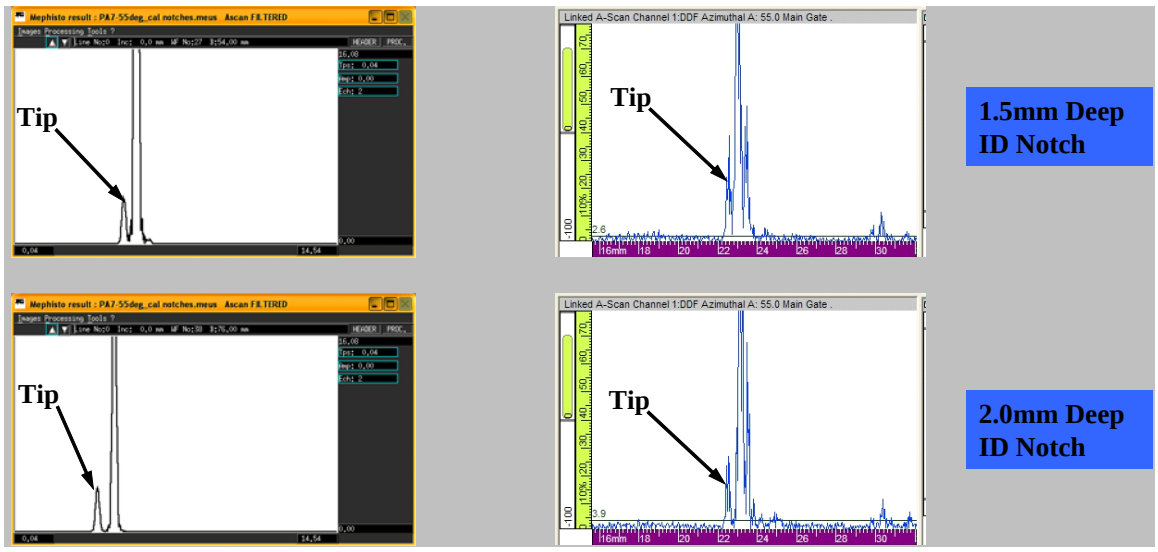

Figure 1.5.1-4. **Simulation to Actual Comparison of 1.5- and 2.0-mm-Deep Notches Using PA7-60/17 UT Technique**

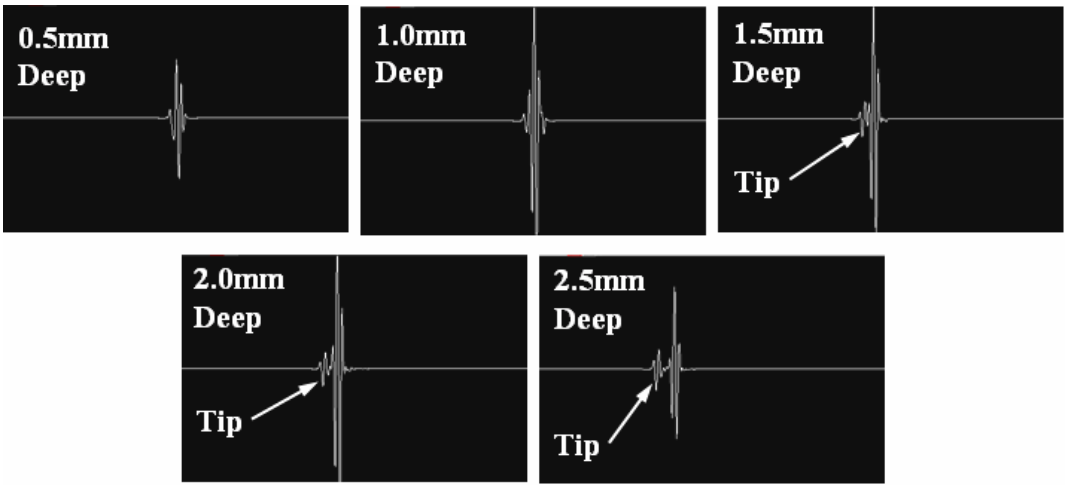

Figure 1.5.1-5. Simulation of 0.5- to 2.5-mm-Deep Notches Using SE5-60 UT Technique

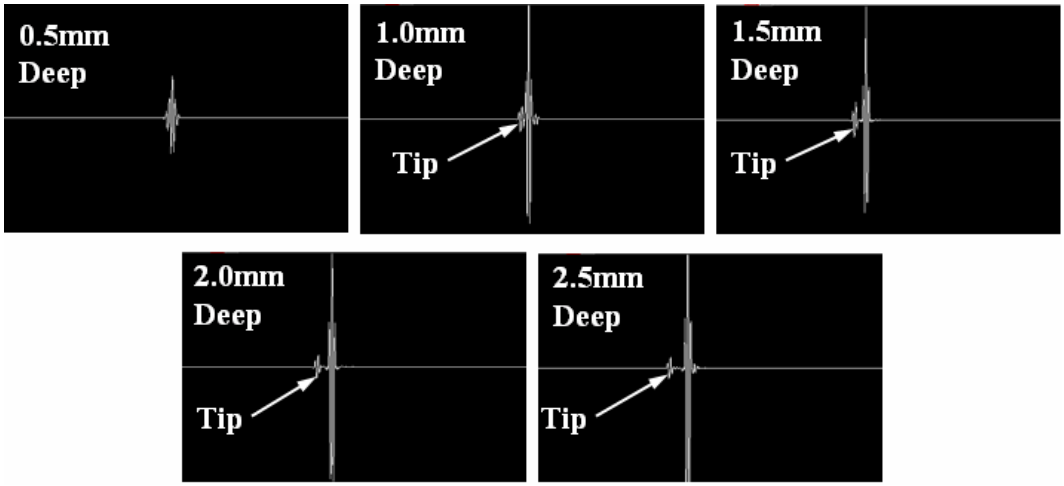

Figure 1.5.1-6. Simulation of 0.5- to 2.5-mm-Deep Notches Using PA7-60/17 UT Technique

Next, height and length dimensions for Flaw W3-1, as discussed in Section 1.6.4 of this report, were input into the model, and simulations were conducted using UT parameters used for the actual scans. Metallography results of Flaw W3-1 indicated a straight portion of the crack that appeared to be caused by fatigue and a brittle extension possibly caused during an unsuccessful attempt to break the sample open at low temperature (Figure 1.6.4-6). Refer to Section 1.6.4 for additional information regarding Flaw W3-1. UT simulations were performed using each crack height separately. Figure 1.5.1-7 shows a view of the straight fatigue crack used for simulation and Figure 1.5.1-8 shows the entire crack height (fatigue plus brittle fracture) used for simulation.

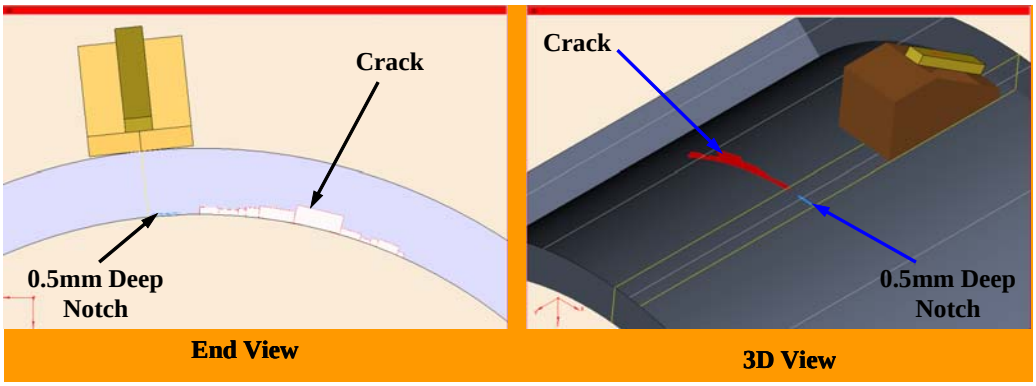

Figure 1.5.1-7. Simulation of Fatigue Portion of Flaw W3-1 (Straight Portion)

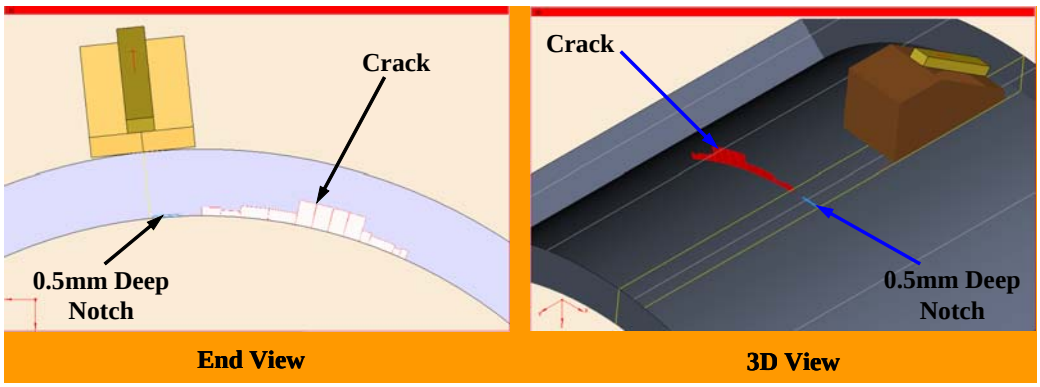

Figure 1.5.1-8. Simulation of Fatigue and Brittle Fracture Combination of Flaw W3-1 (Full Crack Height)

The experimental data for the SE5-60 and the PA7-60/17 techniques was compared to the modeling results. Figures 1.5.1-9 and 1.5.1-10 are C-scan images showing the predicted C-scan image to the actual C-scan image constructed from the experimental data. The predicted results were very similar to the actual (experimental) results with the corner trap signal of the PA7-60/17 technique being narrower than that of the SE5-60 technique. Also, the model accurately predicted that a tip signal could be detected on the portion of the crack having the greatest through-wall height.

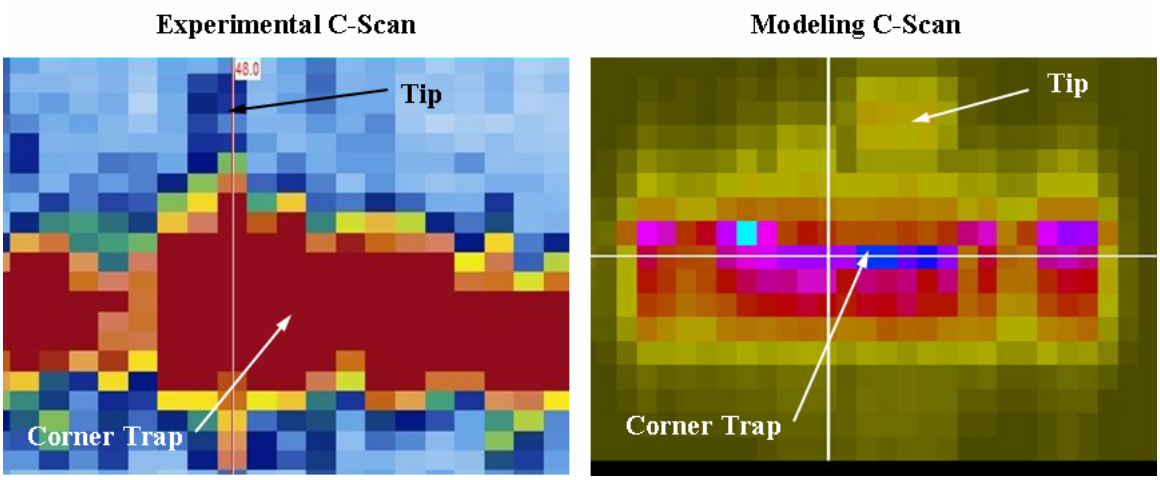

Figure 1.5.1-9. **Comparison of Experimental C-Scan and Predicted C-Scan of W3-1 Fatigue Crack Using Single-Element, 5-MHz, 60-Degree Probe**

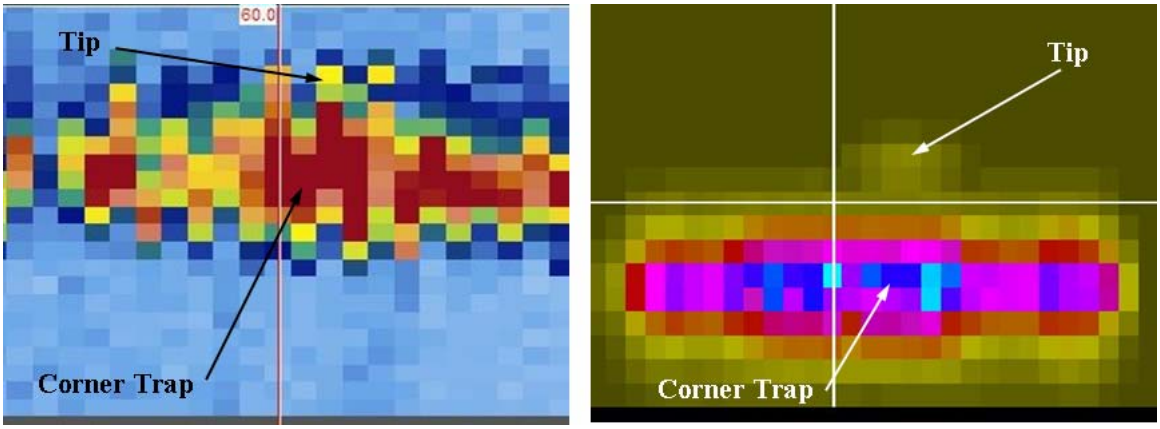

Figure 1.5.1-10. **Comparison of Experimental C-Scan and Predicted C-Scan of W3-1 Fatigue Crack Using PA 7-MHz 60/17 Element Probe at a 60-Degree Angle**

1.5.2 UT Modeling and Simulation of Repair Welds

Weld discontinuities, especially hydrogen-assisted cracking, are a distinct possibility for welds made onto in-service pipelines. Welding onto in-service pipelines, for the purpose of attaching repair branch connections or repair sleeves, results in a relatively high likelihood of hydrogen-assisted cracking due to fast cooling rates.

Current inspection techniques are not reliable in terms of their ability to detect these types of defects. Radiography is not feasible due to the geometry of the welds and the POD issues. Although conventional UT in combination with magnetic-particle inspection is currently recommended by API 1104, UT has not been particularly successful, again due to the changing geometry and inherent problems with signal identification. During this project ultrasonic modeling and simulation software was used to further develop PA technology for reliable detection of weld discontinuities, especially hydrogen-induced cracking, in repair welds.

Lozev et al. investigated the possibility of using PAs with a specific geometry, both at the simulation and experimental level, and came up with a set of ground rules for an initial procedure (see References 1.2-8 and 1.2-9 in Chapter III). During that work, emerging PA technology was combined with UT simulations in the early stages of the procedure development to predict UT beam interactions with cracks, and to determine detection and sizing limitations of the proposed techniques.

During the investigation, the effect of crack orientation on UT detectability was minimized through the use of two optimized linear PA probes (4- and 10-MHz frequencies) developed during the modeling efforts. Simulations were conducted with each set of probe parameters to study the amplitude response when flaws were tilted and skewed at various angles. To validate the UT simulation results and the performance of the optimized transducers, one branch-to-carrier pipe weld for hot taps and one sleeve-to-carrier pipe weld for welded repair sleeves were fabricated. Each validation sample contained hydrogen-assisted cracks in the root and toe areas of the weld. The validation samples were scanned using the 4- and 10-MHz PA probes identified during the modeling efforts. After evaluating the ultrasonic scan data, it was found that better sizing accuracy was achieved using multiple inspection angles with the 4-MHz, 24-element, PA probe. Comparisons of the experimental results and simulation results showed that they were in good agreement with each other.

The UT modeling and simulation work performed during this project built upon the work previously conducted by Lozev et al. (see References 1.2-8 and 1.2-9 in Chapter III) Since the 4-MHz, 24-element probe was shown to have the best performance for this application, all modeling and simulation work was done using that probe. Modeled sound beams used during

the work by Lozev, et al. were 2D models which would not account for part curvature. Consequently, modeling and simulations performed during this project were done using 3D beams. The total aperture of the PA probe was approximately 20 × 8 mm (0.78 × 0.31 in.).

The modeling and simulation was performed in two steps. The first step was to model the beam profiles for each geometry in order to determine the beam dimensions at different focal depths. The second step was to interact the beams with simulated flaws to study the response from different flaw scenarios.

Two hot tap geometries were used for this project. The first, identified as Geometry 7, consisted of a 323-mm (12.75-in.) carrier pipe diameter having a wall thickness of 6.4 mm (0.25 in.). It was not necessary to consider the branch geometry because all the inspection simulations were performed from the pipe side of the connection. However, the branch pipe used for the model had a 114-mm (4.5-in.) diameter resulting in a branch-to-carrier pipe ratio of 0.33. Figure 1.5.2-1 gives a picture representation of the branch-pipe profile used for modeling purposes.

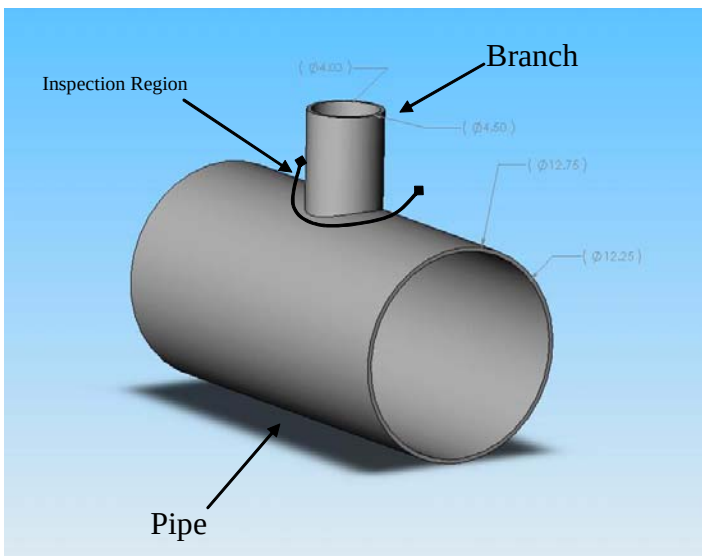

Figure 1.5.2-1. Branch Geometry 7 Setup

For Geometry 7, focal spot calculations were done at depths of 6.25, 9.375, and 12.5 mm. This represented the direct, first, and second leg calculations for the carrier pipe thickness under consideration. These calculations were done at two positions: the saddle (Figure 1.5.2-2) and the crotch position (Figure 1.5.2-3). Beam cross sections were required at these two positions because the direction of propagation of the sound beam relative to the longitudinal axis of the pipe was at the extremes at these two locations. By modeling the beams at these locations, the

integrity of the beam at the extremities of the scan could be determined. The intermediate position between the saddle and the crotch (Figure 1.5.2-4) was not modeled.

Figures 1.5.2-5 through 1.5.2-10 visualizes the beam cross sections for the different configurations considered. The beam appeared to be most distorted in the first leg calculations for the 45-degree angle. There were no calculations for the focusing on the second leg because the beam was still within the footprint of the wedge at this position and calculations were not possible. Figure 1.5.2-11 shows a typical beam cross section capture.

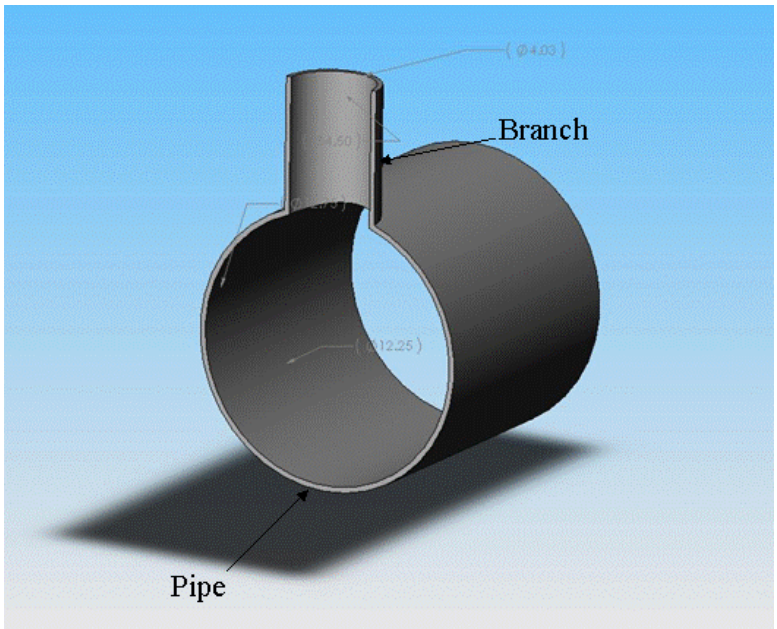

Figure 1.5.2-2. Branch Geometry 7 – Saddle Position Cross Section

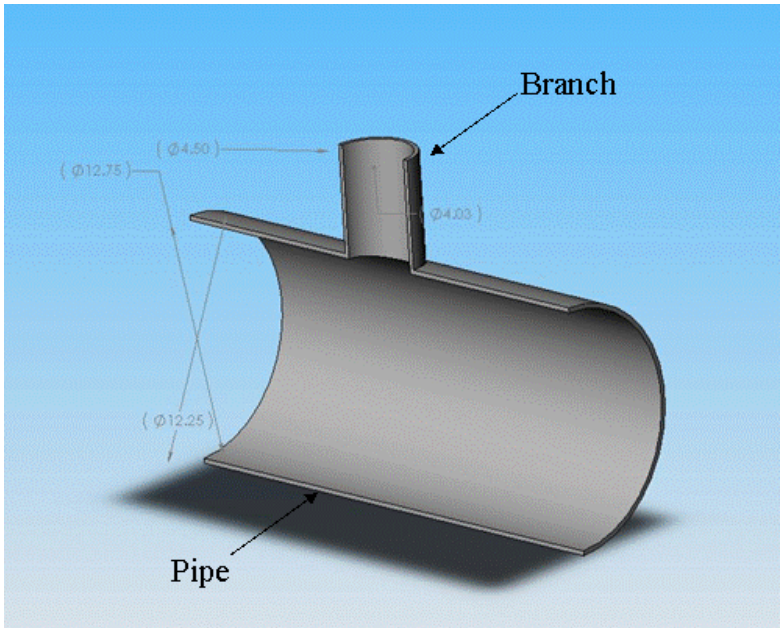

Figure 1.5.2-3. Branch Geometry 7 – Crotch Position Cross Section

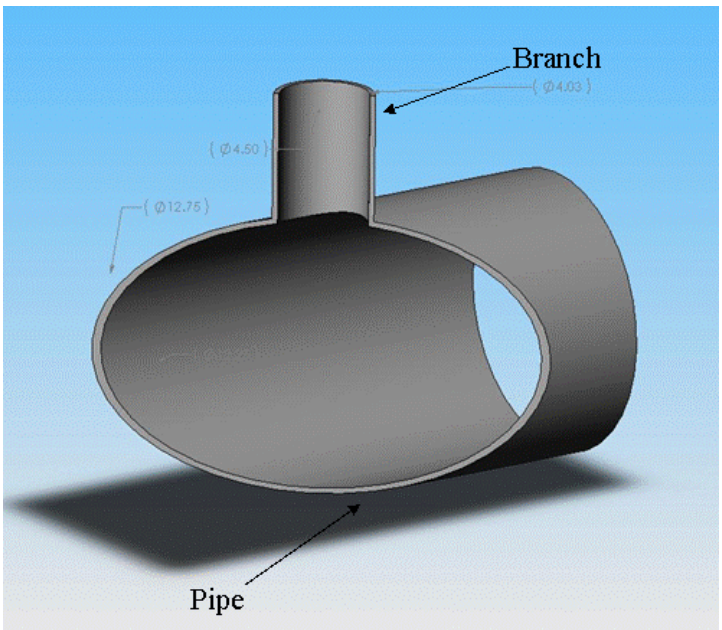

Figure 1.5.2-4. Branch Geometry 7 – 141-Degree Position Cross Section

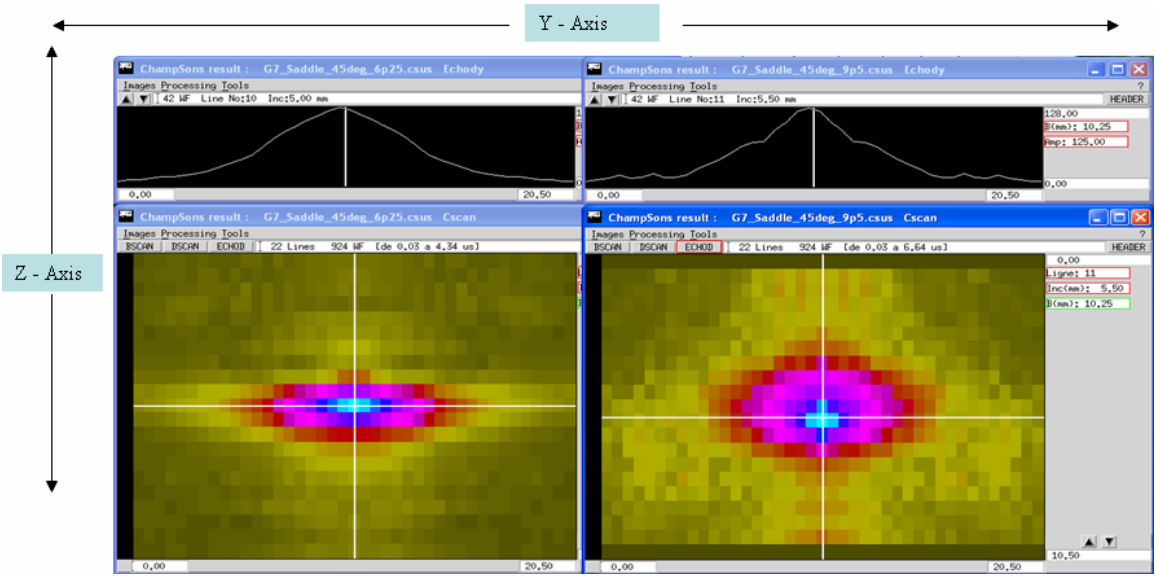

Figure 1.5.2-5. **Beam Cross Sections Capture – Saddle Position at FD 6.25 and 9.375 mm (6.4-mm Wall Thickness), 45-Degree Beam – Geometry 7**

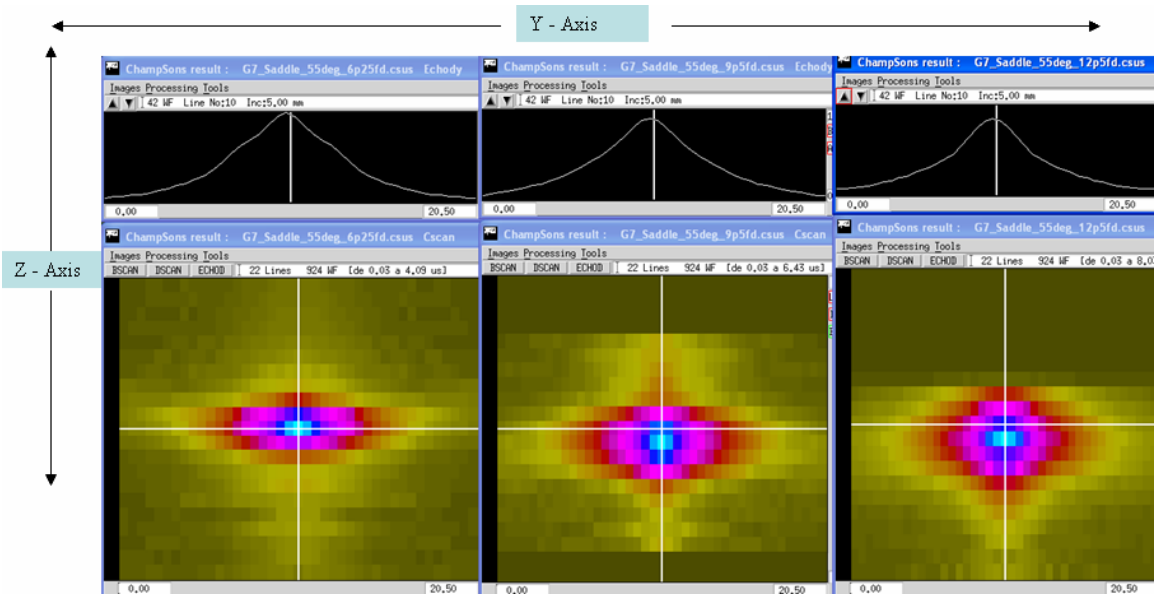

Figure 1.5.2-6. **Beam Cross Sections Capture – Saddle Position at FD 6.25, 9.375, and 12.5 mm (6.4-mm Wall Thickness), 55-Degree Beam – Geometry 7**

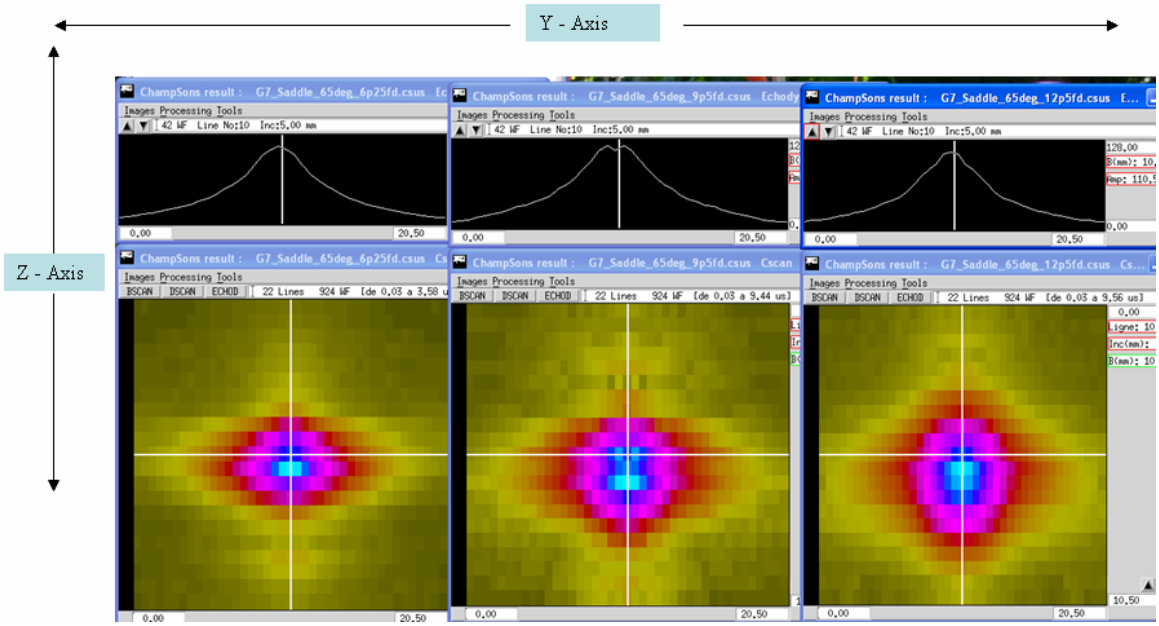

Figure 1.5.2-7. **Beam Cross Sections Capture – Saddle Position at FD 6.25, 9.375, and 12.5 mm (6.4-mm Wall Thickness), 65-Degree Beam – Geometry 7**

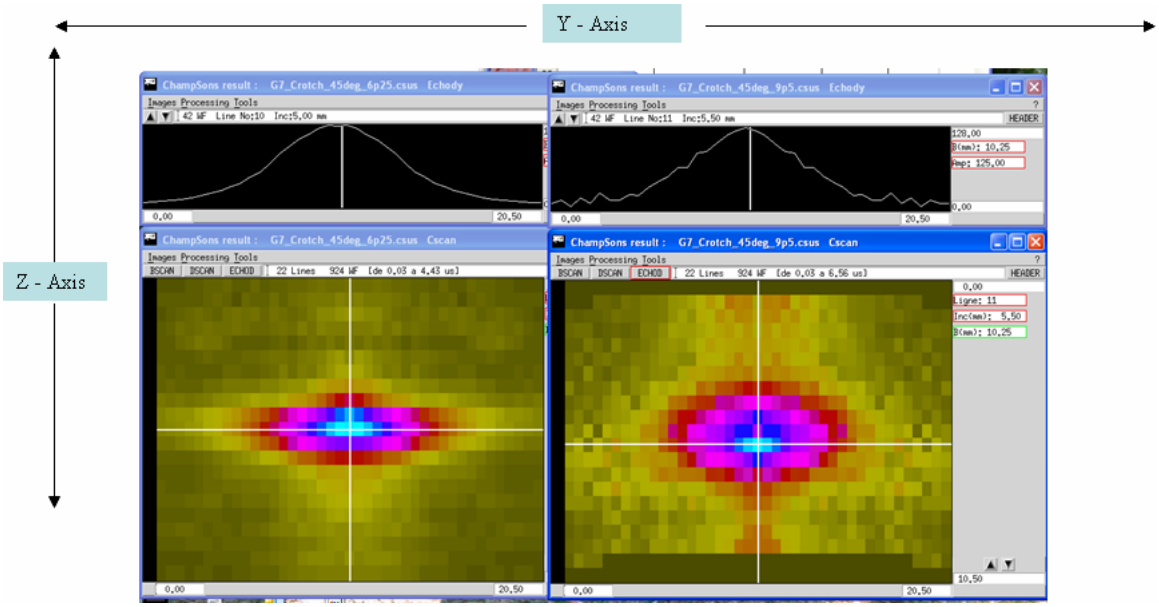

Figure 1.5.2-8. **Beam Cross Sections Capture – Crotch Position at FD 6.25 and 9.375 mm (6.4-mm Wall Thickness), 45-Degree Beam – Geometry 7**

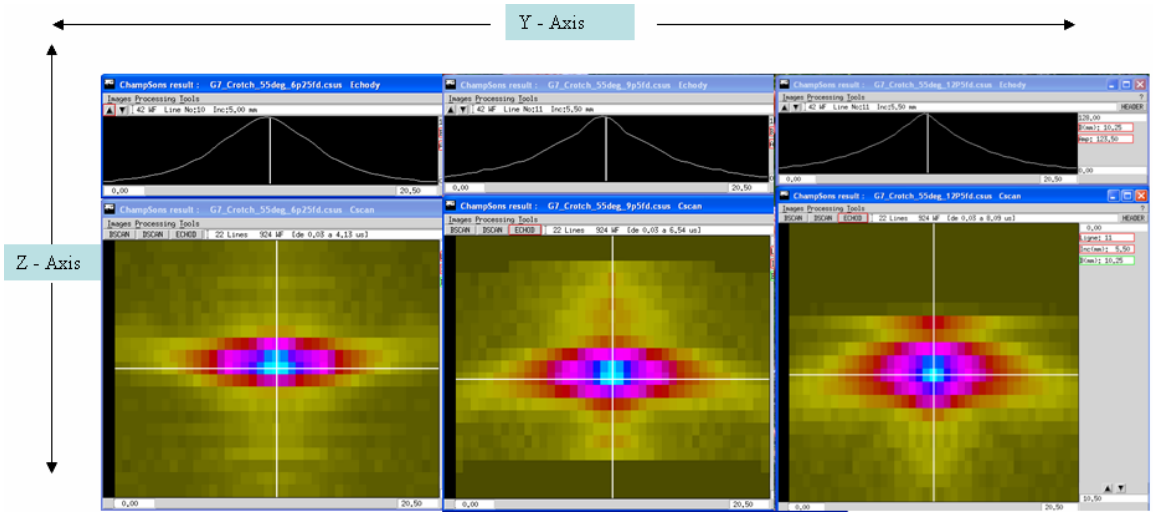

Figure 1.5.2-9. **Beam Cross Sections Capture – Crotch Position at FD 6.25, 9.375, and 12.5 mm (6.4-mm Wall Thickness), 55-Degree Beam – Geometry 7**

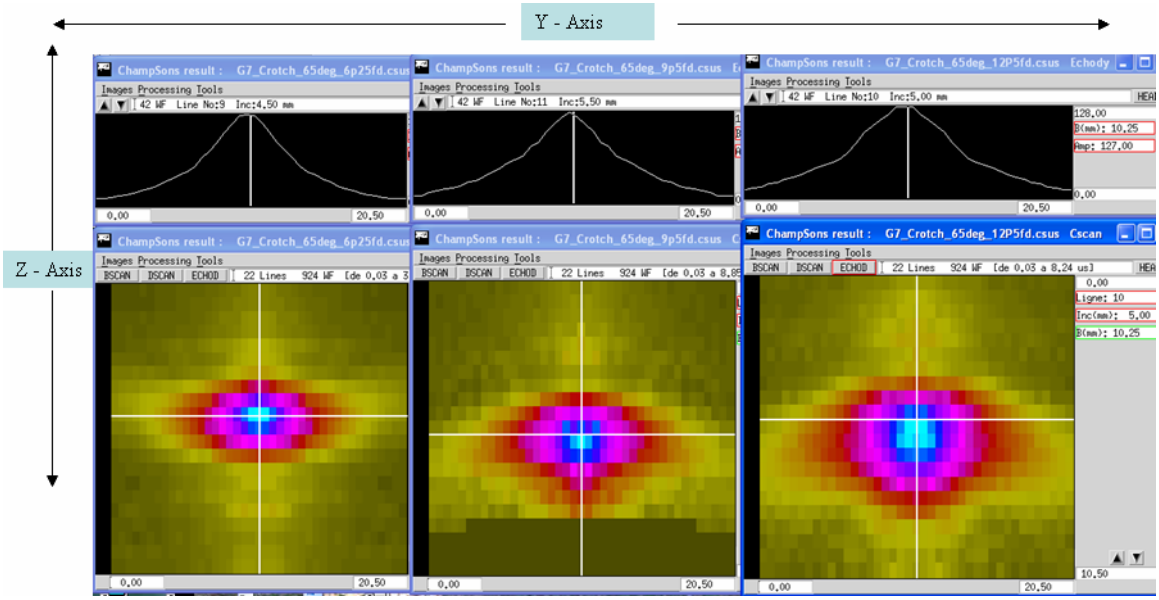

Figure 1.5.2-10. **Beam Cross Sections Capture – Crotch Position at FD 6.25, 9.375, and 12.5 mm (6.4-mm Wall Thickness), 65-Degree Beam – Geometry 7**

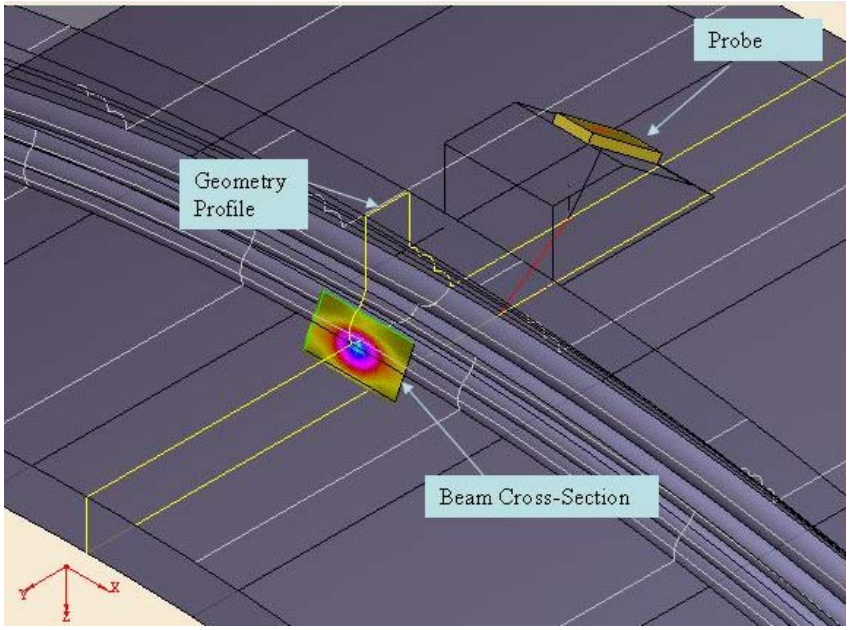

Figure 1.5.2-11. Typical Beam Cross Section Capture

The beam spot size in the focusing direction at the saddle was generally larger than the beam spot size at the crotch position. This was possibly due to the slightly longer sound path and change in beam angle due to the curvature in the saddle position. The beam spot size in the passive beam direction did not show much variation between the saddle and crotch locations. These calculations are tabulated in Tables 1.5.2-1 and 1.5.2-2.

Table 1.5.2-1. **Beam Cross Sections Tabulation – Saddle Position at FD 6.25, 9.375, and 12.5 mm (6.4-mm Wall Thickness), 45-, 55-, and 65-Degree Beams – Geometry 7**

SADDLE SETUP					
	Beam Angle	**6 dB**		**12 dB**	
		Y	**Z**	**Y**	**Z**
Focal Depth = 6.25mm	45	7.0	1.9	10.9	2.5
	55	6.5	1.5	10.3	2.3
	65	6.2	2.5	11.2	3.5
	Beam Angle	**6 dB**		**12 dB**	
		Y	**Z**	**Y**	**Z**
Focal Depth = 9.375mm	45	6.3	3.4	9.7	4.3
	55	5.9	2.1	11.4	3.1
	65	6.1	3.5	12.0	4.8
	Beam Angle	**6 dB**		**12 dB**	
		Y	**Z**	**Y**	**Z**
Focal Depth = 12.5mm	45	NA	NA	NA	NA
	55	5.5	2.6	11.0	3.5
	65	6.5	4.1	13.0	5.1

Table 1.5.2-2. **Beam Cross Sections Tabulation – Crotch Position at FD 6.25, 9.375, and 12.5 mm (6.4-mm Wall Thickness), 45-, 55-, and 65-Degree Beams – Geometry 7**

CROTCH SETUP					
	Beam Angle	**6 dB**		**12 dB**	
		Y	**Z**	**Y**	**Z**
Focal Depth = 6.25mm	45	7.4	1.8	11.1	2.8
	55	6.8	1.5	10.7	2.5
	65	6.4	2.3	11.5	3.2
	Beam Angle	**6 dB**		**12 dB**	
		Y	**Z**	**Y**	**Z**
Focal Depth = 9.375mm	45	7.2	2.6	10.3	3.8
	55	7.0	1.9	11.8	3.0
	65	6.6	2.4	12.0	3.8
	Beam Angle	**6 dB**		**12 dB**	
		Y	**Z**	**Y**	**Z**
Focal Depth = 12.5mm	45	NA	NA	NA	NA
	55	6.4	2.3	12.4	3.3
	65	7.1	4.0	13.3	4.9

The second geometry, identified as Geometry 8, consisted of a 914-mm (36-in.) pipe diameter with a 10.7-mm (0.421-in.) thickness. The branch pipe diameter was 557 mm (18 in.) which resulted in a branch-to-pipe diameter ratio of 0.5. Figure 1.5.2-12 shows a picture representation of the branch-pipe profile used for modeling purposes.

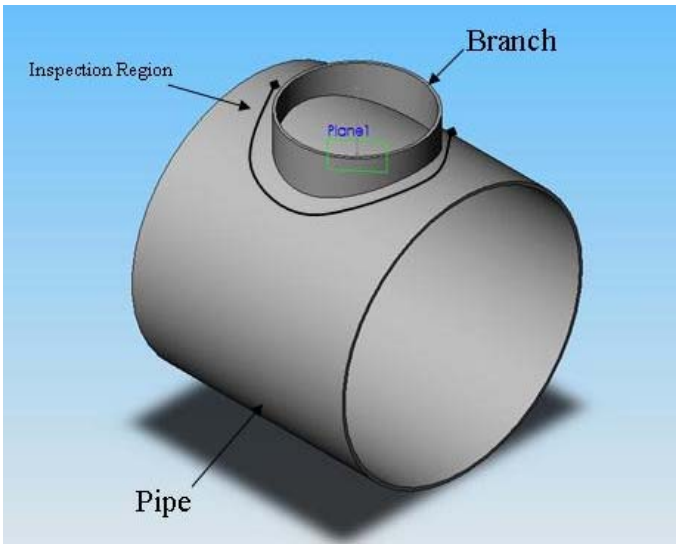

Figure 1.5.2-12. Branch Geometry Setup for Geometry 8

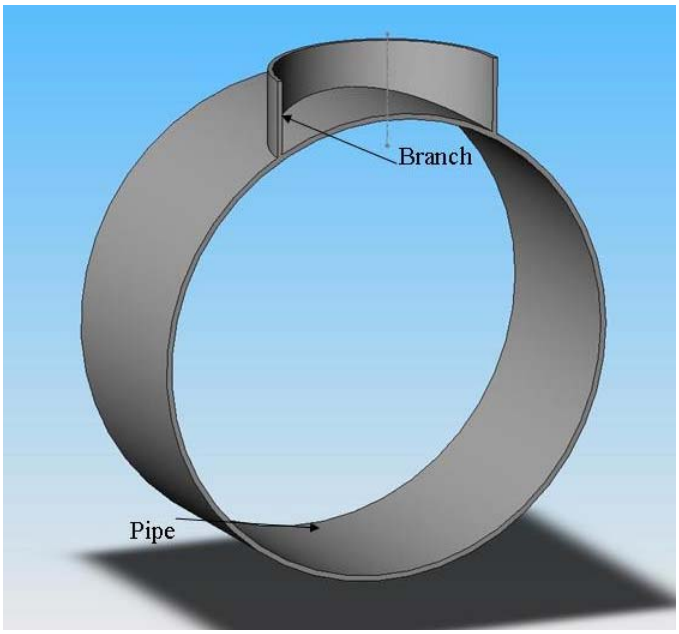

Figure 1.5.2-13. Branch Geometry 8 – Saddle Position Cross Section

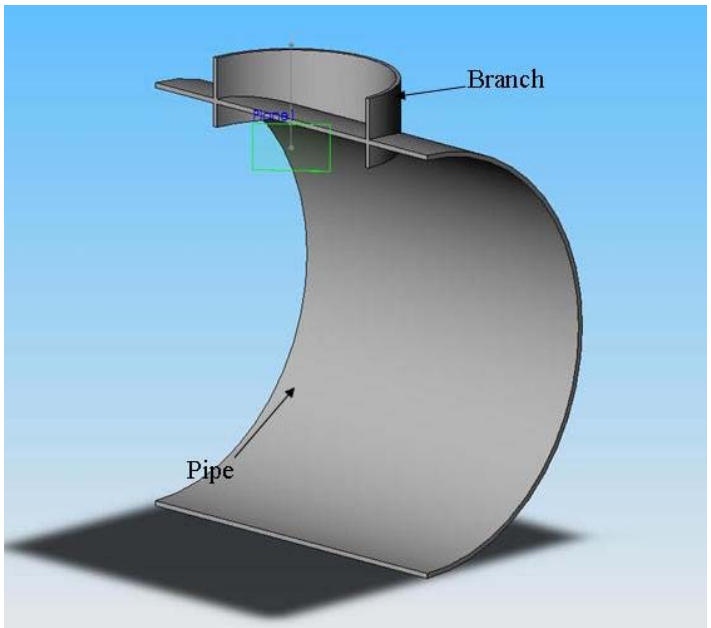

Figure 1.5.2-14. Branch Geometry 8 – Crotch Position Cross Section

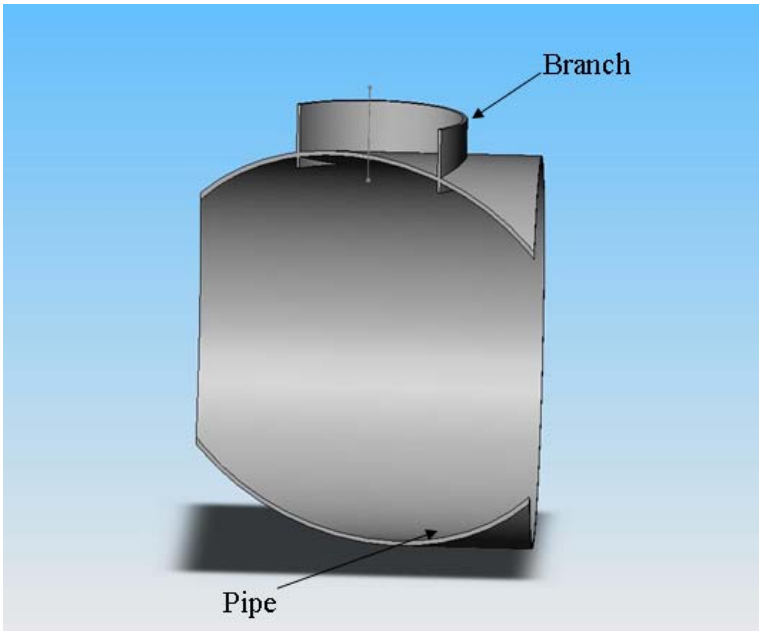

Figure 1.5.2-15. Branch Geometry 8 – 141-Degree Position Cross Section

As was done with Geometry 7, the focal spot calculations were performed at the direct, first and second leg depths which for Geometry 8 resulted in 10-, 15-, and 20-mm depths. These calculations were also done at two positions; the saddle (Figure 1.5.2-13) and the crotch position (Figure 1.5.2-14). The position shown in Figure 1.5.2-15, which is an intermediate between the saddle and the crotch, was not modeled in this beam cross section.

Analysis of the beam cross sections in Figures 1.5.2-16 through 1.5.2-18 at the saddle position and Figures 1.5.2-19 through 1.5.2-21 for the crotch position show very little difference in the beam cross section between the two positions. This is likely due to the larger diameter of the carrier pipe on which the transducer is positioned. However, in both cases, there was an increase in the spot size at a 65-degree angle. The spot sizes for 45- and 55-degree angles were similar in size. Tables 1.5.2-3 and 1.5.2-4 give the tabulated results for all of these calculations.

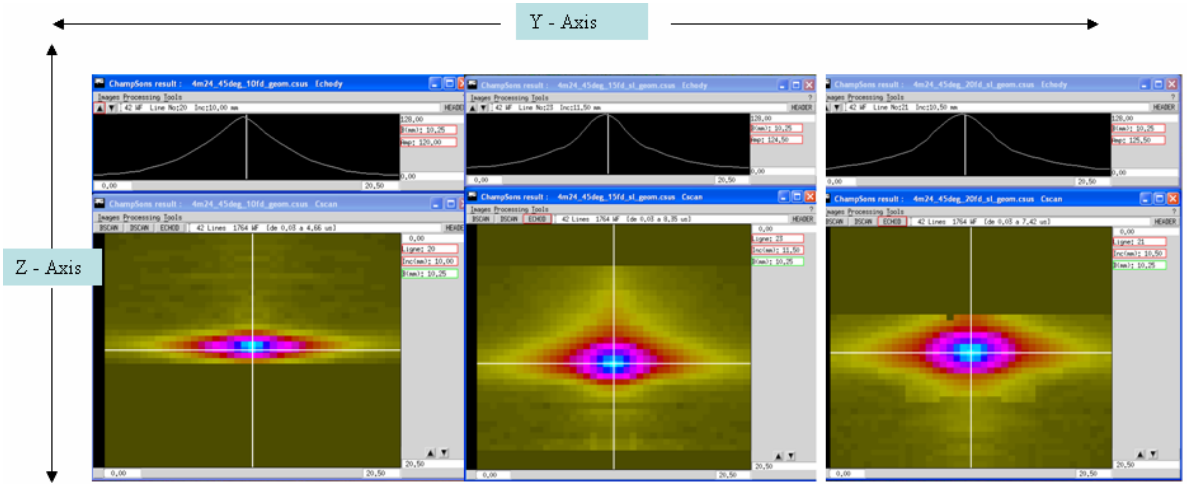

Figure 1.5.2-16. Beam Cross Sections Capture – Saddle Position at FD 10, 15, and 20 mm (10.7-mm Wall Thickness), 45-Degree Beam – Geometry 8

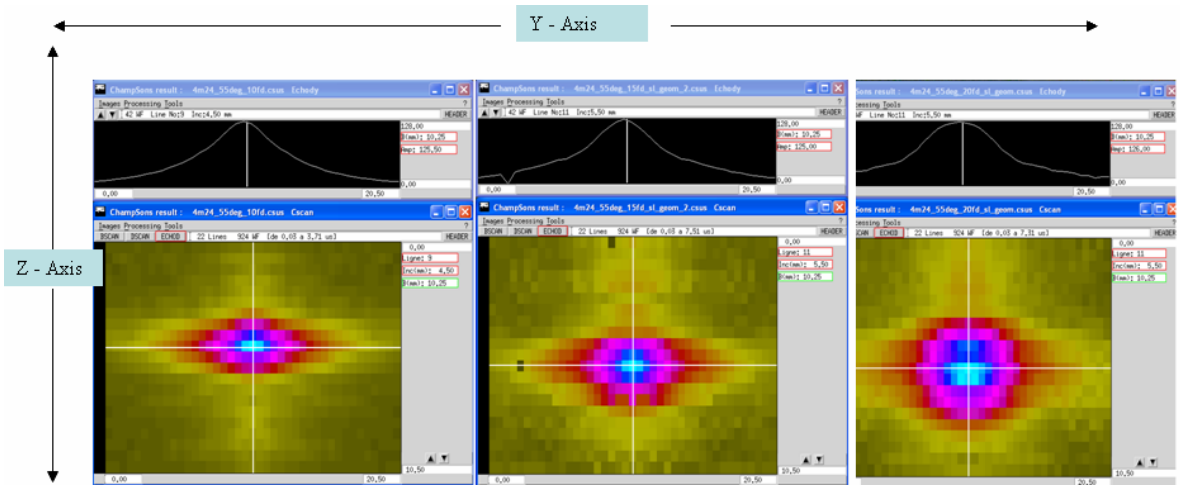

Figure 1.5.2-17. **Beam Cross Sections Capture – Saddle Position at FD 10, 15, and 20 mm (10.7-mm Wall Thickness), 55-Degree Beam – Geometry 8**

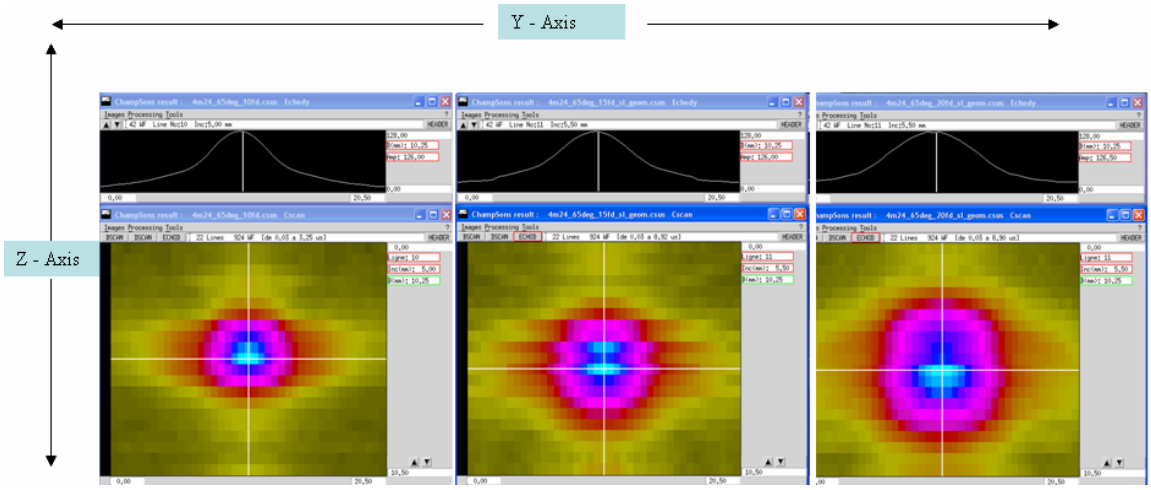

Figure 1.5.2-18. **Beam Cross Sections Capture – Saddle Position at FD 10, 15, and 20 mm (10.7-mm Wall Thickness), 65-Degree Beam – Geometry 8**

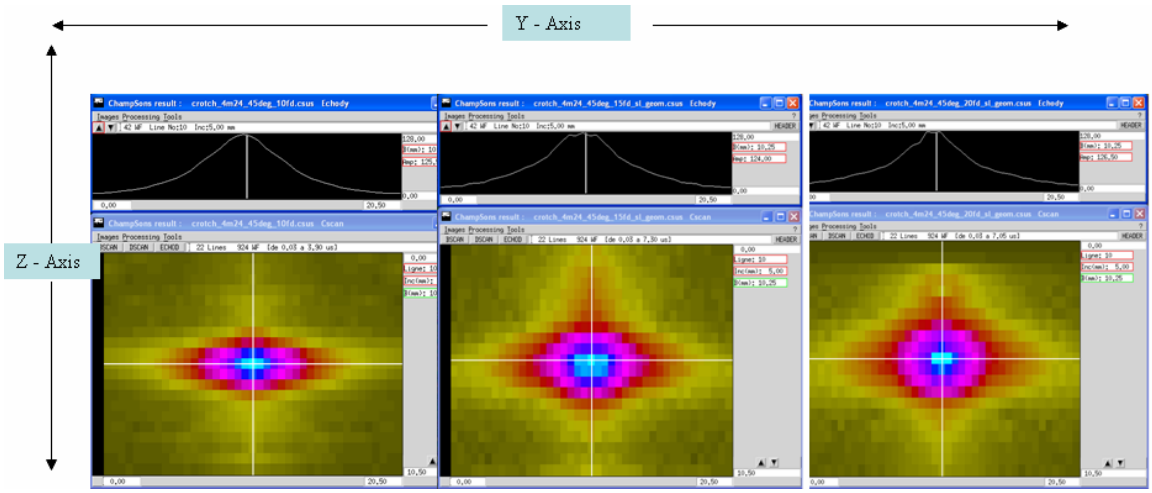

Figure 1.5.2-19. **Beam Cross Sections Capture – Crotch Position at FD 10, 15, and 20 mm (10.7-mm Wall Thickness), 45-Degree Beam – Geometry 8**

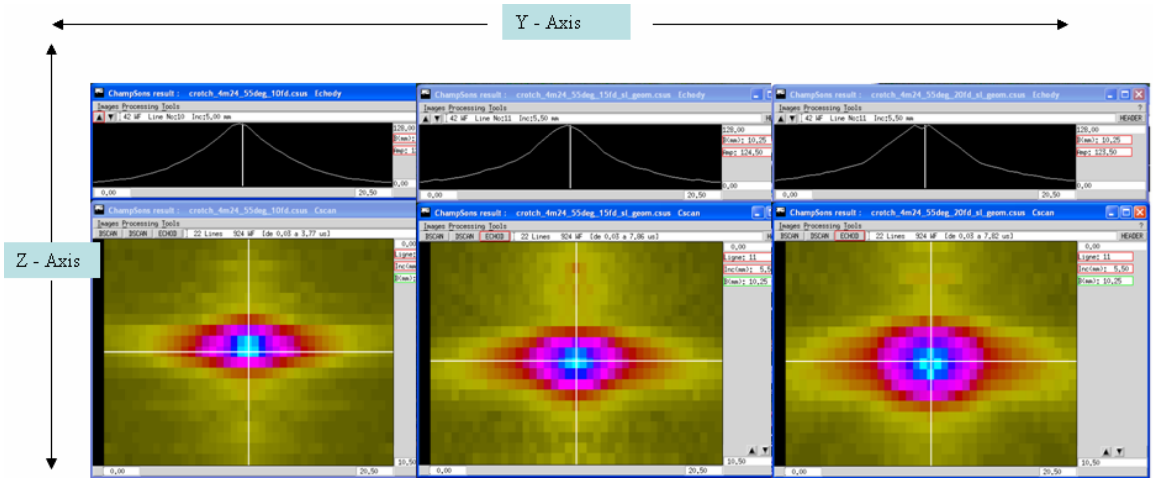

Figure 1.5.2-20. **Beam Cross Sections Capture – Crotch Position at FD 10, 15, and 20 mm (10.7-mm Wall Thickness), 55-Degree Beam – Geometry 8**

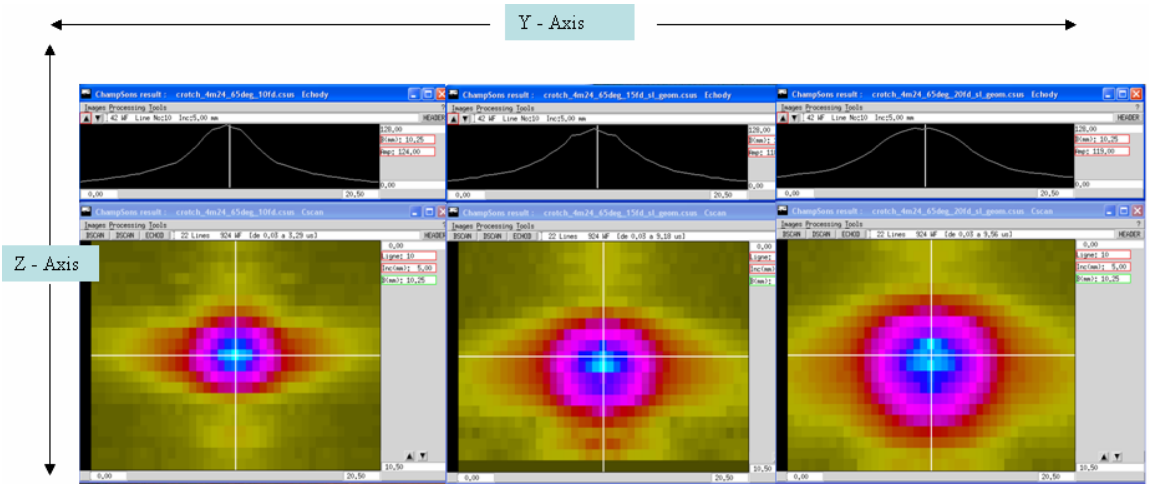

Figure 1.5.2-21. **Beam Cross Sections Tabulation – Crotch Position at FD 10, 15, and 20 mm (10.7-mm Wall Thickness), 65-Degree Beam – Geometry 8**

Table 1.5.2-3. **Beam Cross Sections Tabulation – Saddle Position at FD 10, 15, and 20 mm (10.7-mm Wall Thickness) – Geometry 8**

SADDLE SETUP					
	Beam Angle	6 dB		12 dB	
		Y	Z	Y	Z
Focal Depth = 10mm	45	5.9	1.9	10.3	2.8
	55	6.2	2.0	11.0	2.9
	65	5.7	3.0	11.0	4.3
	Beam Angle	6 dB		12 dB	
		Y	Z	Y	Z
Focal Depth = 15mm	45	5.0	3.0	10.9	3.5
	55	5.9	2.8	12.5	3.5
	65	7.2	4.0	14.0	5.8
	Beam Angle	6 dB		12 dB	
		Y	Z	Y	Z
Focal Depth = 20mm	45	6.0	3.4	11.8	5.5
	55	6.8	3.9	12.7	5.1
	65	8.1	5.5	13.4	7.5

Table 1.5.2-4. Beam Cross Sections Tabulation – Crotch Position at FD 10, 15, and 20 mm (10.7-mm Wall Thickness) – Geometry 8

CROTCH SETUP					
	Beam Angle	6 dB		12 dB	
		Y	Z	Y	Z
Focal Depth = 10mm	45	6.4	2.0	10.8	3.0
	55	6.3	1.9	11.0	2.8
	65	5.7	2.9	11.3	4.0
	Beam Angle	6 dB		12 dB	
		Y	Z	Y	Z
Focal Depth = 15mm	45	6.5	2.8	12.3	6.0
	55	6.1	3.1	12.0	3.8
	65	6.9	4.0	13.0	5.5
	Beam Angle	6 dB		12 dB	
		Y	Z	Y	Z
Focal Depth = 20mm	45	5.8	2.9	12.3	4.6
	55	6.7	3.3	13.2	4.1
	65	8.2	4.9	14.4	6.8

After building the beam models, the next step was to simulate a UT examination. Previous work done in this regard used a flaw height of 0.5 to 1.0 mm with flaw tilt angles in the range of -60 to 60 degrees (see References 1.2-8 and 1.2-9 in Chapter III). The previous studies indicated that the most significant and unpredictable misorientation of hydrogen cracks in repair welds resulted mainly from the tilt of the cracks. The main idea of this phase was to understand the effect of the tilt of the flaw on the amplitude response and is an extension of the previous work on other geometries under consideration. Figures 1.5.2-22 and 1.5.2-23 show typical toe crack and root crack interaction setups for this case. A total of six flaws were modeled during this phase. The six flaws consisted of a root and toe crack at the saddle position, crotch position, and 141-degree position.

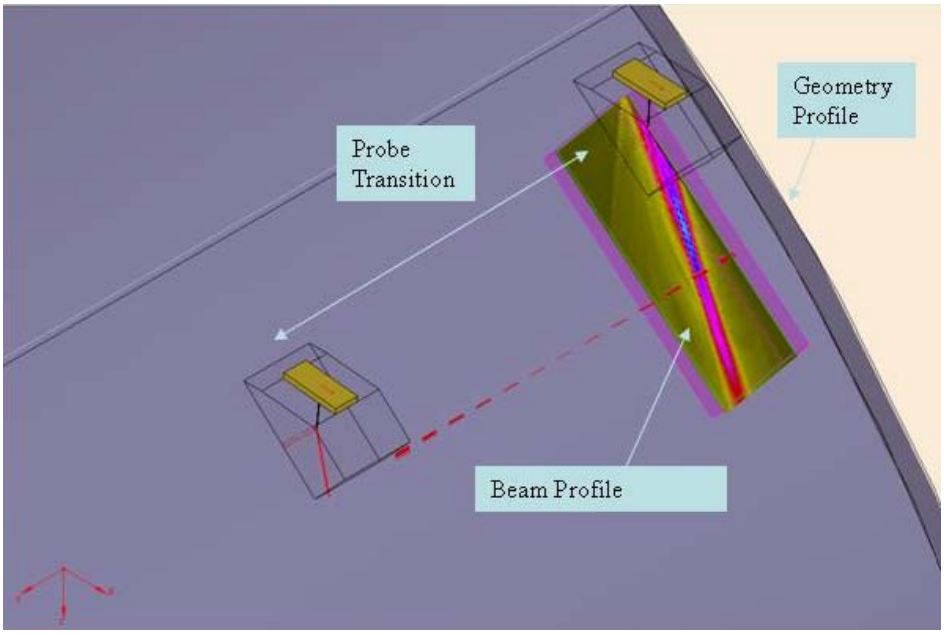

Figure 1.5.2-22. Typical Toe Crack Interaction Setup

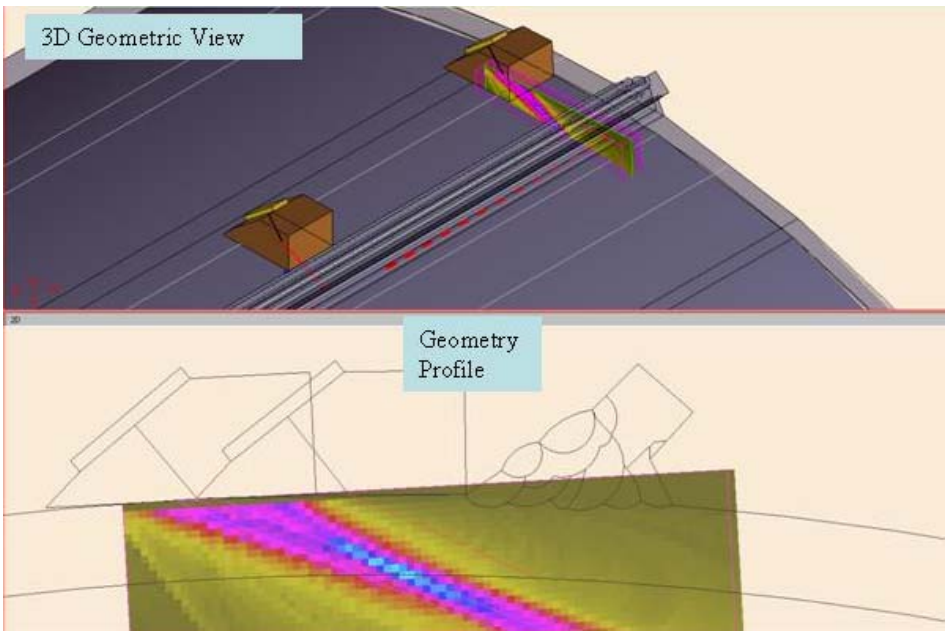

Figure 1.5.2-23. Typical Root Crack Interaction Setup

Modal Analysis of Flaw Signals

The modal analysis capture in Figure 1.5.2-24 shows the color coding of the different flaw interaction modes to analyze the source of the reflection, e.g., tip reflection or corner trap reflection. Note that sound paths of the different "modes" of the beam are color coded and illustrated on the right-hand side of this capture. Modal analysis essentially splits the beam flaw interaction into the different components of the beam. This provides greater insight into what exactly is happening when the beam hits the flaw. The various reflection components for this application are as follows:

- **Direct Reflection**, also denoted by 'Td_T', also read as: Transverse wave hitting the defect and coming back as a transverse wave. The color indication on the echodynamics and the B-scan is yellow.

- **Second Leg Reflection**, also denoted by:

    - 'TTd_T': Transverse (T) wave hitting the backwall, hitting the defect and coming back to the probe as T. The color indication on the echodynamics and the B-scan is orange.

    - 'TTd_TT': Transverse (T) wave hitting the backwall, hitting the defect as T, hitting the backwall again as T and coming back to the probe as T. The color indication on the echodynamics and the B-scan is pink.

- **Third Leg Reflection**, denoted by:

    - 'TTTd_TT': Transverse (T) wave hitting the backwall, hitting the front wall as T, hitting the defect, then hitting the backwall as T and returning to the probe as T. The color indication on the echodynamics and the B-scan is cream.

    - 'TTTd_TTT': Transverse (T) wave hitting the backwall, hitting the frontwall as T, hitting the defect as T, bouncing back to the front wall as T, hitting the backwall as T, and returning to the probe as T. The color indication on the echodynamics and B-scan is given as brown.

Mode conversions from transverse (T) to longitudinal (L) were not found in the simulations performed and, therefore, are not addressed in this report.

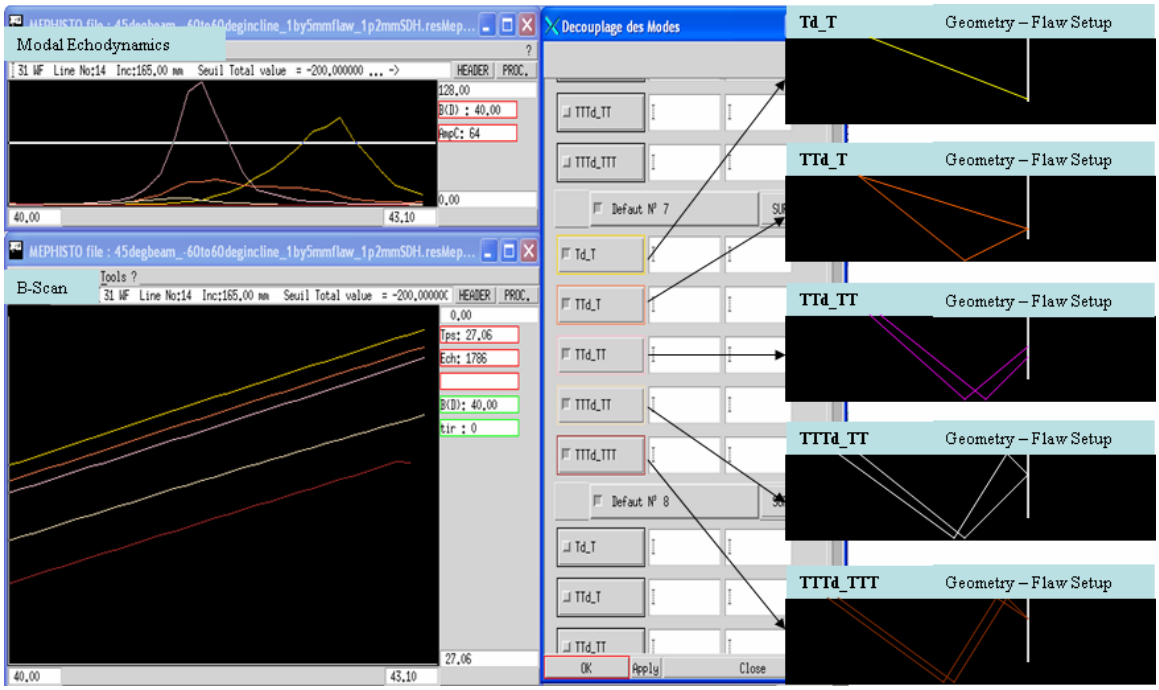

Figure 1.5.2-24. **Modal Analysis Capture – Shows the Color Coding of the Different Flaw Interaction Modes to Analyze the Source of the Reflection, e.g., Tip Reflection or Corner Trap Reflection.** (Sound paths are illustrated on the right-hand side.)

<u>Geometry 7 Interactions:</u>

Figures 1.5.2-25 to 1.5.2-27 show the interaction captures for the saddle position of Geometry 7. The plots on the left are for the toe crack interaction and the ones on the right are the root crack interaction. The responses show the echodynamic, B-scan, and C-scan from the top to bottom in that order. The root crack did not show up at 45- and 55-degree beam angle because the probe travel was stopped by the weld. However, the root crack was clearly detectable at 65 degrees. For the toe crack, the response showed very vaguely at the 45-degree angle, but was clearly detected at angles of 55 and 65 degrees.

Figure 1.5.2-28 shows the dB plot of the amplitude response with respect to a 1.2-mm SDH as the 0-dB reference. The plot on the left is for the toe crack and the one on the right is for the root crack. The signal responses can be characterized for each of the cracks as follows:

Toe Crack at the Saddle Position

- Flaw tilt of -60 to +60 degrees
- 45-degree beam showed a net 16-dB drop in amplitude. It appeared that there was a loss of signal from the flaw and the beam did not adequately reach it at higher positive tilt angles of the flaw
- Flaw tilt of 0 to ±30 degrees
- 55-degree beam showed a rise of about 6 dB
- 65-degree beam showed a rise of about 12 dB
- Flaw tilt of ±30 degree to ±60 degree
- 45-degree beam showed 8-dB fall in amplitude
- 55-degree beam showed 18-dB fall in amplitude
- 65-degree beam showed 22-dB fall in amplitude.

Root Crack at the Saddle Position

- Flaw tilt of -60 to +10 degrees
- 45-degree beam showed no response
- 55-degree beam showed no response
- 65-degree beam showed 35-dB rise in amplitude.
- Flaw tilt of +10 to +60 degree
- 45-degree beam showed no response
- 55-degree beam showed response at +50- and +60-degree inclinations of the flaw; however, the response was very weak
- 65-degree beam showed 30-dB fall in amplitude.

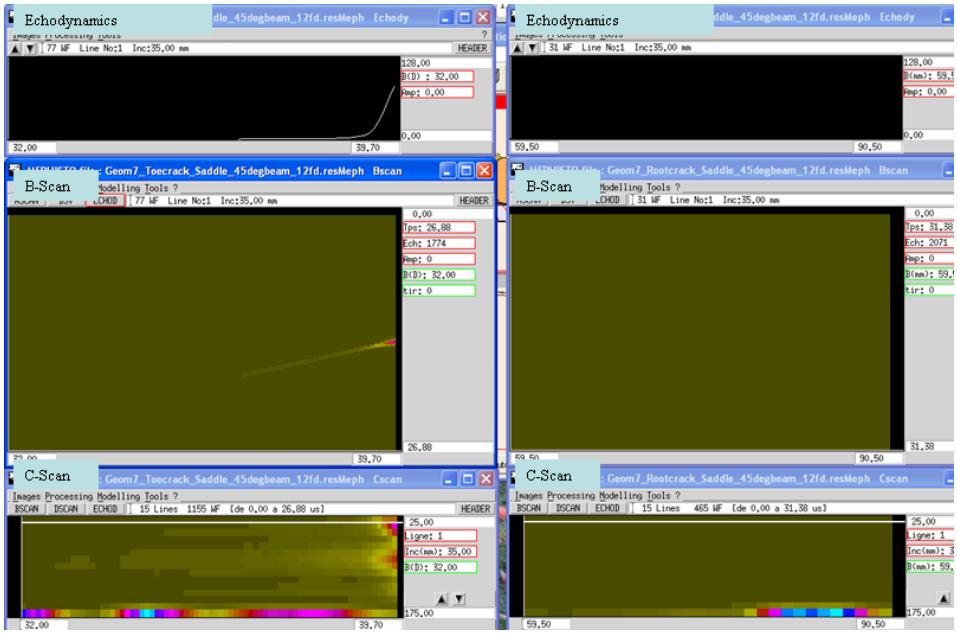

Figure 1.5.2-25. **Interaction Calculations Capture – 1-mm Crack Height at Saddle Position, 45-Degree Beam (Toe Crack – Left, Root Crack – Right) – Geometry 7**

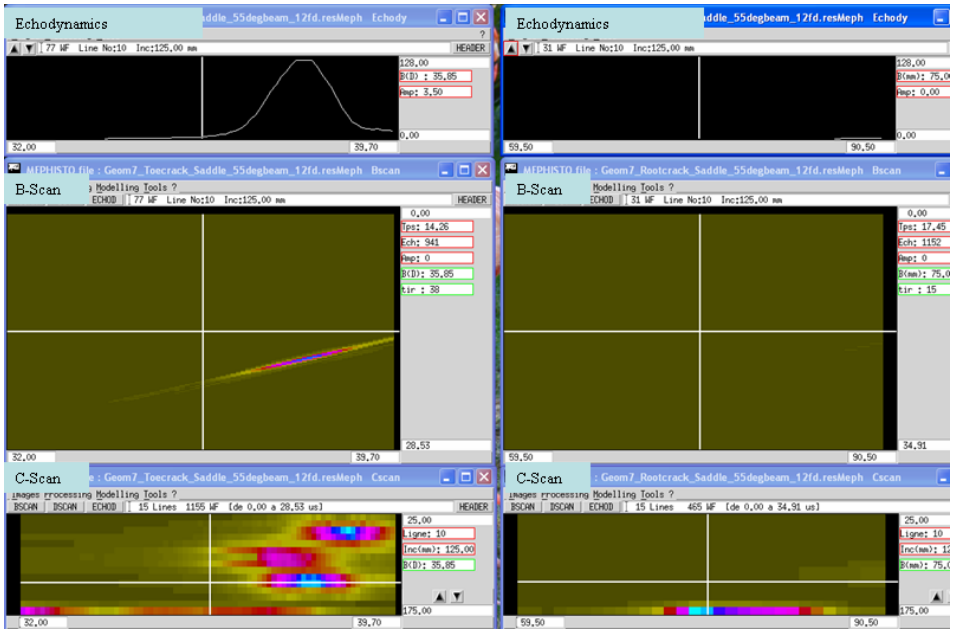

Figure 1.5.2-26. **Interaction Calculations Capture – 1-mm Crack Height at Saddle Position, 55-Degree Beam (Toe Crack – Left, Root Crack – Right) – Geometry 7**

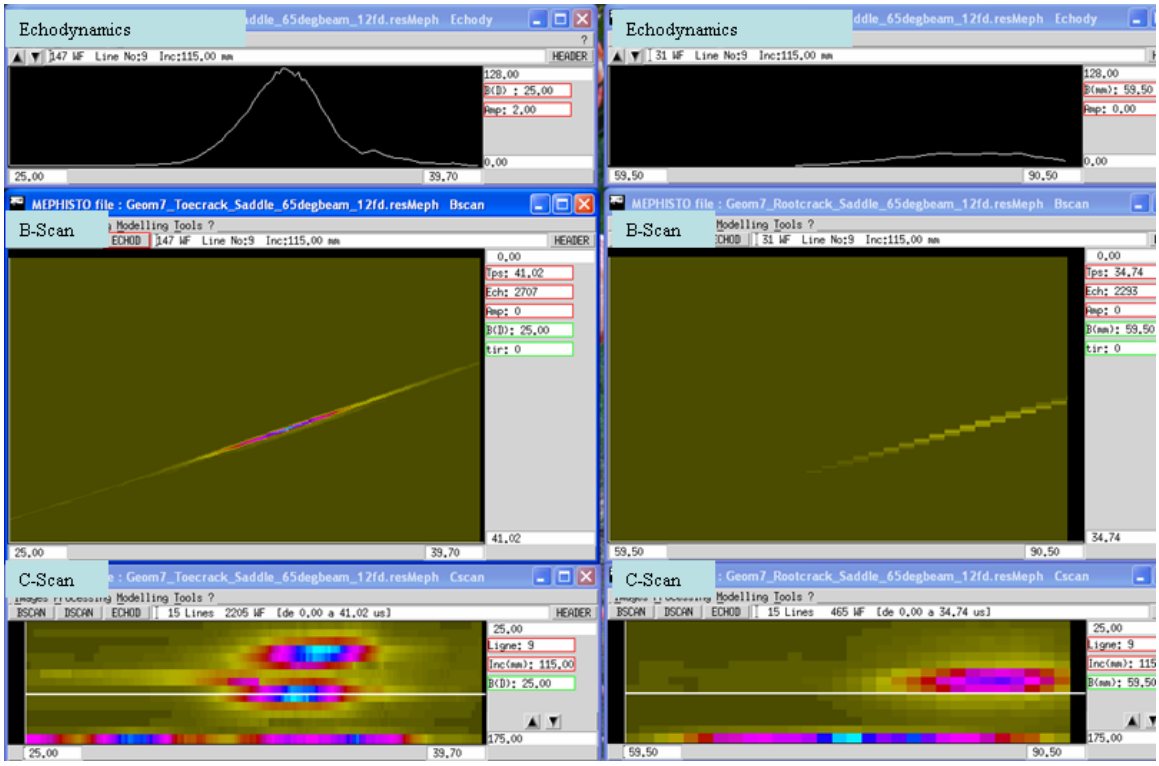

Figure 1.5.2-27. **Interaction Calculations Capture – 1-mm Crack Height at Saddle Position, 65-Degree Beam (Toe Crack – Left, Root Crack – Right) – Geometry 7**

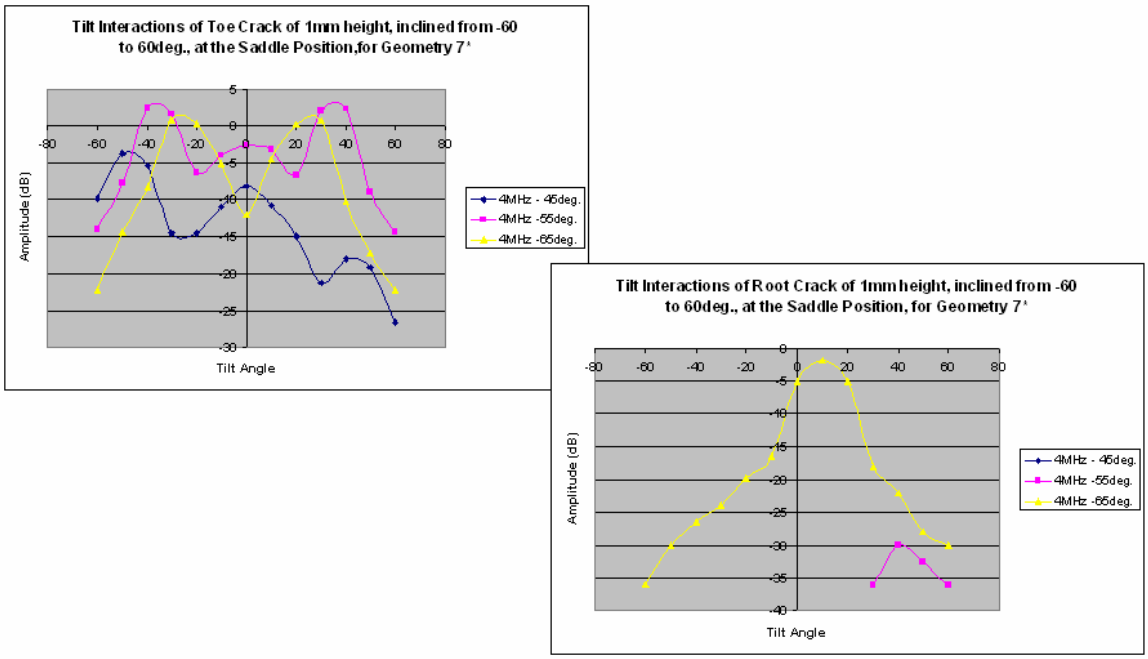

Figure 1.5.2-28. (dB) Interaction Calculations Plot – 1-mm Crack Height at Saddle Position, 45-, 55-, and 65-Degree Beam (Toe Crack – Left, Root Crack – Right) – Geometry 7

Figures 1.5.2-29 to 1.5.2-31 show the interaction captures for the crotch position of Geometry 7. The plots on the left are for the toe crack interaction and those on the right are for the root crack interaction. The response from the root crack was non-existent at the 45-degree angle. There was a slight response at 55 degrees and a full-echodynamic response at 65 degrees. The toe crack was barely detectable at 45 degrees. However, there was a full-echodynamic response at 55 and 65 degrees.

Figure 1.5.2-32 shows the dB plot of the amplitude response with respect to the 1.2-mm SDH as the 0-dB reference. The plot on the left is for the toe crack and the one on the right is for the root crack. The responses can be characterized for each of the cracks as follows:

Toe Crack at the Crotch Position

- Flaw tilt of -60 to +60 degrees
- 45-degree beam showed a net 20-dB drop in amplitude
- Flaw tilt of 0 to ±30 degrees
- 55-degree beam showed a rise of about 10 dB
- 65-degree beam showed a rise of about 12 dB
- Flaw tilt of ±30 degrees to ±60 degrees
- 55-degree beam showed 15-dB fall in amplitude
- 65-degree beam showed 25-dB fall in amplitude.

Root Crack at the Crotch Position

- Flaw tilt of -60 to +30 degrees
- 45-degree beam showed no response.
- 55-degree beam showed 32-dB rise in amplitude
- 65-degree beam showed 34-dB rise in amplitude
- Flaw tilt of +30 to +60 degrees
- 45-degree beam showed no response
- 55-degree beam showed 20-dB fall in amplitude
- 65-degree beam showed 25-dB fall in amplitude.

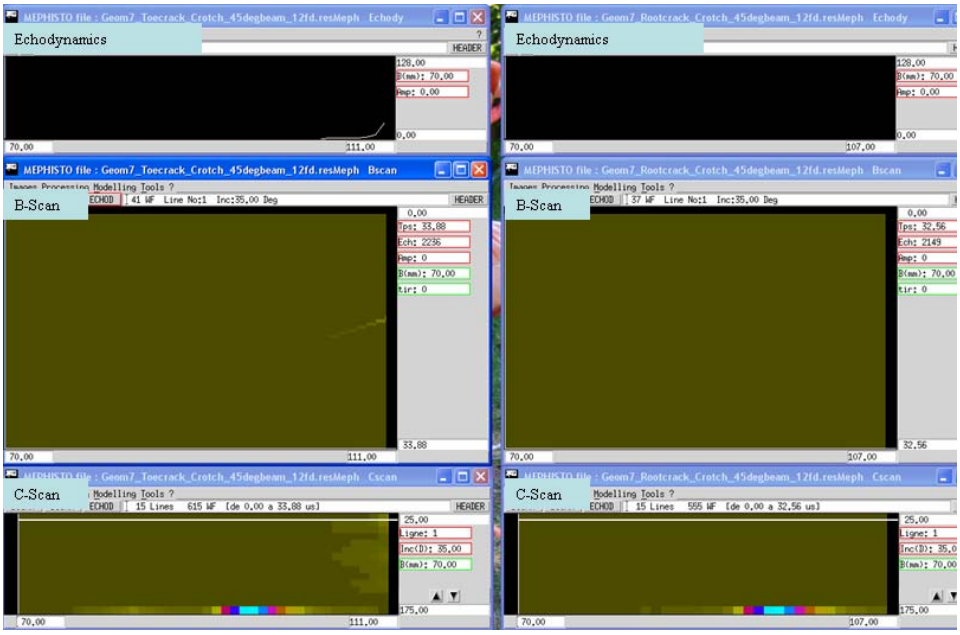

Figure 1.5.2-29. **Interaction Calculations Capture – 1-mm Crack Height at Crotch Position, 45-Degree Beam (Toe Crack – Left, Root Crack – Right) – Geometry 7**

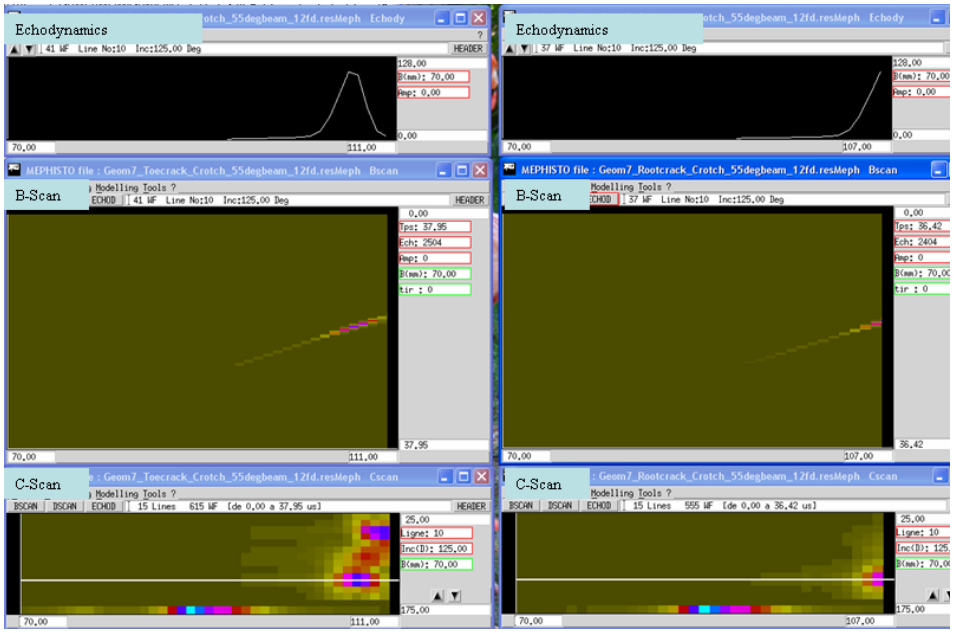

Figure 1.5.2-30. **Interaction Calculations Capture – 1-mm Crack Height at Crotch Position, 55-Degree Beam (Toe Crack – Left, Root Crack – Right) – Geometry 7**

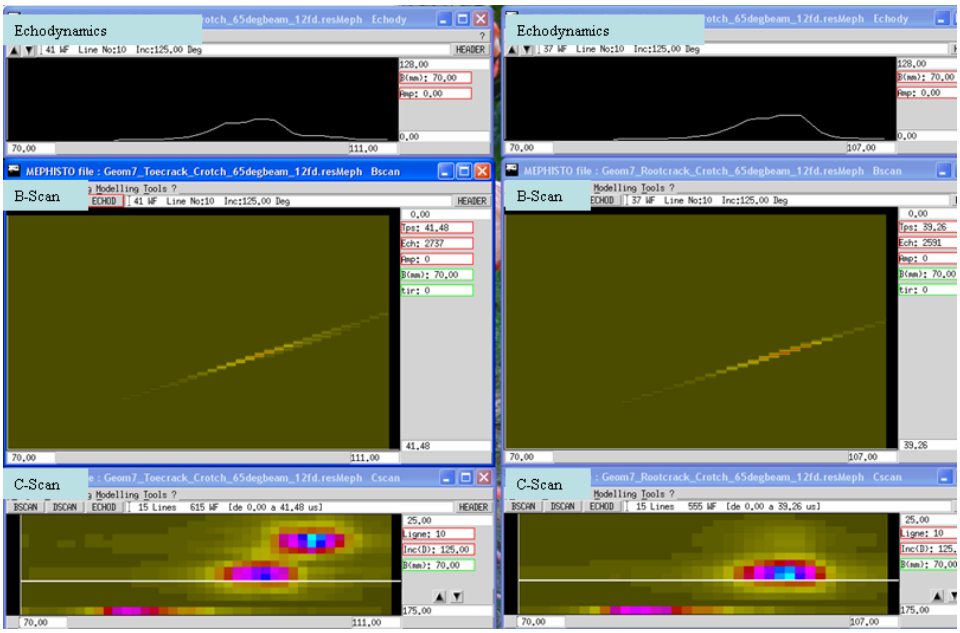

Figure 1.5.2-31. **Interaction Calculations Capture – 1-mm Crack Height at Crotch Position, 65-Degree Beam (Toe Crack – Left, Root Crack – Right) – Geometry 7**

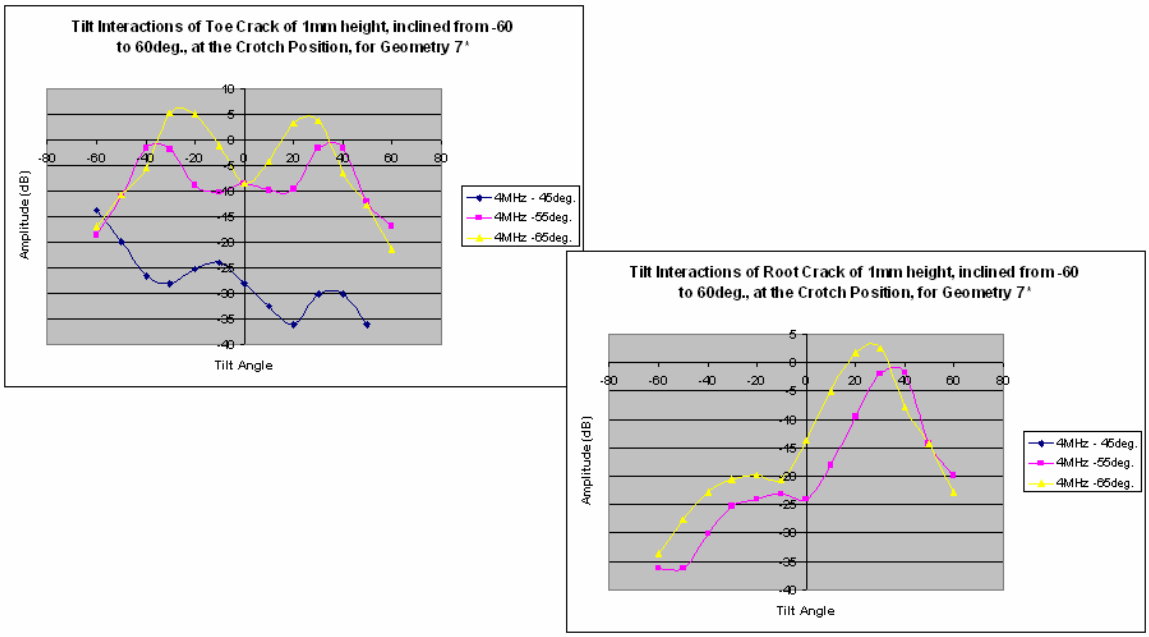

Figure 1.5.2-32. **(dB) Interaction Calculations Plot – 1-mm Crack Height at Crotch Position, 45-, 55-, and 65-Degree Beam (Toe Crack – Left, Root Crack – Right) – Geometry 7**

Figures 1.5.2-33 to 1.5.2-35 show the interaction captures for the 141-degree cross section position of Geometry 7. The plots on the left are for the toe crack interactions and those on the right are for root crack interactions. The response from the root crack was non-existent at the 45-degree angle. There was a slight response at the 55-degree angle and a full-echodynamic response at the 65-degree angle.

Figure 1.5.2-36 shows the dB plot of the amplitude response with respect to the 1.2-mm SDH as the 0-dB reference. The plot on the left is for the toe crack and the one on the right is for the root crack. The responses can be characterized for each of the cracks as follows:

<u>Toe Crack at the 141-Degree Position</u>

- Flaw tilt of -60 to +60 degrees
- 45-degree beam showed a net 20-dB drop in amplitude
- Flaw tilt of -20 to 0 degrees
- 55-degree beam showed a rise of about 5 dB
- 65-degree beam showed a drop of 6 dB
- Flaw tilt of 0 to +20 degree
- 55-degree beam showed a drop of 5 dB
- 65-degree beam showed a drop of about 6 dB
- Flaw tilt of -20 degrees to -30 degrees
- 55-degree beam showed a 7-dB rise in amplitude
- 65-degree beam showed a 15-dB fall in amplitude
- Flaw tilt of -30 to -60 degrees
- 55-degree beam showed 17-dB fall in amplitude
- 65-degree beam showed 35-dB fall in amplitude followed by a sudden rise of 10 dB at about 10 degrees
- Flaw tilt of +30 to +60 degrees
- Both 55 and 65-degree beams showed a 15-dB fall in amplitude.

<u>Root Crack at the 141-Degree Position</u>

- Flaw tilt of -60 to + 30 degrees
- 45-degree beam showed only a slight response for the +50- and +60-degree beams
- 55-degree beam showed 25-dB rise in amplitude
- 65-degree beam showed 32-dB rise in amplitude
- Flaw tilt of +30 to +60 degrees
- 45-degree beam showed no response
- 55-degree beam showed 6-dB fall in amplitude
- 65-degree beam showed 17-dB fall in amplitude.

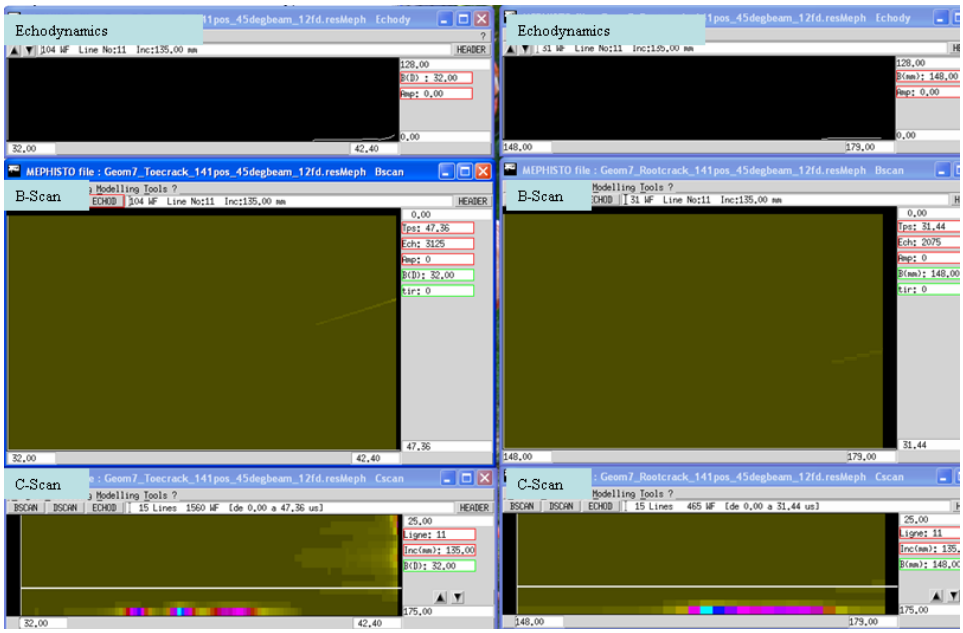

Figure 1.5.2-33. **Interaction Calculations Capture – 1-mm Crack Height at 141-Degree Position, 45-Degree Beam (Toe Crack – Left, Root Crack – Right) – Geometry 7**

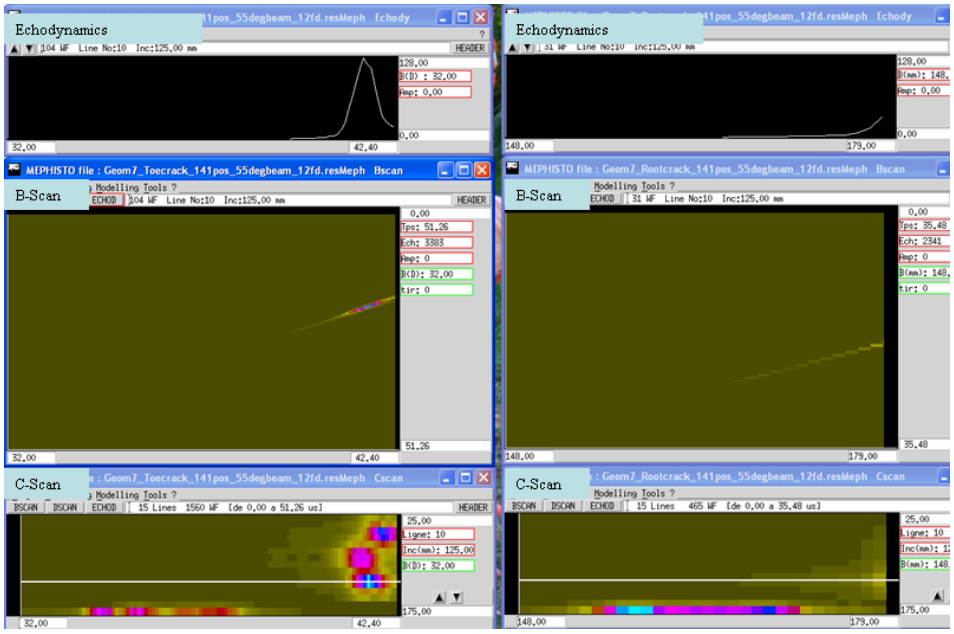

Figure 1.5.2-34. **Interaction Calculations Capture – 1-mm Crack Height at 141-Degree Position, 55-Degree Beam (Toe Crack – Left, Root Crack – Right) – Geometry 7**

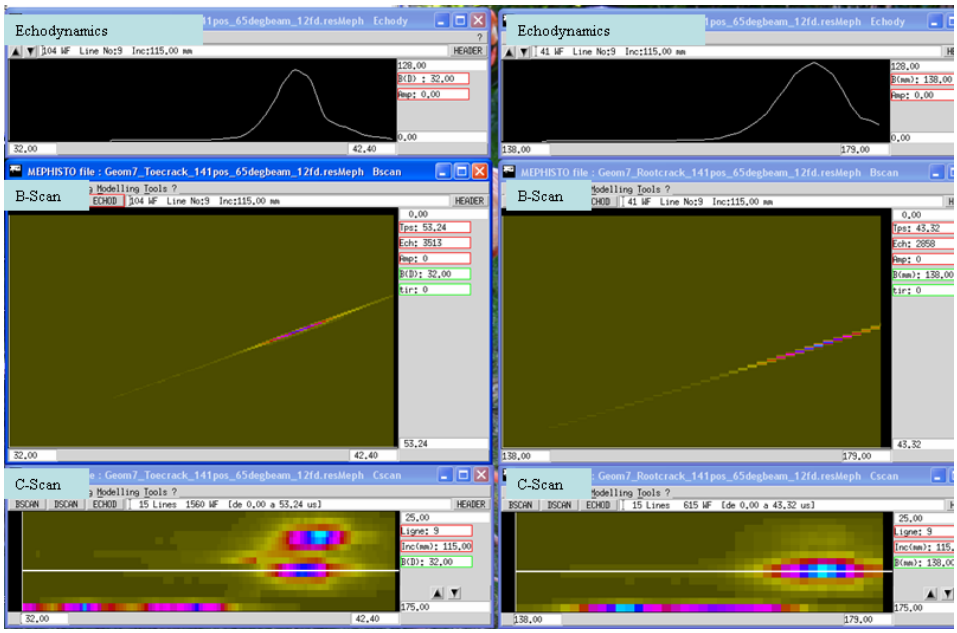

Figure 1.5.2-35. **Interaction Calculations Capture – 1-mm Crack Height at 141-Degree Position, 65-Degree Beam (Toe Crack – Left, Root Crack – Right) – Geometry 7**

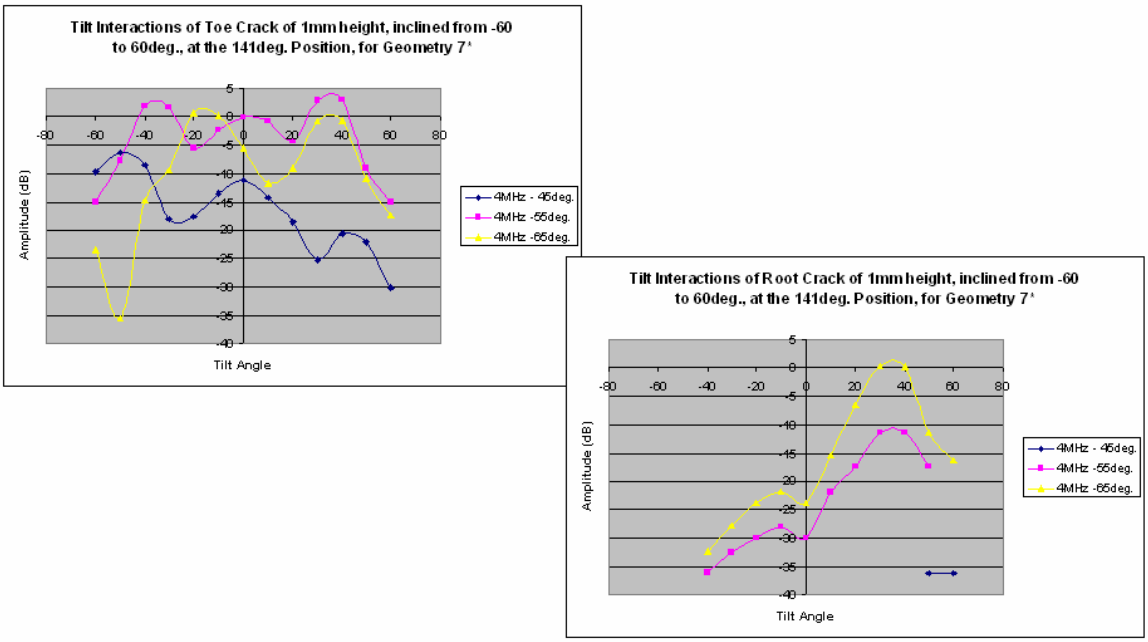

Figure 1.5.2-36. **(dB) Interaction Calculations Plot – 1-mm Crack Height at 141-Degree Position, 45-, 55-, and 65-Degree Beam (Toe Crack – Left, Root Crack – Right) – Geometry 7**

Geometry 7 Modal Analysis:

Modal analysis was done for one particular flaw case on Geometry 7 to analyze the different reflections which come from the beam to flaw interaction. The case chosen was a toe and root flaw at the saddle position having a height of 1 mm (0.04 in.). The analysis was performed at a beam angle of 65 degrees with amplitude comparisons made relative to a 1.2-mm (0.047-in.) SDH. All of the Figures 1.5.2-37 through 1.5.2-49 show the capture of the toe crack response: the modal echodynamics, B-scan and C-scan on the right with calculations for the echodynamics and B-scan of the modal analysis on the left.

Modal Analysis results in Figures 1.5.2-37 through 1.5.2-42 shows that for negative tilt angles, the corner trap was the dominant part of the reflected signal, with little or no reflection from the flaw face. Figure 1.5.2-43 and 1.5.2-44 shows a transition phase where flaws tilted at 0 and 10 degrees had a significant response from both the flaw face and the corner trap. Figures 1.5.2-45 to 1.5.2-49 shows that for positive tilt angles of +10 degree or greater, the flaw face signal was dominant with very little corner trap response.

Figures 1.5.2-50 through 1.5.2-54 illustrates the modal echodynamics for the same beam with the root crack response. Since the modeled root crack was not open to the ID or OD surface it did not have a corner trap for this particular geometry. Consequently, the reflected signal consisted only of flaw face reflections throughout the entire tilt range of -60 to +60 degree.

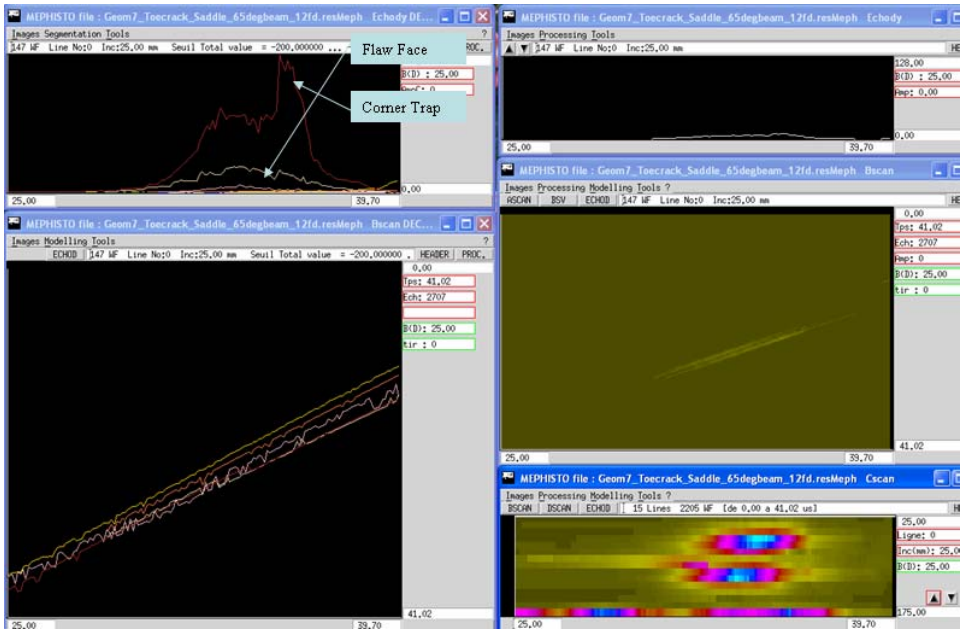

Figure 1.5.2-37. Modal Analysis – Toe Flaw on Saddle, 65-Degree Beam; -60-Degree Flaw Tilt – Geometry 7

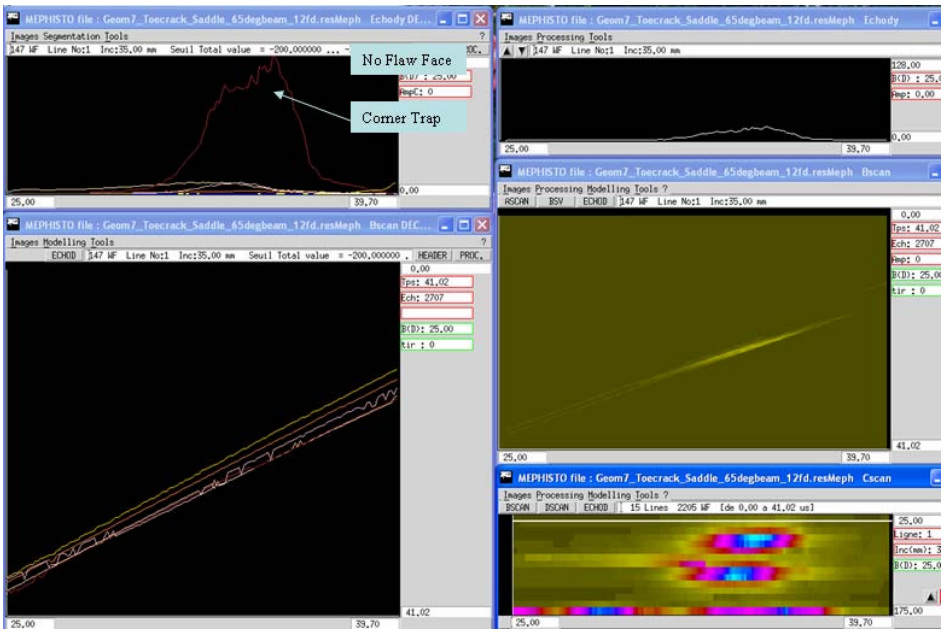

Figure 1.5.2-38. Modal Analysis – Toe Flaw on Saddle, 65-Degree Beam; -50-Degree Flaw Tilt – Geometry 7

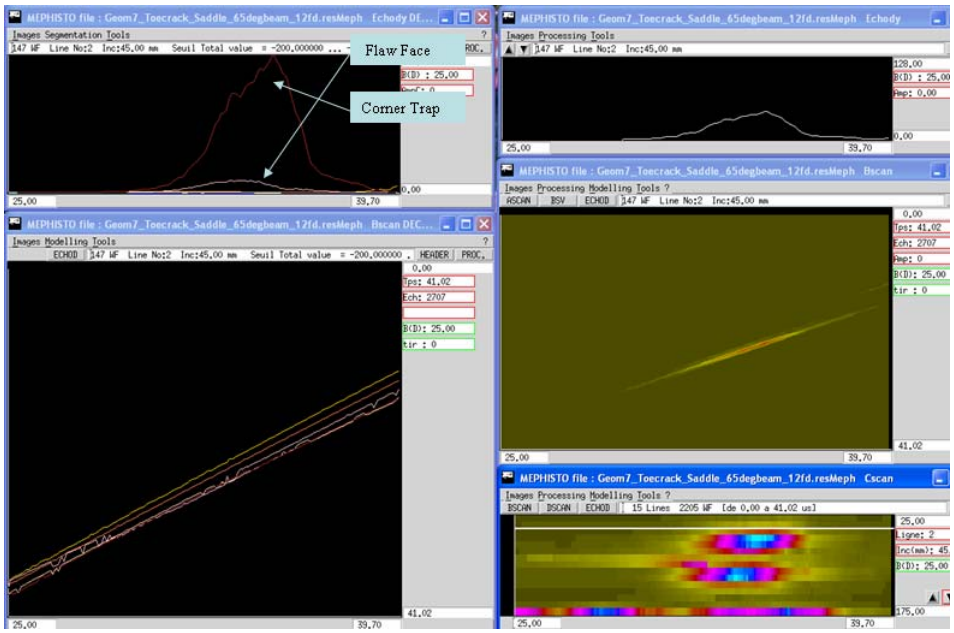

Figure 1.5.2-39. Modal Analysis – Toe Flaw on Saddle, 65-Degree Beam -40-Degree Flaw Tilt – Geometry 7

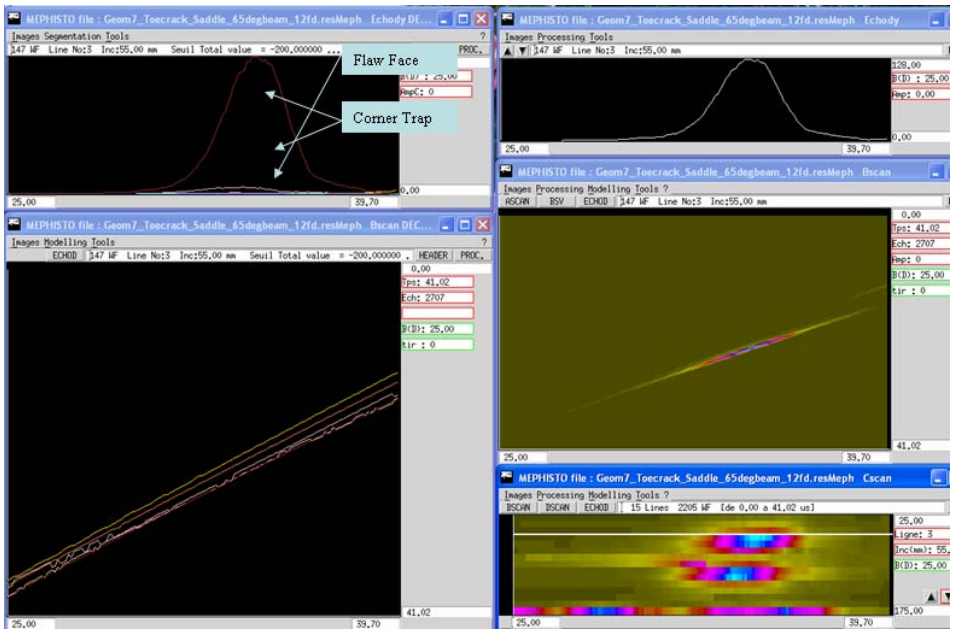

Figure 1.5.2-40. Modal Analysis – Toe Flaw on Saddle, 65-Degree Beam; -30-Degree Flaw Tilt – Geometry 7

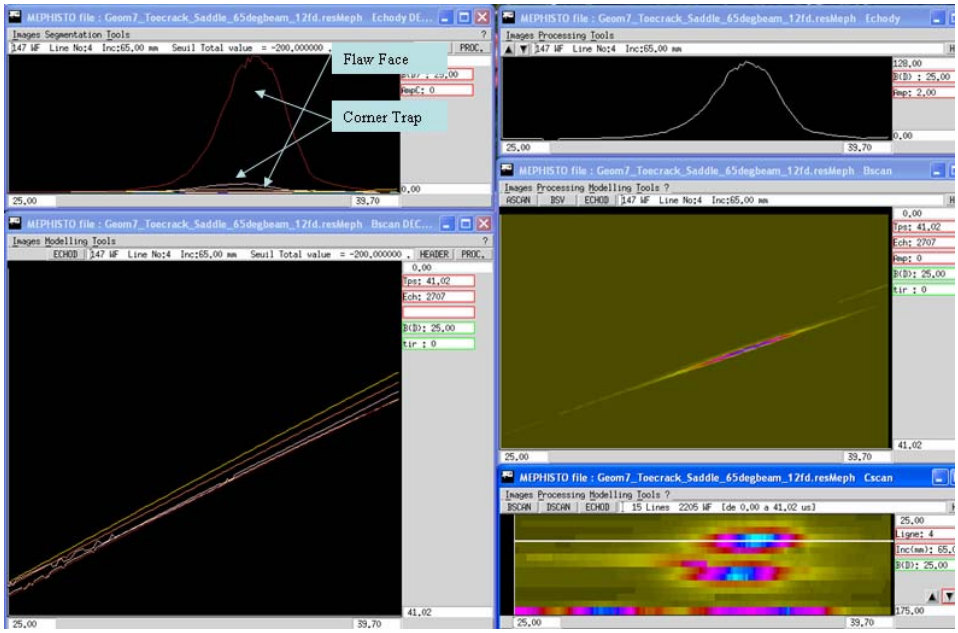

Figure 1.5.2-41. Modal Analysis – Toe Flaw on Saddle, 65-Degree Beam; -20-Degree Flaw Tilt – Geometry 7

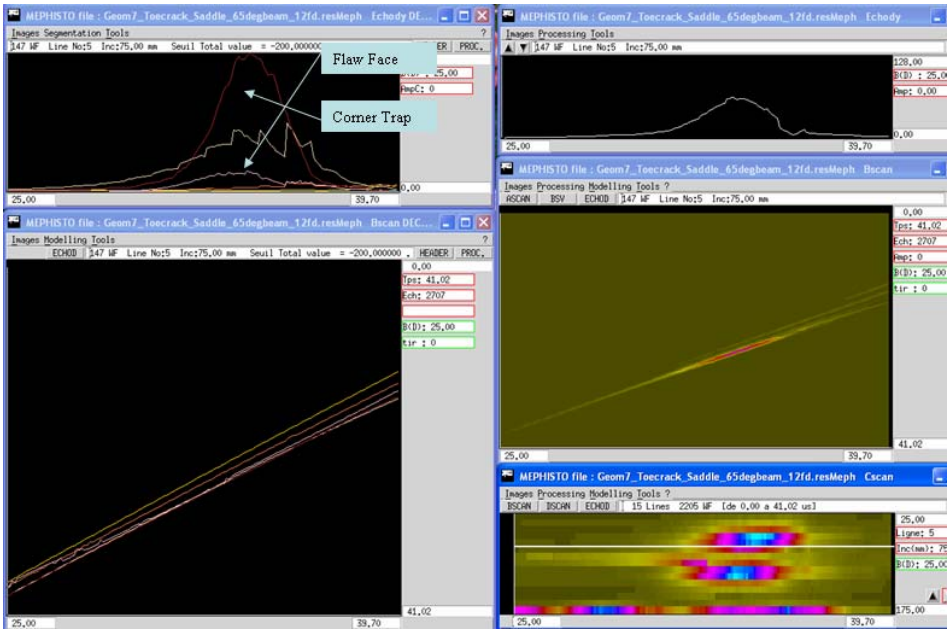

Figure 1.5.2-42. Modal Analysis – Toe Flaw on Saddle, 65-Degree Beam; -10-Degree Flaw Tilt – Geometry 7

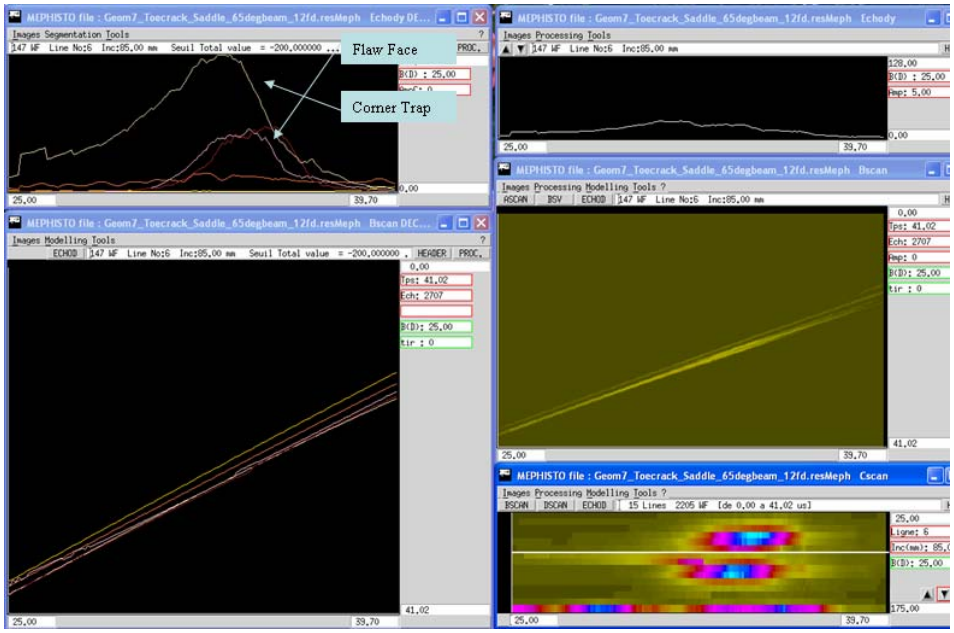

Figure 1.5.2-43. Modal Analysis – Toe Flaw on Saddle, 65-Degree Beam; 0-Degree Flaw Tilt – Geometry 7

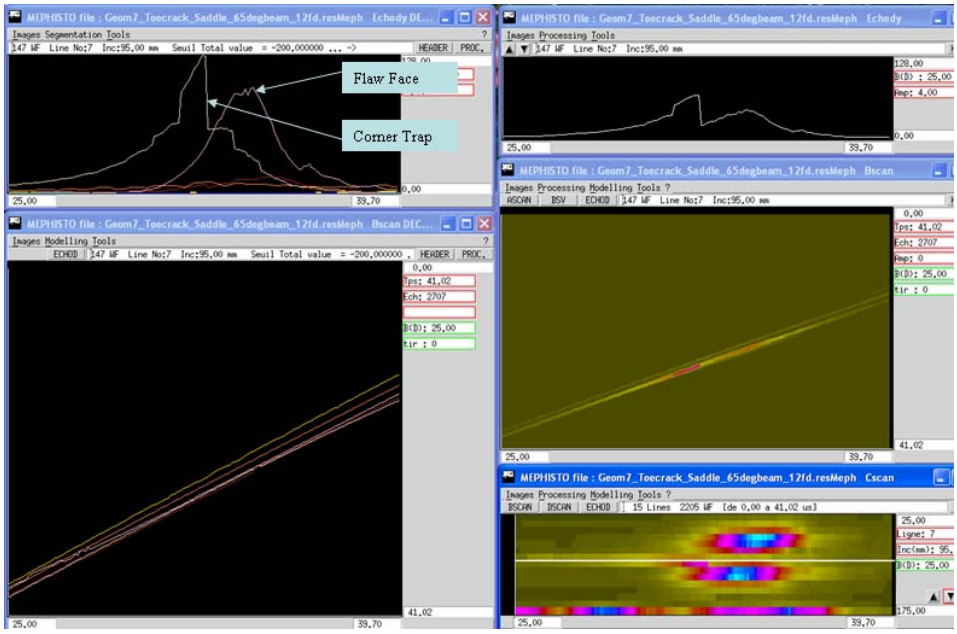

Figure 1.5.2-44. Modal Analysis – Toe Flaw on Saddle, 65-Degree Beam; 10-Degree Flaw Tilt – Geometry 7

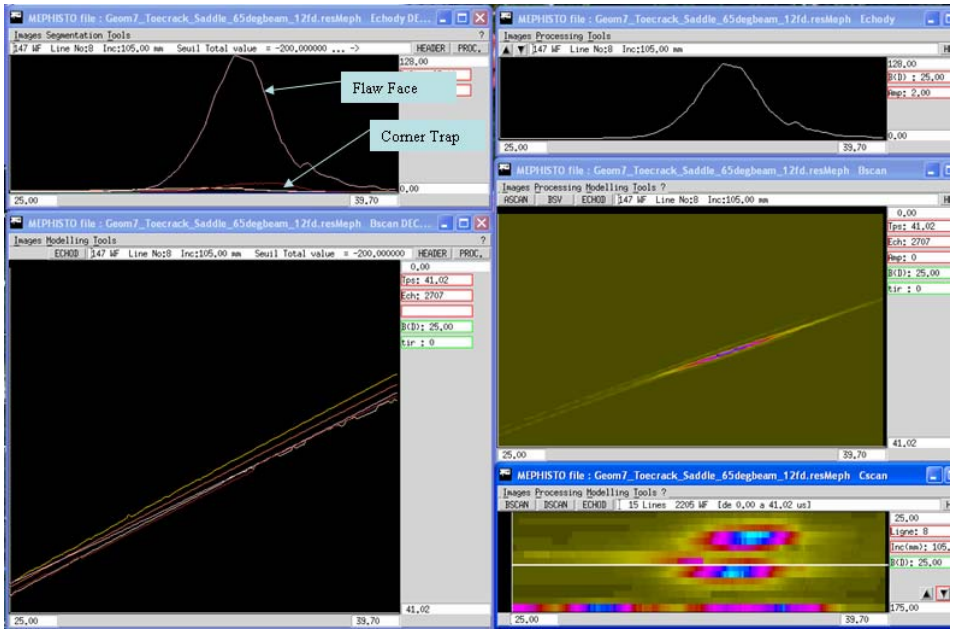

Figure 1.5.2-45. Modal Analysis – Toe Flaw on Saddle, 65-Degree Beam; 20-Degree Flaw Tilt – Geometry 7

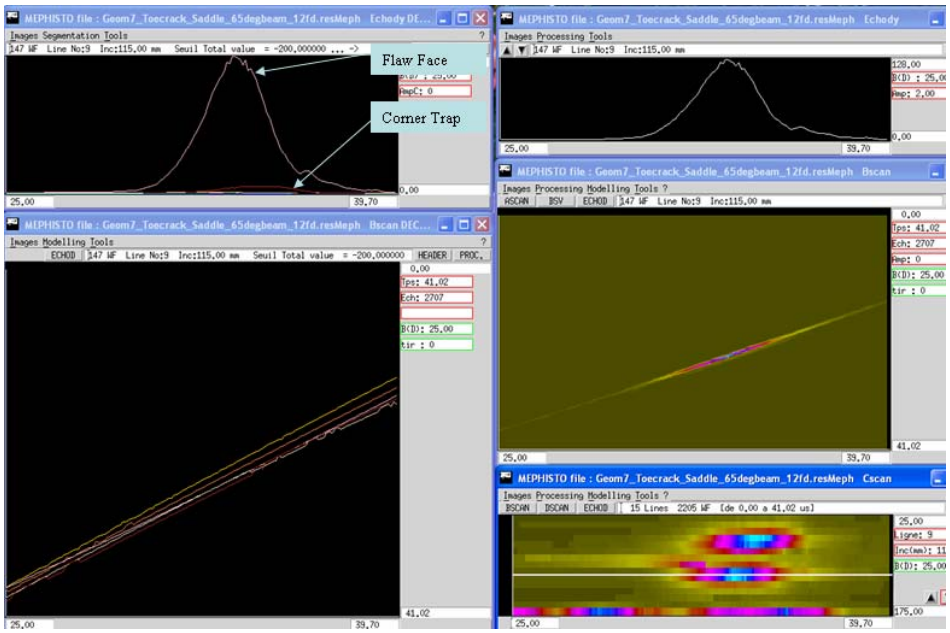

Figure 1.5.2-46. Modal Analysis – Toe Flaw on Saddle, 65-Degree Beam; 30-Degree Flaw Tilt – Geometry 7

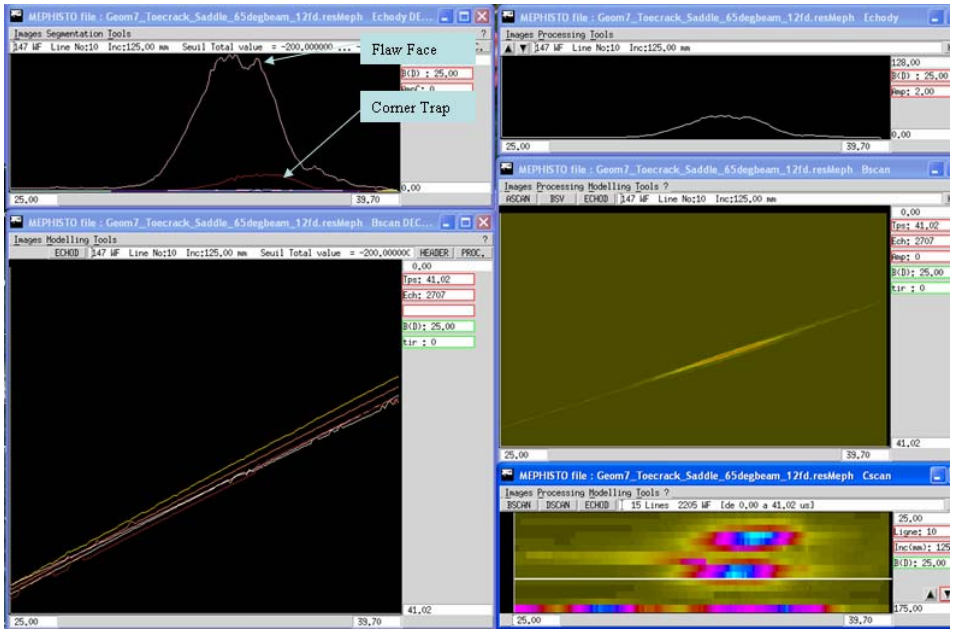

Figure 1.5.2-47. Modal Analysis – Toe Flaw on Saddle, 65-Degree Beam; 40-Degree Flaw Tilt – Geometry 7

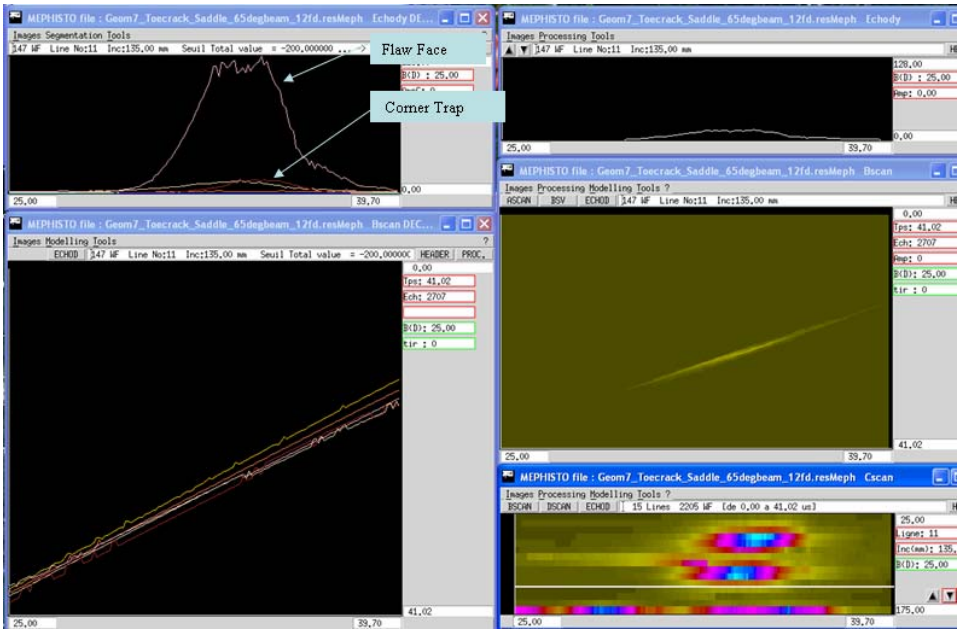

Figure 1.5.2-48. Modal Analysis – Toe Flaw on Saddle, 65-Degree Beam; 50-Degree Flaw Tilt – Geometry 7

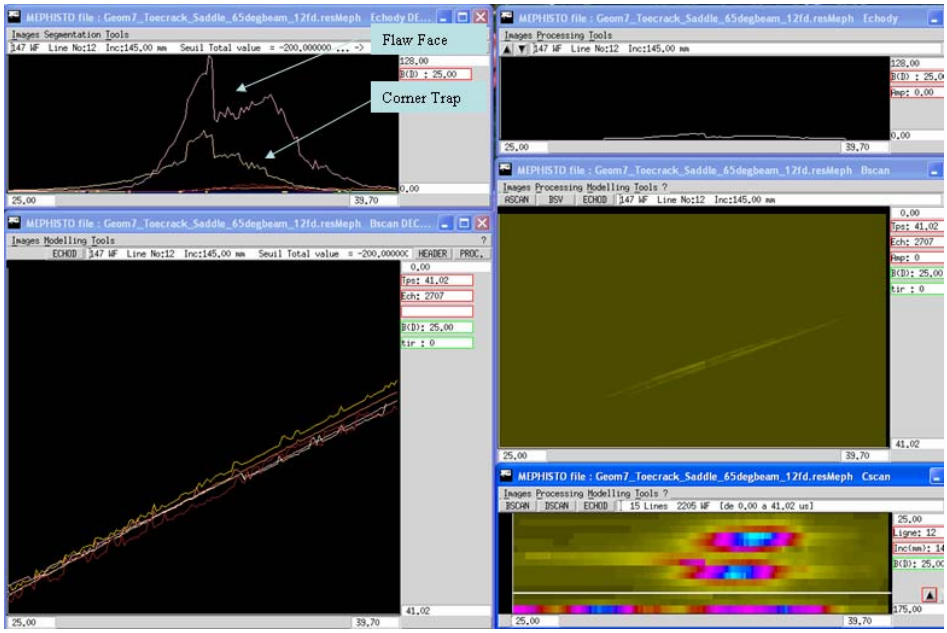

Figure 1.5.2-49. Modal Analysis – Toe Flaw on Saddle, 65-Degree Beam; 60-Degree Flaw Tilt – Geometry 7

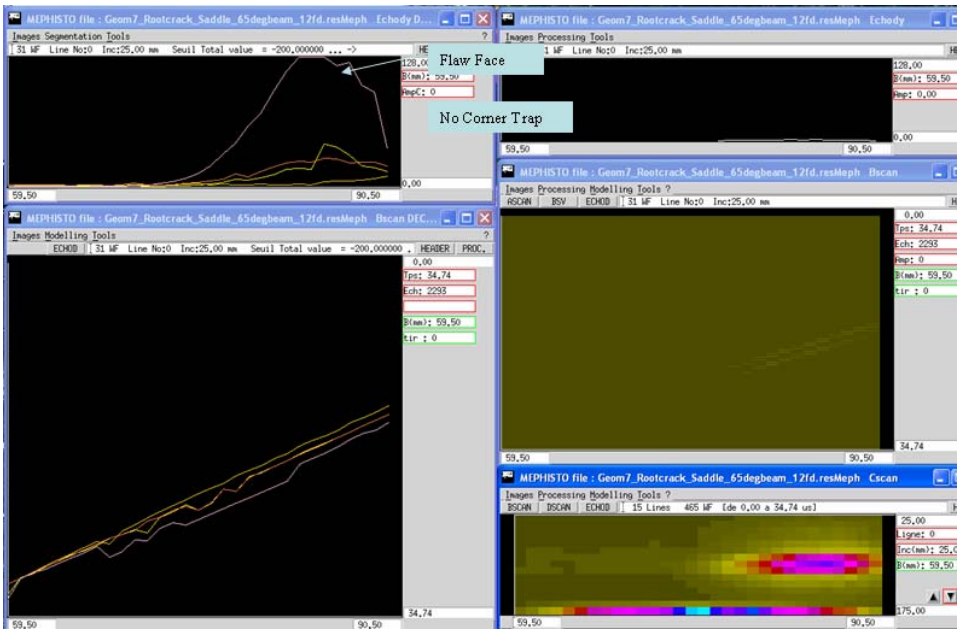

Figure 1.5.2-50. Modal Analysis – Root Flaw on Saddle, 65-Degree Beam; -60-Degree Flaw Tilt – Geometry 7

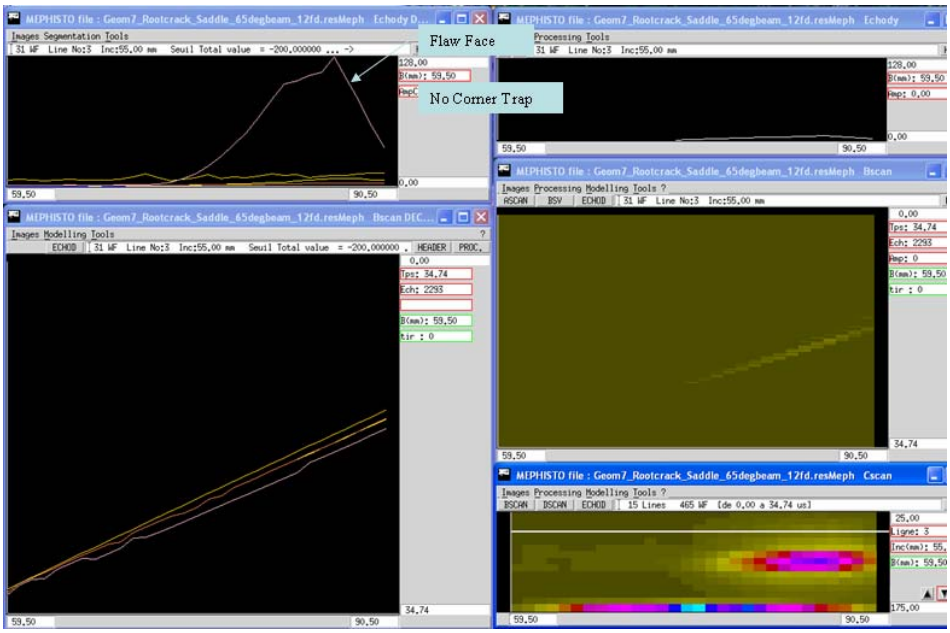

Figure 1.5.2-51. Modal Analysis – Root Flaw on Saddle, 65-Degree Beam; -30-Degree Flaw Tilt – Geometry 7

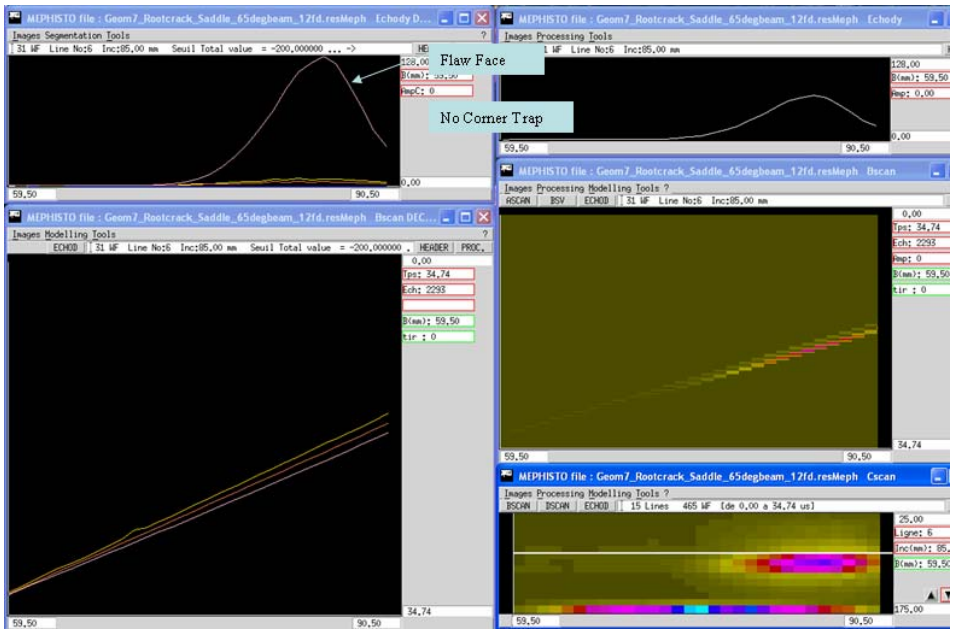

Figure 1.5.2-52. Modal Analysis – Root Flaw on Saddle, 65-Degree Beam; 0-Degree Flaw Tilt – Geometry 7

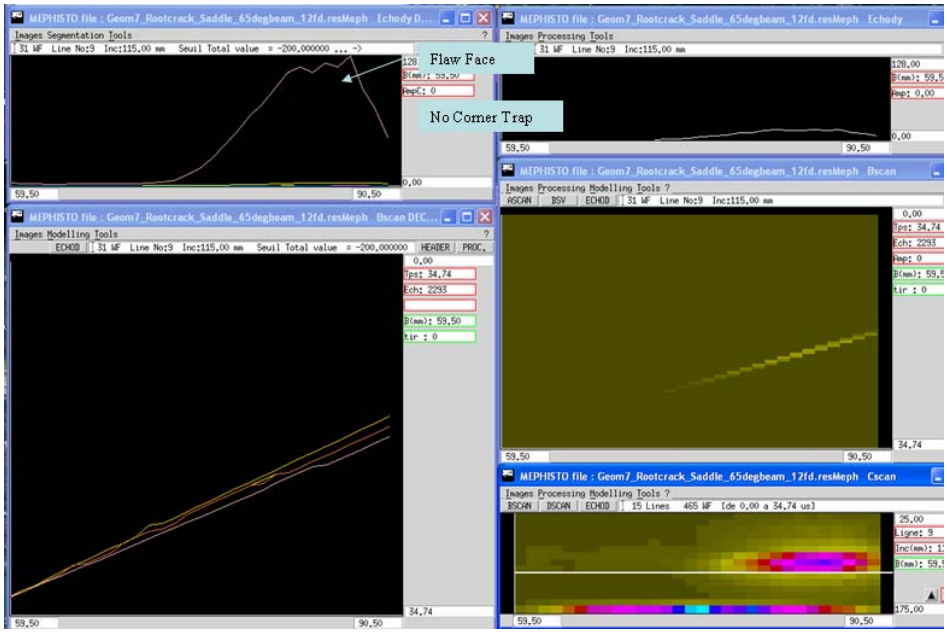

Figure 1.5.2-53. Modal Analysis – Root Flaw on Saddle, 65-Degree Beam; 30-Degree Flaw Tilt – Geometry 7

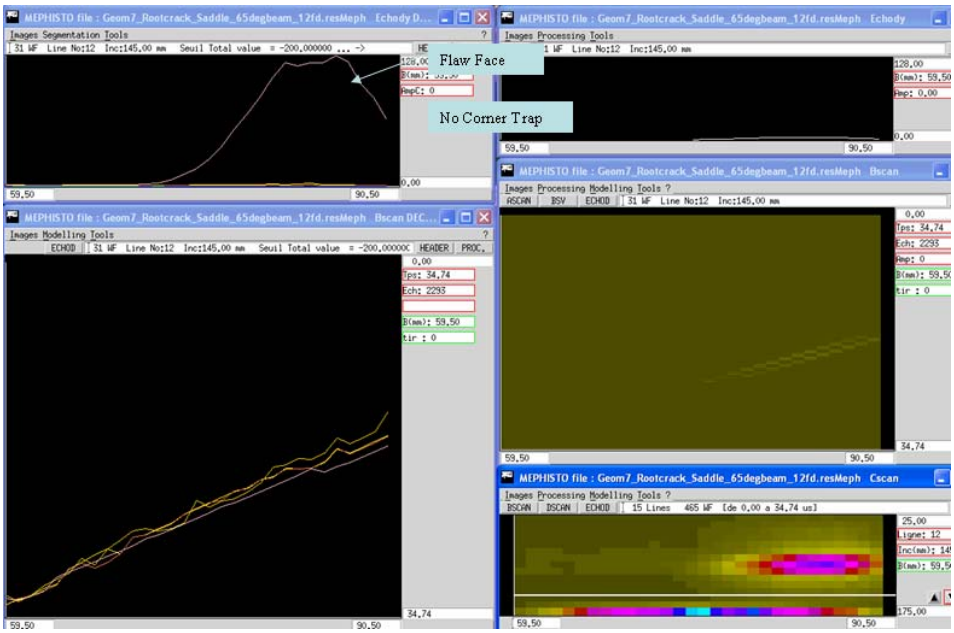

Figure 1.5.2-54. Modal Analysis – Root Flaw on Saddle, 65-Degree Beam; 60-Degree Flaw Tilt – Geometry 7

Geometry 8 Interactions:

Figures 1.5.2-55, 1.5.2-56, and 1.5.2-57 show the interaction captures for the saddle position of Geometry 8. The plots on the left in the figures show the toe crack interaction and the ones on the right show the root crack interaction. The responses show the echodynamic, B-scan and C-scan from the top to bottom in that order. The root crack did not show up at the 45-degree beam angle and showed up only slightly at the 55-degree beam angle. It was only at an angle of 65 degree that the response began to show up clearly. However, for the toe crack, the response was available at all of the angles.

Figure 1.5.2-58 shows the dB plot of the amplitude response with respect to the 1.2-mm SDH as the 0-dB reference. The plot on the left is for the toe crack and the one on the right is for the root crack. The responses can be characterized for each of the cracks as follows:

Toe Crack at the Saddle Position

- Flaw tilt of 0 to ±30 degree
- 45- and 55-degree beams showed a drop in amplitude of the crack of about 6 dB
- 65-degree beam showed a rise in amplitude of about 15 dB
- Flaw tilt of ±30 degrees to ±60 degrees
- 45-degree beam showed a 6-dB rise in amplitude followed by a 12-dB fall
- 55-degree beam showed a 15-dB fall in amplitude steadily from this point
- 65-degree beam showed a rapid 30-dB fall in amplitude over this range of positive tilt and 25-dB fall with negative tilt
- Toe crack at the saddle position having no corner trap response
- The calculation was done only for the 65-degree beam in order to compare it with the corner trap response. This calculation is shown as the blue plot in Figure 1.5.2-58
- There is a 15-dB rise in the signal on the -60 to +20 degree inclination of the crack
- The +20- and +60-degree inclination part of the response followed a similar response when a corner trap was present. That is, the response showed a rapid 30-dB fall in the amplitude over the range of tilt.

Root Crack at the Saddle Position

- Flaw tilt of -60 to +20 degrees
- All beams showed a 32-dB rise in amplitude
- There was no response from the 45-degree beam as it did not reach the root crack because of probe contact with the weld
- Flaw tilt of +20 to +60 degree
- All the beams showed a 22-dB fall in amplitude
- There is no response from the 45-degree beam as it did not reach the root crack because of probe contact with the weld.

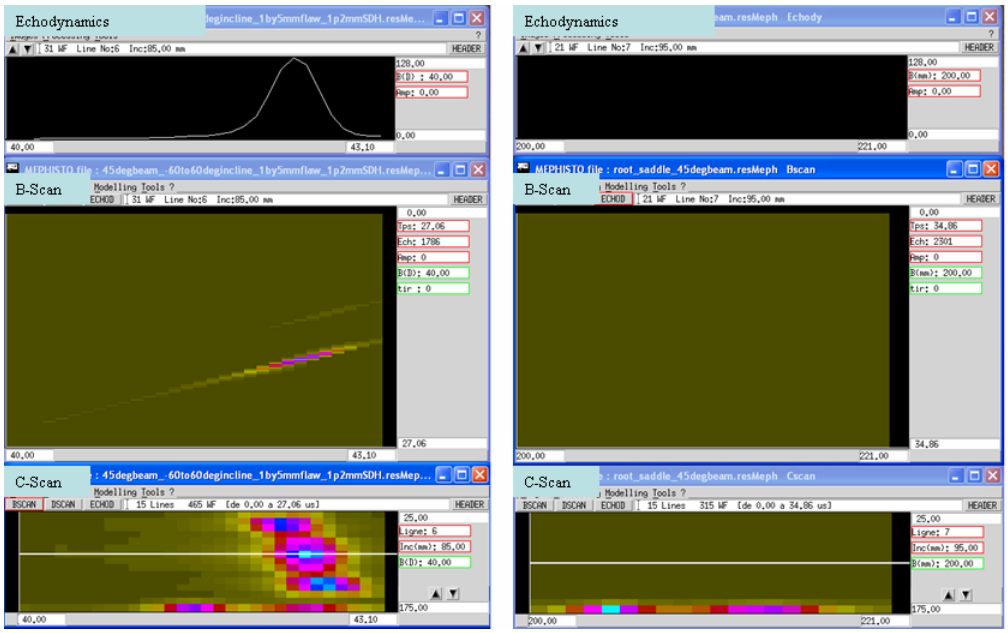

Figure 1.5.2-55. **Interaction Calculations Capture – 1-mm Crack Height at Saddle Position, 45-Degree Beam (Toe Crack – Left, Root Crack – Right) – Geometry 8**

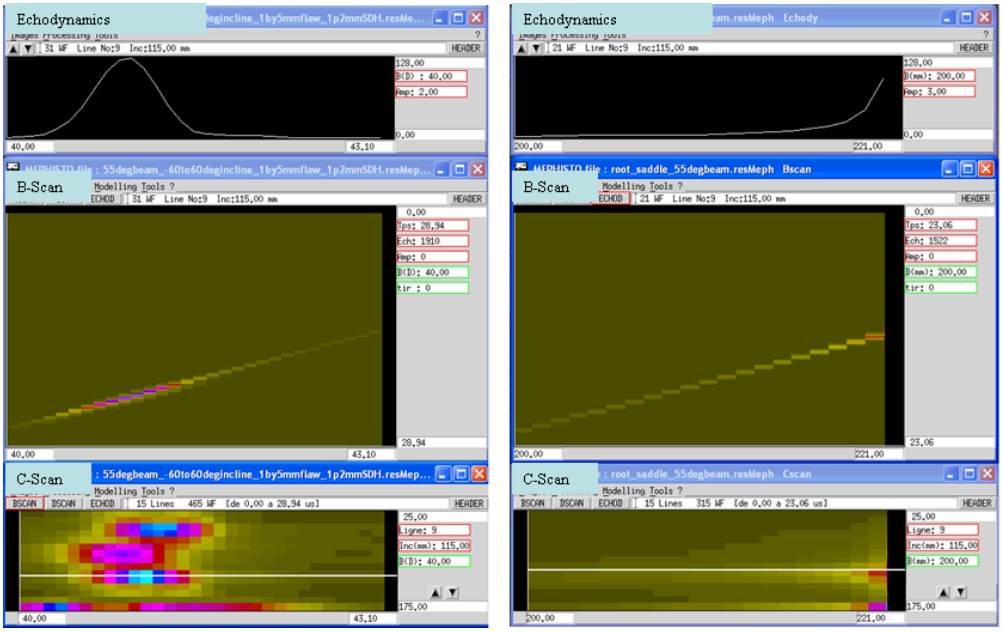

Figure 1.5.2-56. **Interaction Calculations Capture – 1-mm Crack Height at Saddle Position, 55-Degree Beam (Toe Crack – Left, Root Crack – Right) – Geometry 8**

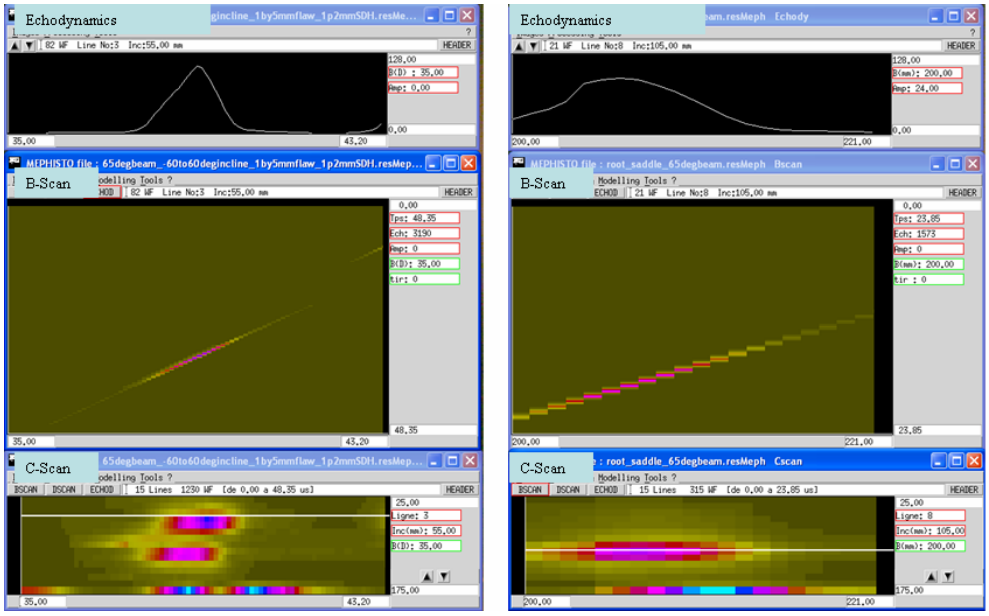

Figure 1.5.2-57. **Interaction Calculations Capture – 1-mm Crack Height at Saddle Position, 65-Degree Beam (Toe Crack – Left, Root Crack – Right) – Geometry 8**

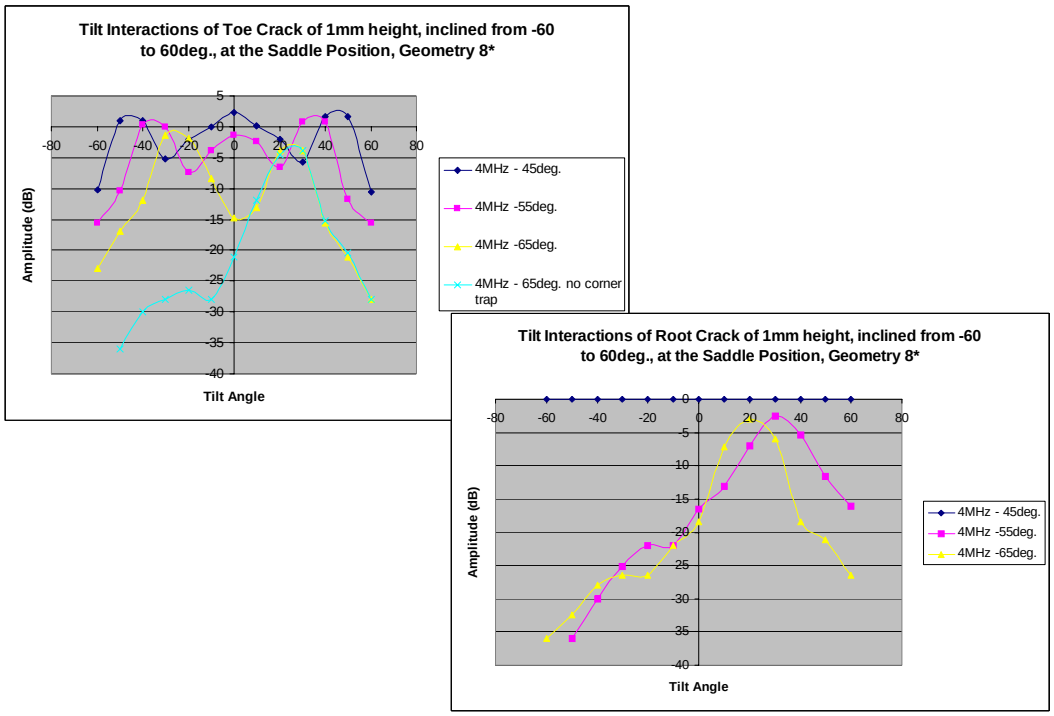

Figure 1.5.2-58. **(dB) Interaction Calculations Plot – 1-mm Crack Height at Saddle Position, 45-, 55-, and 65-Degree Beam (Toe Crack – Left, Root Crack – Right) – Geometry 8**

Figures 1.5.2-59, 1.5.2-60, and 1.5.2-61 show the interaction captures for the crotch position of Geometry 8. The plots on the left of the figure show the toe crack interaction and the ones on the right show the root crack interaction. The responses show the echodynamic, B-scan and C-scan from the top to bottom in that order. The root crack did not show up when using the 45-degree beam angle and showed up very slightly with the 55-degree beam angle. It was only at the 65-degree angle that the response began to show up clearly. However, for the toe crack, the response was available at all of the angles.

Figure 1.5.2-62 shows the dB plot of the amplitude response with respect to the 1.2-mm SDH as the 0-dB reference. The plot on the left is for the toe crack and the one on the right is for the root crack. The responses can be characterized for each of the cracks as follows:

<u>Toe Crack at the Crotch Position</u>

- Flaw tilt of 0 to ±20 degrees
- 45- and 55-degree beams showed a fall in amplitude of about 8 dB
- 65-degree beam showed a rise in amplitude of about 8 dB
- Flaw tilt of ±20 degrees to ±60 degrees
- 45-degree beam showed a 10-dB rise in amplitude followed by a 20-dB fall
- 55-degree beam showed a 10 dB rise in amplitude followed by a 15-dB fall
- 65-degree beam showed a rapid 25-dB fall in amplitude over this period.

<u>Root Crack at the Crotch Position</u>

- Flaw tilt of -60 to 0 degree
- No 45-degree beam response
- No 55-degree beam response for initial angles. This was followed by a 7-dB rise in amplitude at higher tilt angles
- 65-degree beam showed a similar 15-dB rise in amplitude followed by a slight fall of about 2 dB
- Flaw tilt of 0 to +30 degrees
- 20- to 22-dB rise in the amplitude in this range for the 55- and 65-degree beams
- Flaw tilt of +30 to +60 degrees
- 13-dB drop in the 55-degree beam response
- 25-dB drop in the 65-degree beam response.

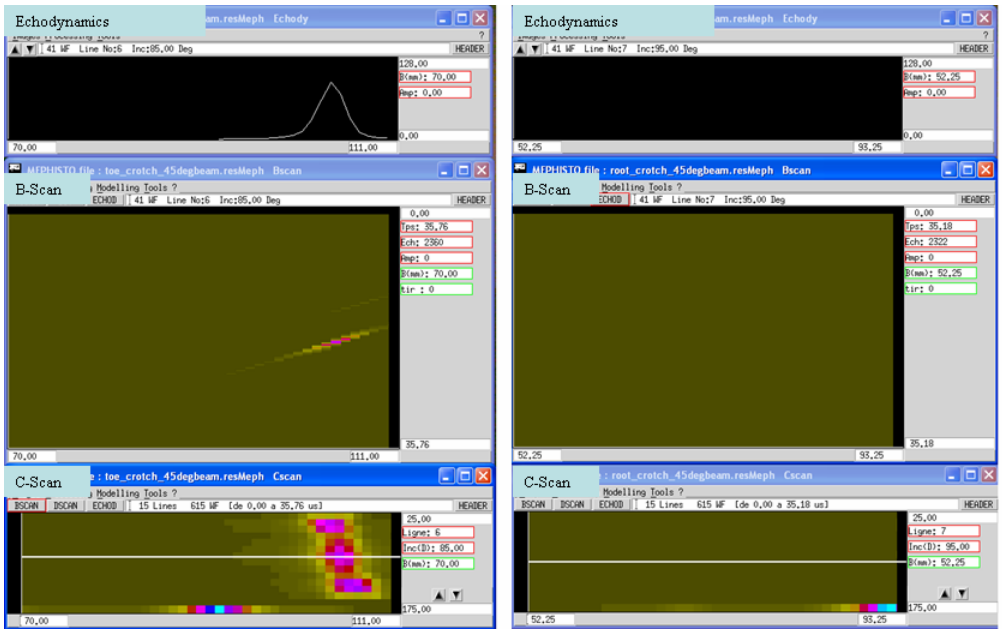

Figure 1.5.2-59. **Interaction Calculations Capture – 1-mm Crack Height at Crotch Position, 45-Degree Beam (Toe Crack – Left, Root Crack – Right) – Geometry 8**

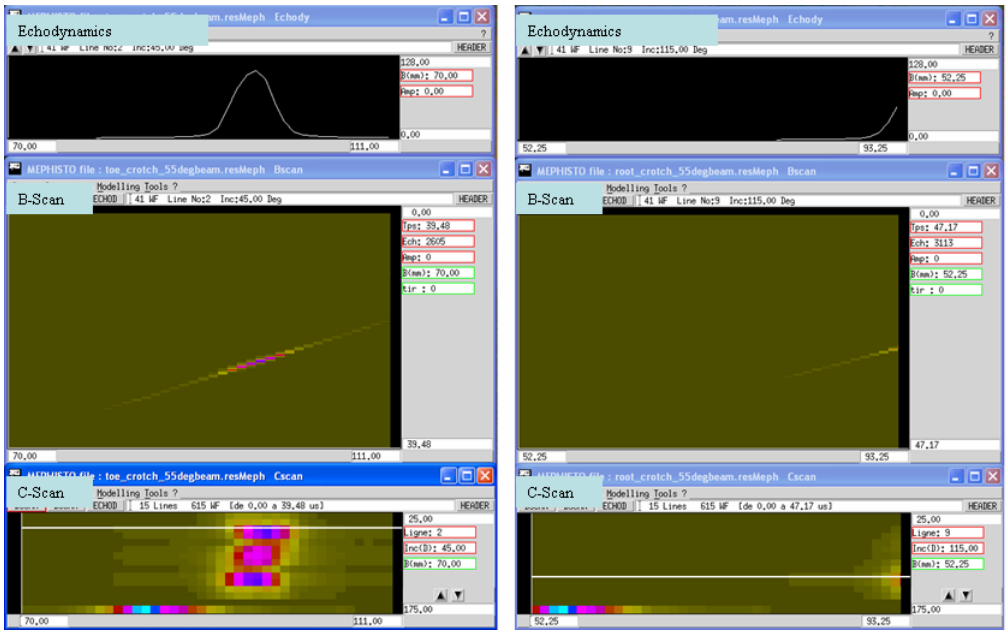

Figure 1.5.2-60. **Interaction Calculations Capture – 1-mm Crack Height at Crotch Position, 55-Degree Beam (Toe Crack – Left, Root Crack – Right) – Geometry 8**

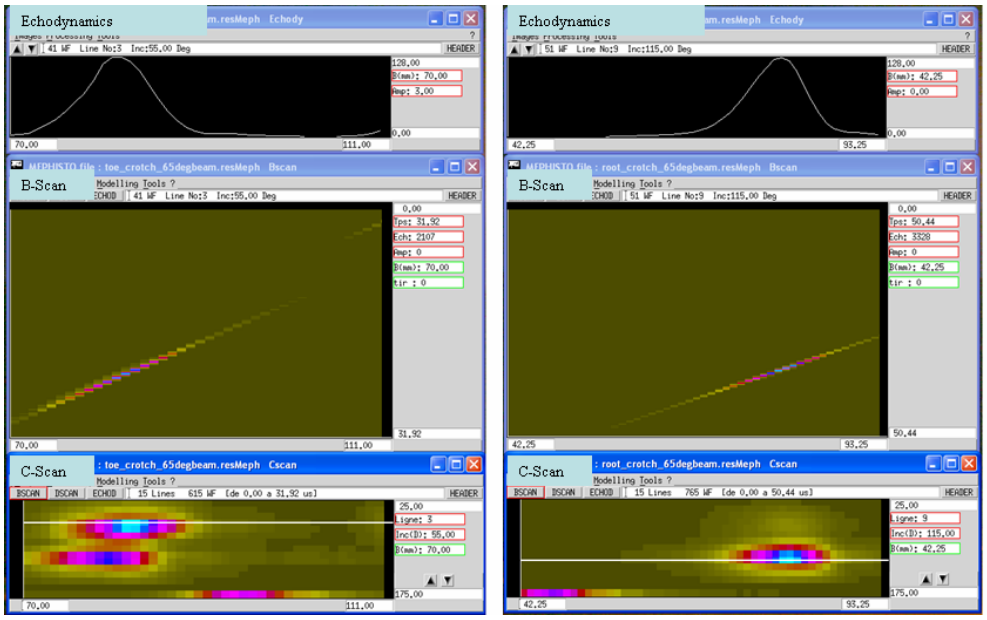

Figure 1.5.2-61. **Interaction Calculations Capture – 1-mm Crack Height at Crotch Position, 65-Degree Beam (Toe Crack – Left, Root Crack – Right) – Geometry 8**

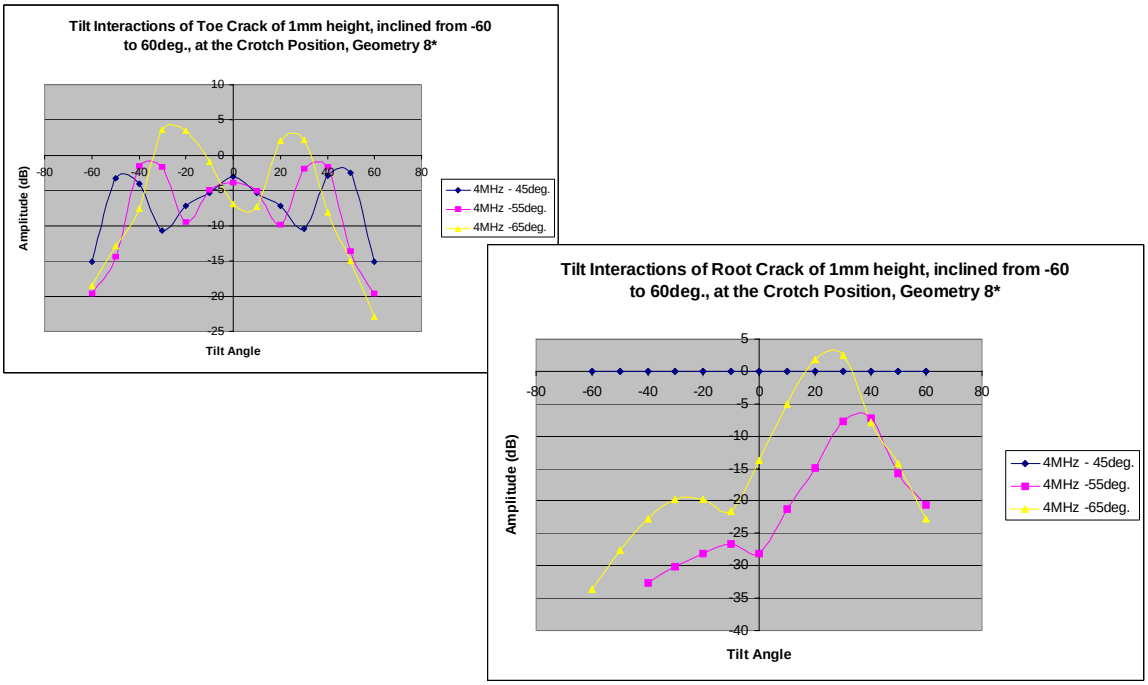

Figure 1.5.2-62. **(dB) Interaction Calculations Plot – 1-mm Crack Height at Crotch Position, 45-, 55-, and 65-Degree Beam (Toe Crack – Left, Root Crack – Right) – Geometry 8**

Figures 1.5.2-63, 1.5.2-64, and 1.5.2-65 show the interaction captures for the 141 degree cross section position. The plots on the left of the figure show the toe crack interaction and the ones on the right show the root crack interaction. The responses show the Echodynamic, B-scan and C-scan from the top to bottom in that order. The root crack did not show up at the 45 degree beam angle and showed up only slightly at the 55 degree beam angle. It was only at the 65 degree angle that the response began to show up clearly. However, for the toe crack, the response was available at all of the angles. Figure 1.5.2-66 shows the dB plot of the amplitude response with respect to the 1.2-mm SDH as the 0-dB reference. The plot on the left is for the toe crack and the one on the right is for the root crack. The responses can be characterized for each of the cracks as follows:

<u>Toe Crack at the 141-Degree Position</u>

- Flaw tilt of 0 to ±20 degrees
- 45- and 55-degree beams showed a 5-dB fall
- 65-degree beam showed a 12-dB rise
- Flaw tilt of ±20 to ±40 degrees
- 45-degree beam showed a 3-dB fall followed by a 7-dB rise
- 55-degree beam showed a 6-dB rise
- 65-degree beam showed a 12-dB rise
- Flaw tilt of ±40 degrees to ±60 degrees
- 45-degree beam showed a 12-dB fall
- 55-degree beam showed a 20-dB fall
- 65-degree beam showed a 12-dB fall.

<u>Root Crack at the 141 degree Position</u>

- There was no detection of the flaw by the 45-degree beam
- Flaw tilt of -60 to -40 degrees
- There was no detection for the 55-degree beam
- About a 5-dB rise for the 65-degree beam
- Flaw tilt of -40 to -10 degrees
- About a 5-dB rise for the 55-degree beam
- About another 5-dB rise for the 65-degree beam
- Flaw tilt of -10 to +30 degrees
- 20-dB rise for the 55-degree beam
- 30-dB rise for the 65-degree beam
- Flaw tilt of +30 to +60 degrees
- 10-dB fall for the 55-degree beam
- 25-dB fall for the 65-degree beam.

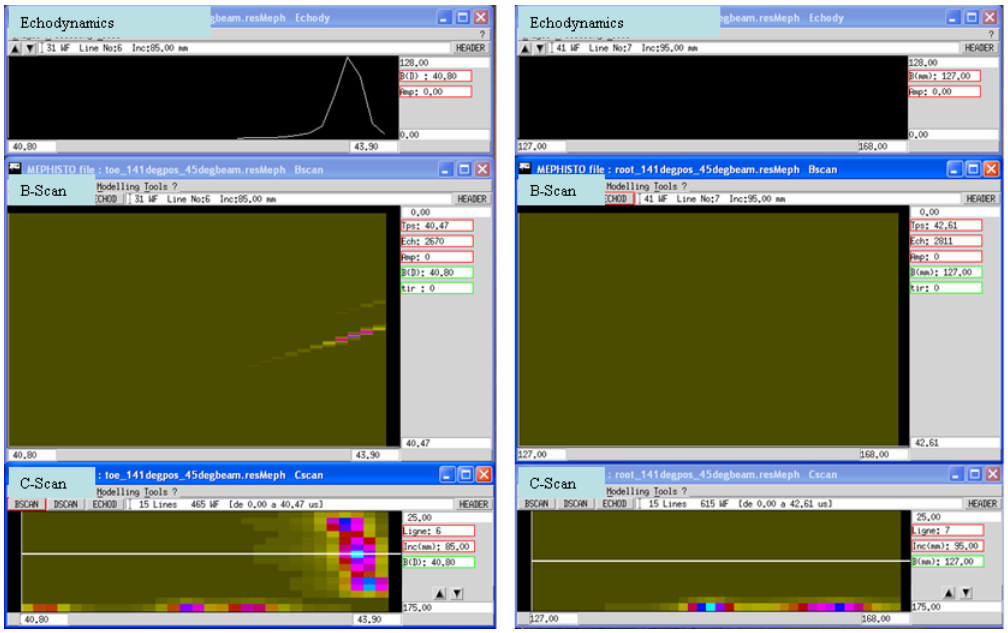

Figure 1.5.2-63. **Interaction Calculations Capture – 1-mm Crack Height at 141-Degree Position, 45-Degree Beam (Toe Crack – Left, Root Crack – Right) – Geometry 8**

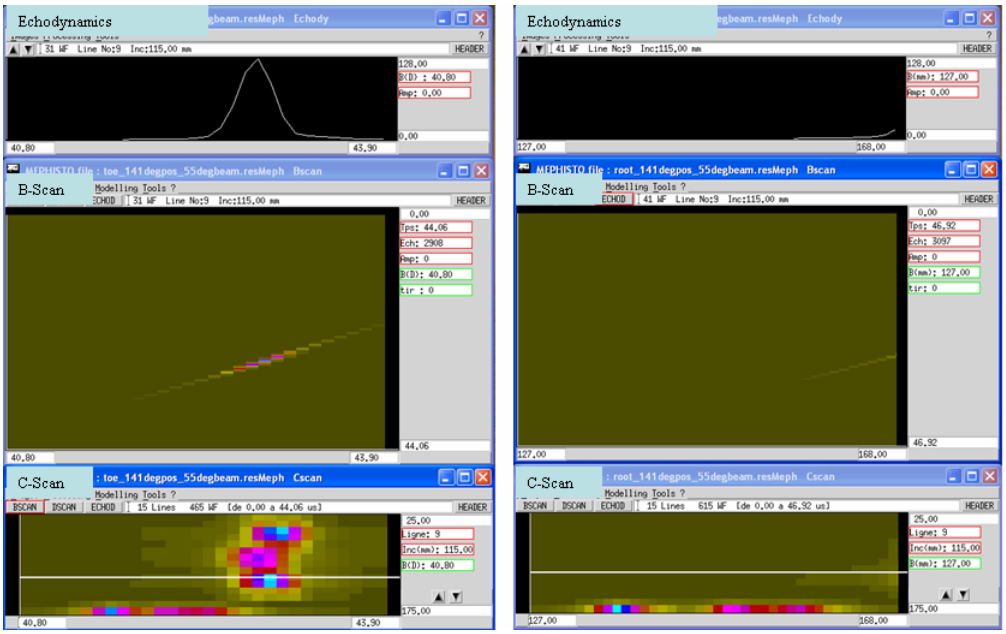

Figure 1.5.2-64. **Interaction Calculations Capture – 1-mm Crack Height at 141-Degree Position, 55-Degree Beam (Toe Crack – Left, Root Crack – Right) – Geometry 8**

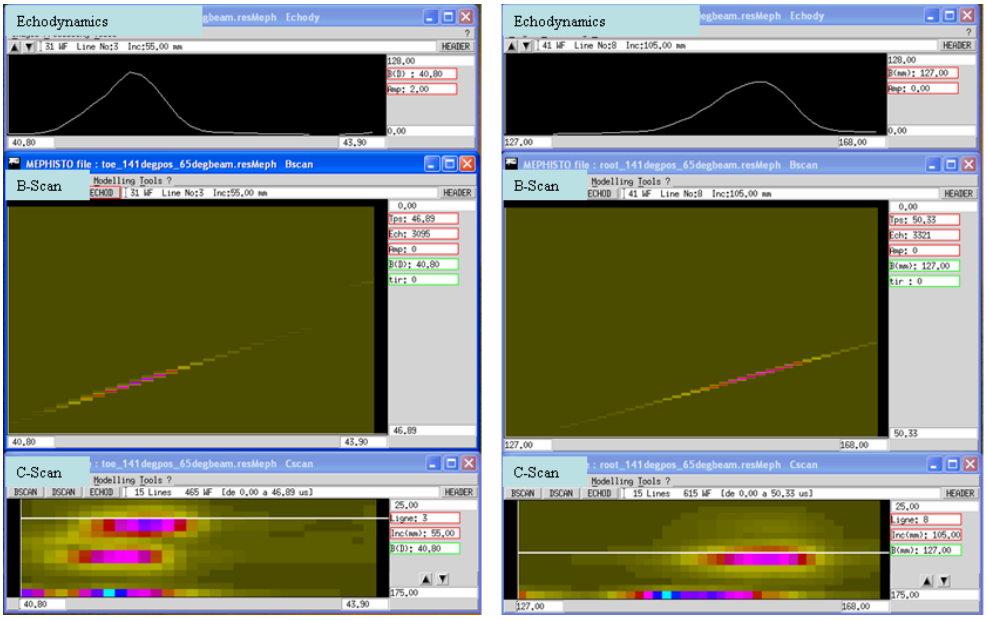

Figure 1.5.2-65. **Interaction Calculations Capture – 1-mm Crack Height at 141-Degree Position, 65-Degree Beam (Toe Crack – Left, Root Crack – Right) – Geometry 8**

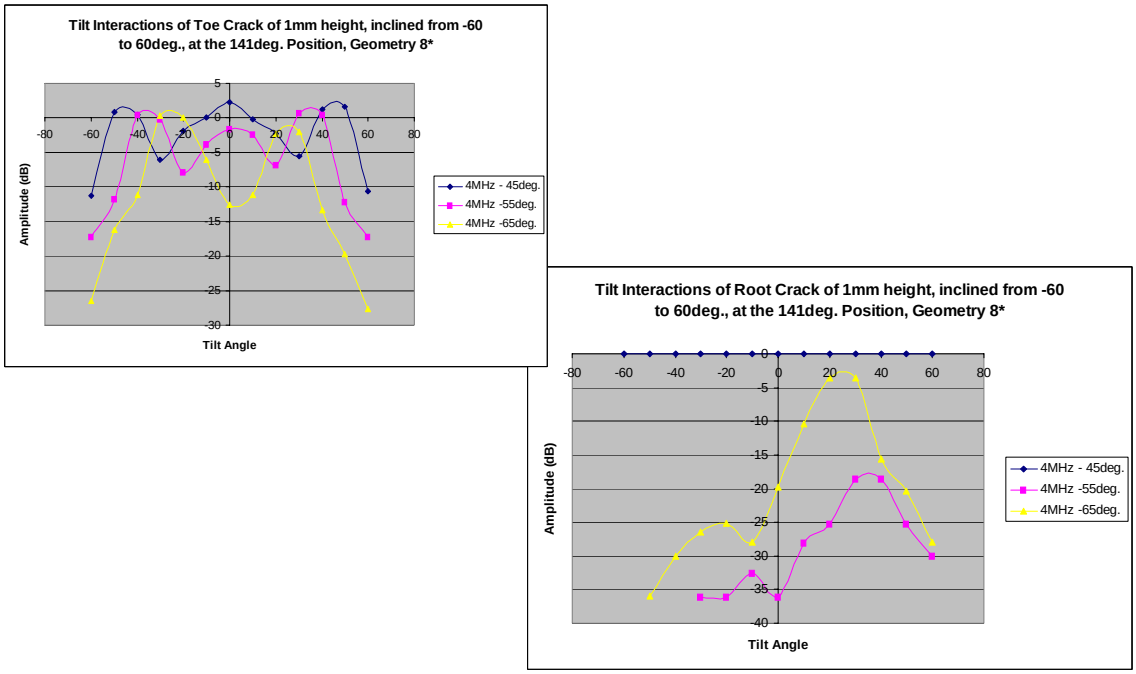

Figure 1.5.2-66. **(dB) Interaction Calculations Plot – 1-mm Crack Height at 141-Degree Position, 45-, 55-, and 65-Degree Beam (Toe Crack – Left, Root Crack – Right) – Geometry 8**

Geometry 8 Modal Analysis:

Modal analysis was done for one particular flaw case on Geometry 8 to analyze the different reflections which come from the beam flaw interaction. The case chosen was a toe flaw at the saddle position having a height of 1 mm (0.04 in.). The analysis was performed at a 45-degree beam angle with amplitude comparisons made relative to a 1.2-mm (0.047-in.)-diameter SDH. All of the Figures 1.5.2-67 through 1.5.2-84 show the capture of the modal echodynamics, B- and C-scan on the right with calculations for the echodynamics and B-scan of the modal analysis on the left.

Modal analysis results in Figures 1.5.2-67 through 1.5.2-74 shows that for flaw tilt angles from -60 to +10 degrees the corner trap was the dominant part of the reflected signal, and there was little or no reflection from the flaw face. Figures 1.5.2-75 and 1.5.2-76 shows a transition phase where flaws tilted at +20 and +30 degrees had significant response from both the flaw face and the corner trap. Figures 1.5.2-77 through 1.5.2-79 shows that for tilt angles of +40 to +60 degrees, the flaw face signal was dominant and there was very little corner trap response. This was likely caused by the flaw face being perpendicular to the beam, which provided a good reflection from the crack face.

It is important to note that a corner trap is produced only on surface-breaking flaws. Therefore, toe cracks had a strong corner trap response since they were open to the OD surface. Root cracks, however, did not form a corner trap condition for this particular geometry, resulting in reflections only from the crack face as shown in Figures 1.5.2-80 through 1.5.2-84. Figure 1.5.2-85 shows the comparison of the 3-mm height flaw with and without corner trap signals. The reason for this comparison was to see the influence of corner trap as the flaw becomes a significant percentage of the beam spread. In this case, the beam size at the second leg was about 5 mm for the 45-degree beam. Figure 1.5.2-86 shows the dB amplitude comparison of the signals with and without corner trap. It was obvious that the corner trap signal made up a significant portion of the amplitude response.

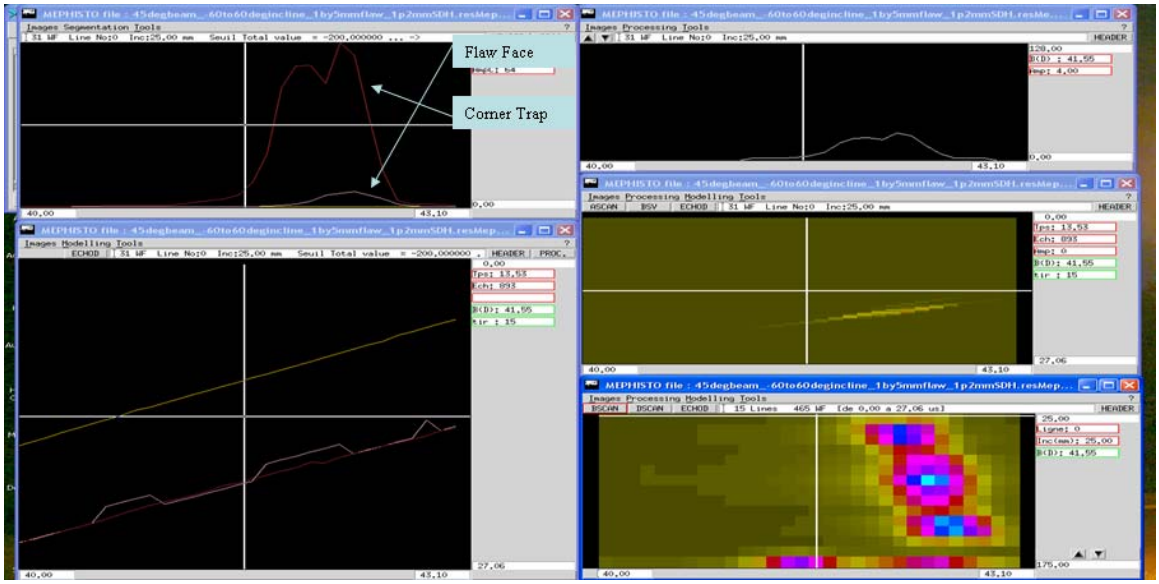

Figure 1.5.2-67. Modal Analysis – Toe Flaw on Saddle, 45-Degree Beam; -60-Degree Flaw Tilt – Geometry 8

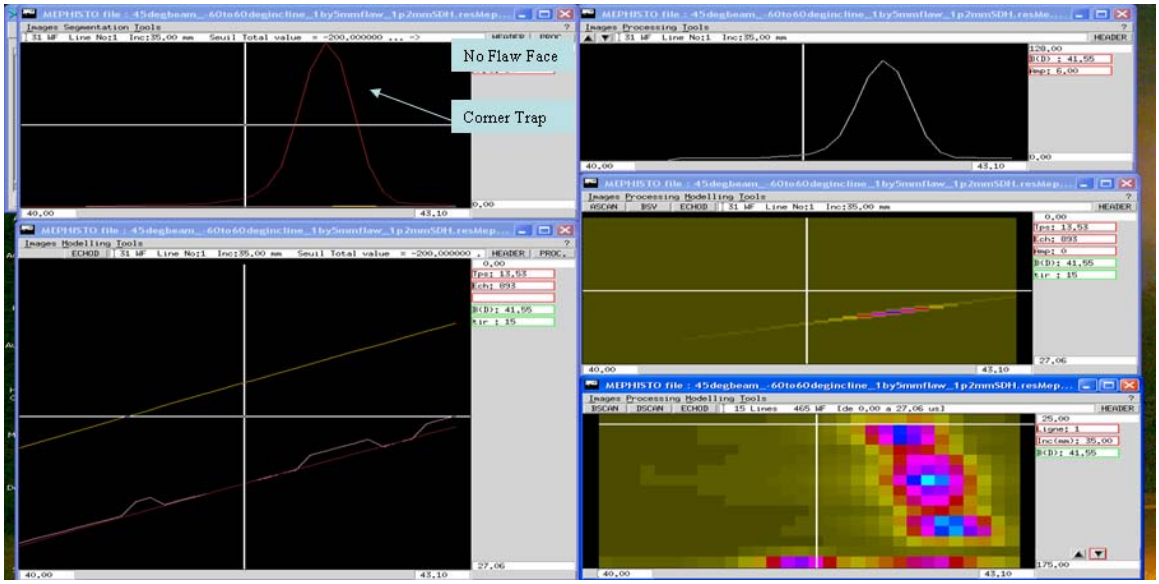

Figure 1.5.2-68. Modal Analysis – Toe Flaw on Saddle, 45-Degree Beam; -50-Degree Flaw Tilt – Geometry 8

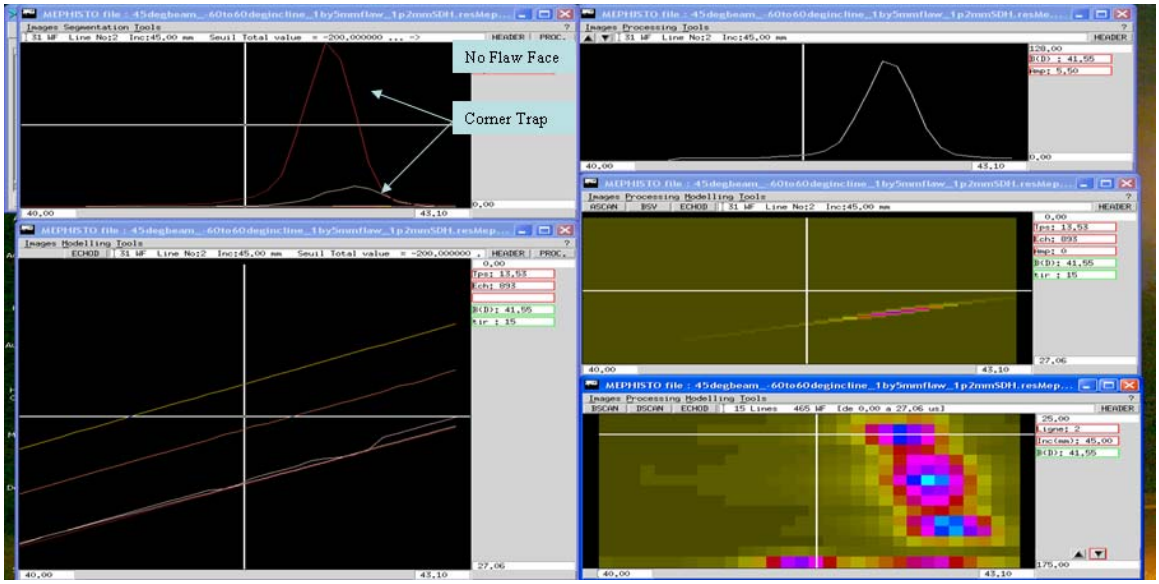

Figure 1.5.2-69. **Modal Analysis – Toe Flaw on Saddle, 4-Degree Beam; -40-Degree Flaw Tilt – Geometry 8**

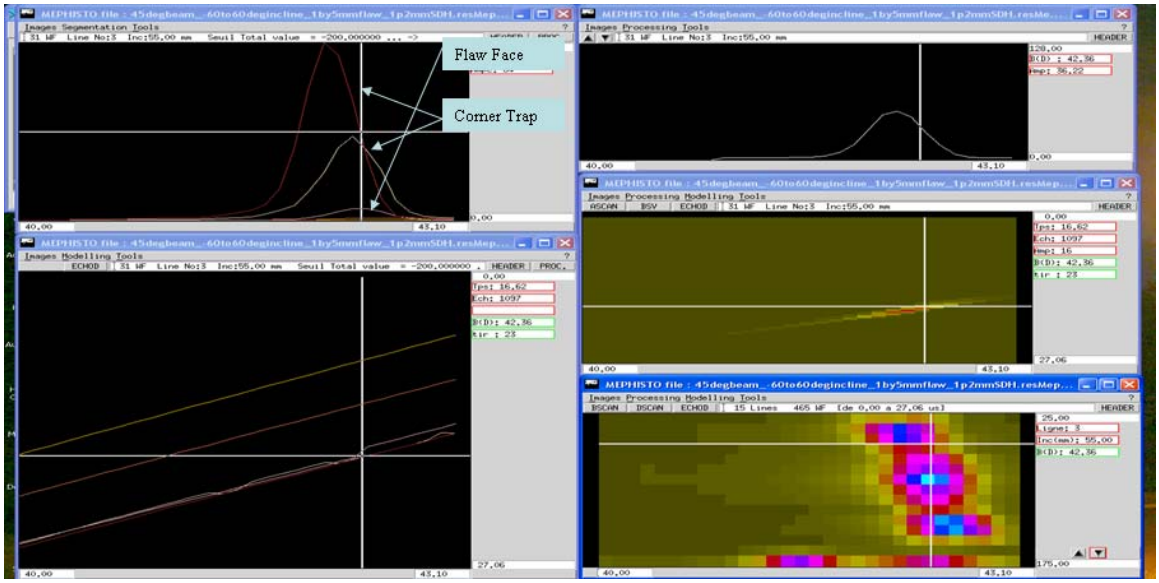

Figure 1.5.2-70. **Modal Analysis – Toe Flaw on Saddle, 45-Degree Beam; -30-Degree Flaw Tilt – Geometry 8**

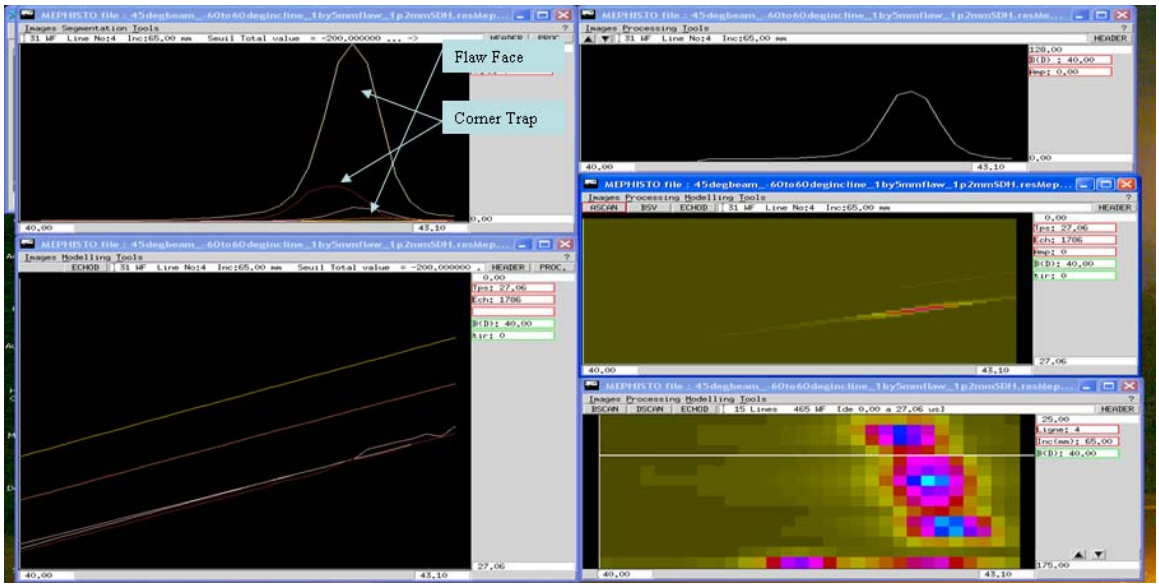

Figure 1.5.2-71. Modal Analysis – Toe Flaw on Saddle, 45-Degree Beam; -20-Degree Flaw Tilt – Geometry 8

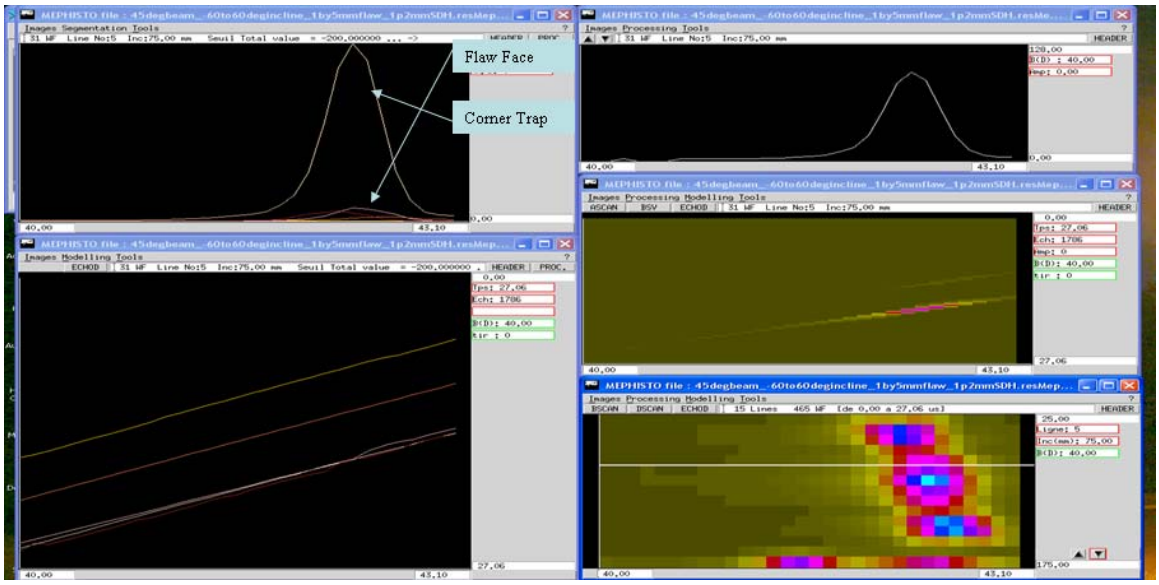

Figure 1.5.2-72. Modal Analysis – Toe Flaw on Saddle, 45-Degree Beam; -10-Degree Flaw Tilt – Geometry 8

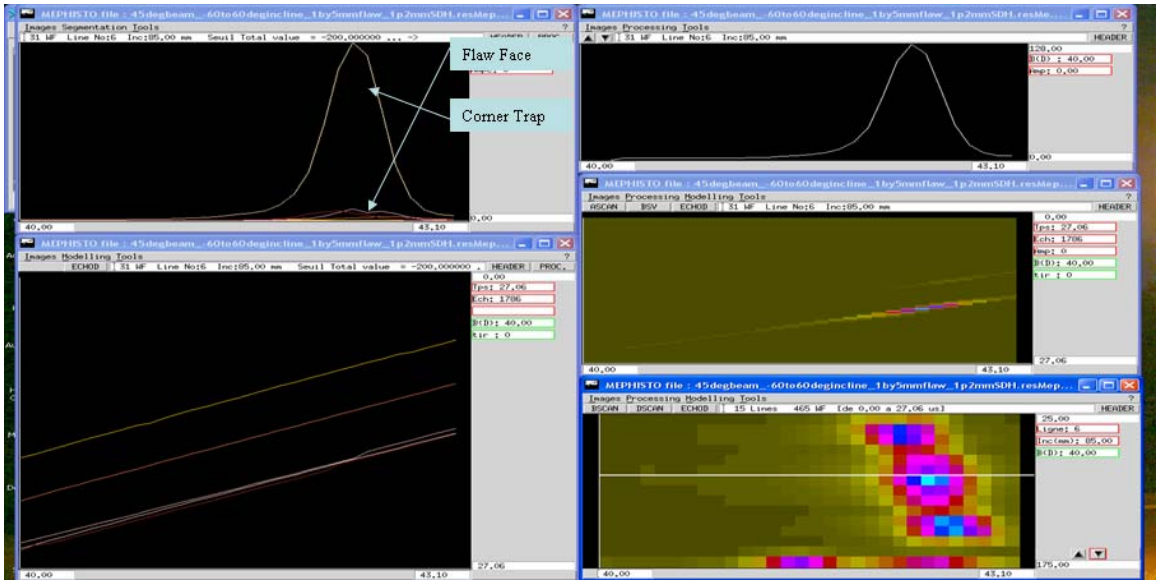

Figure 1.5.2-73. Modal Analysis – Toe Flaw on Saddle, 45-Degree Beam; 0-Degree Flaw Tilt –Geometry 8

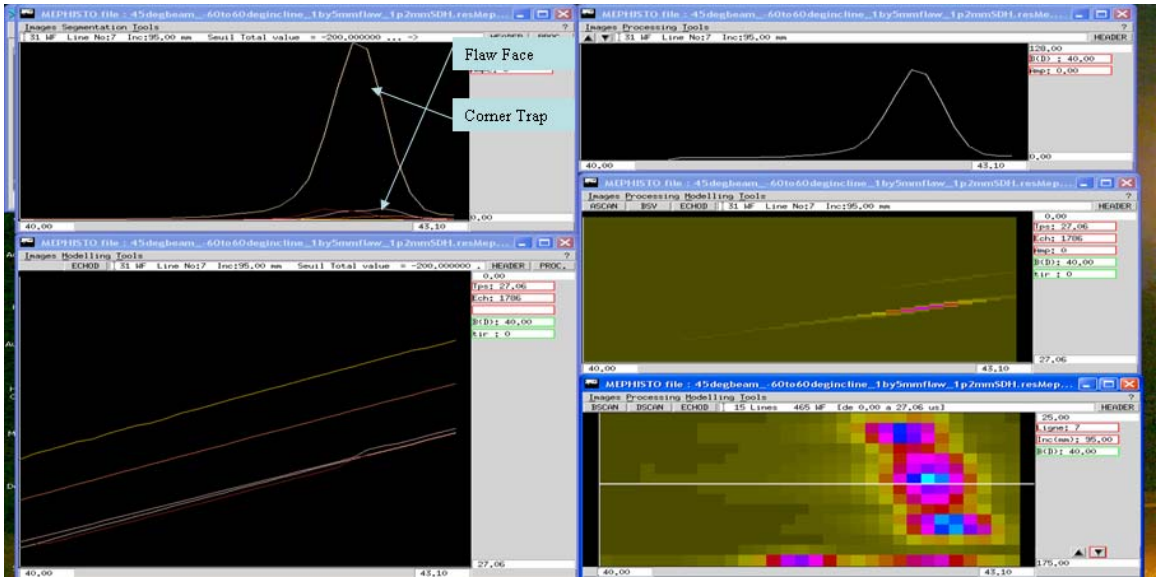

Figure 1.5.2-74. Modal Analysis – Toe Flaw on Saddle, 45-Degree Beam; 10-Degree Flaw Tilt – Geometry 8

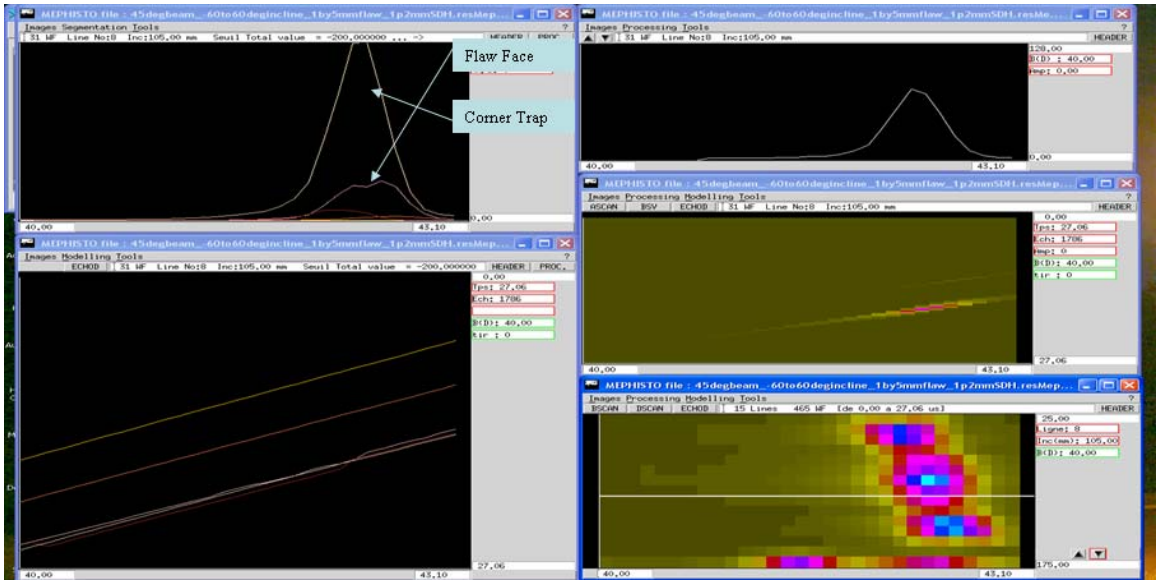

Figure 1.5.2-75. Modal Analysis – Toe Flaw on Saddle, 45-Degree Beam; 20-Degree Flaw Tilt – Geometry 8

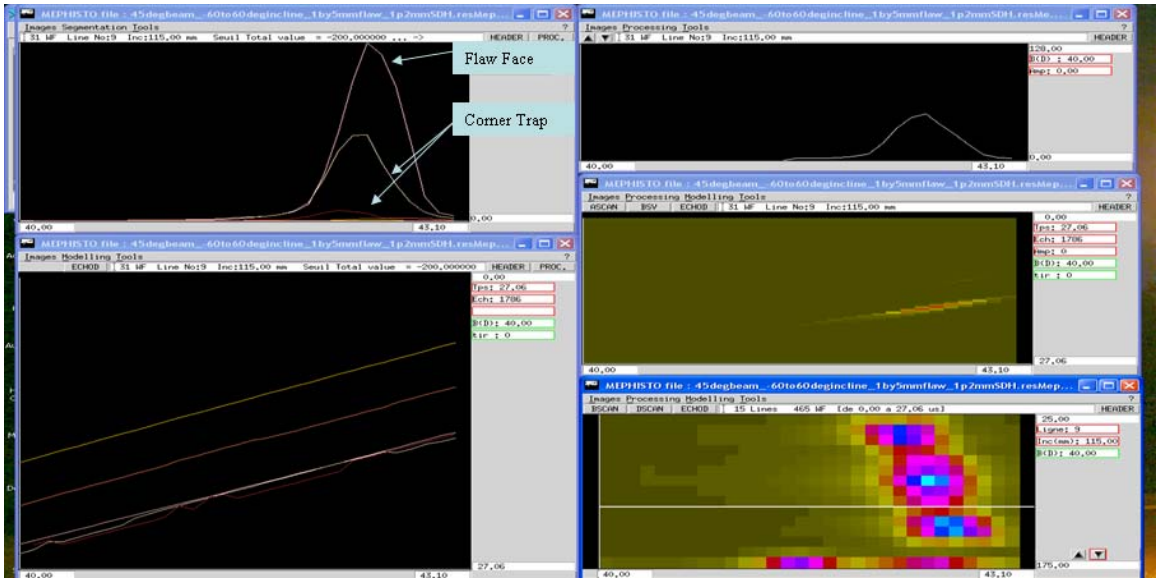

Figure 1.5.2-76. Modal Analysis – Toe Flaw on Saddle, 45-Degree Beam; 30-Degree Flaw Tilt – Geometry 8

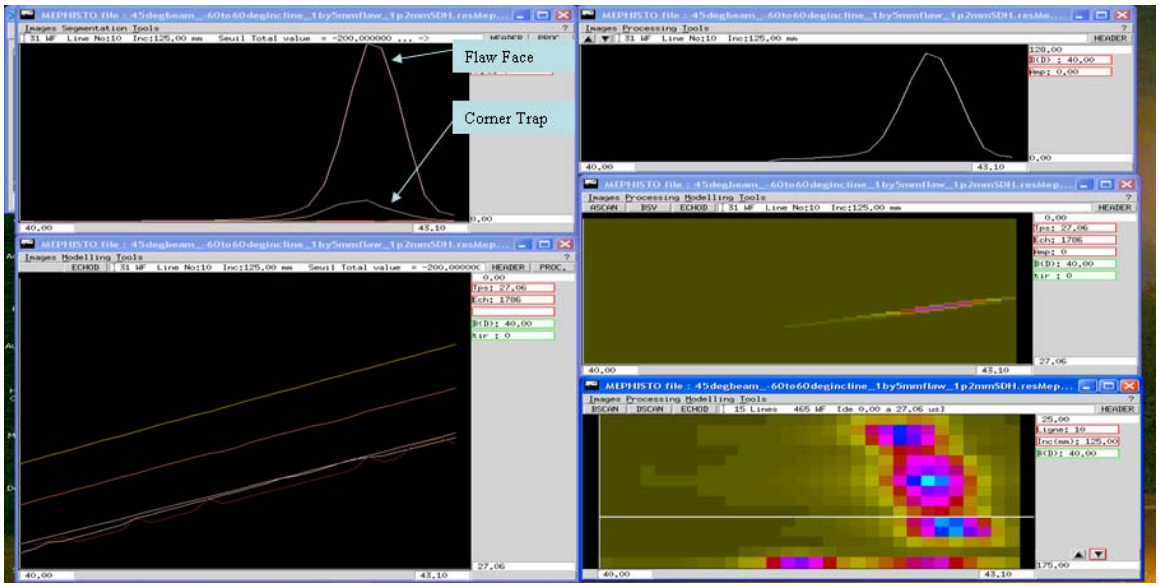

Figure 1.5.2-77. Modal Analysis – Toe Flaw on Saddle, 45-Degree Beam; 40-Degree Flaw Tilt – Geometry 8

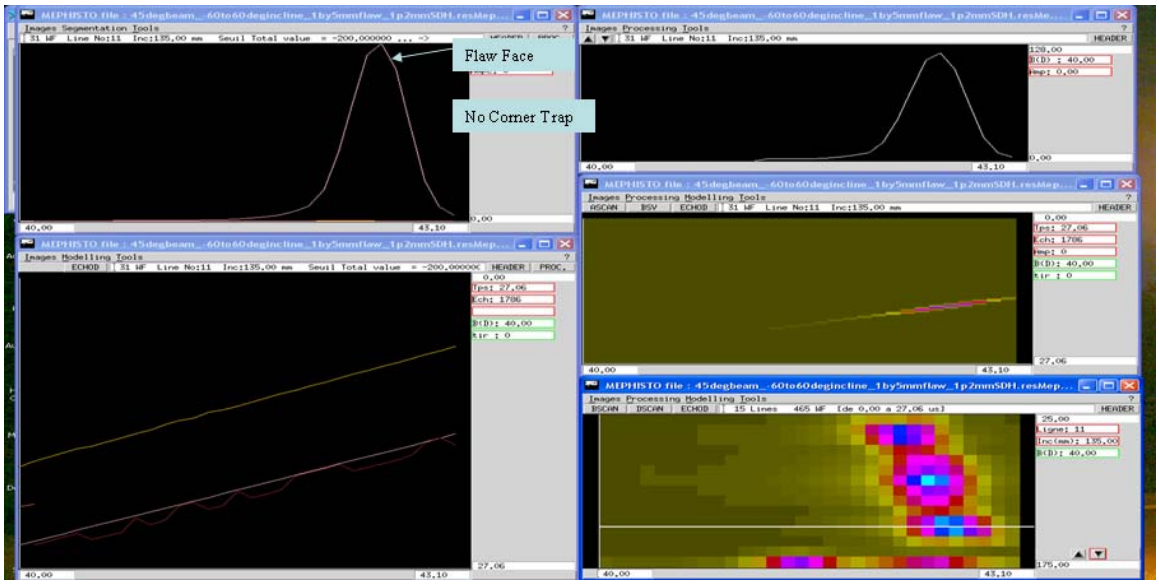

Figure 1.5.2-78. Modal Analysis – Toe Flaw on Saddle, 45-Degree Beam; 50-Degree Flaw Tilt – Geometry 8

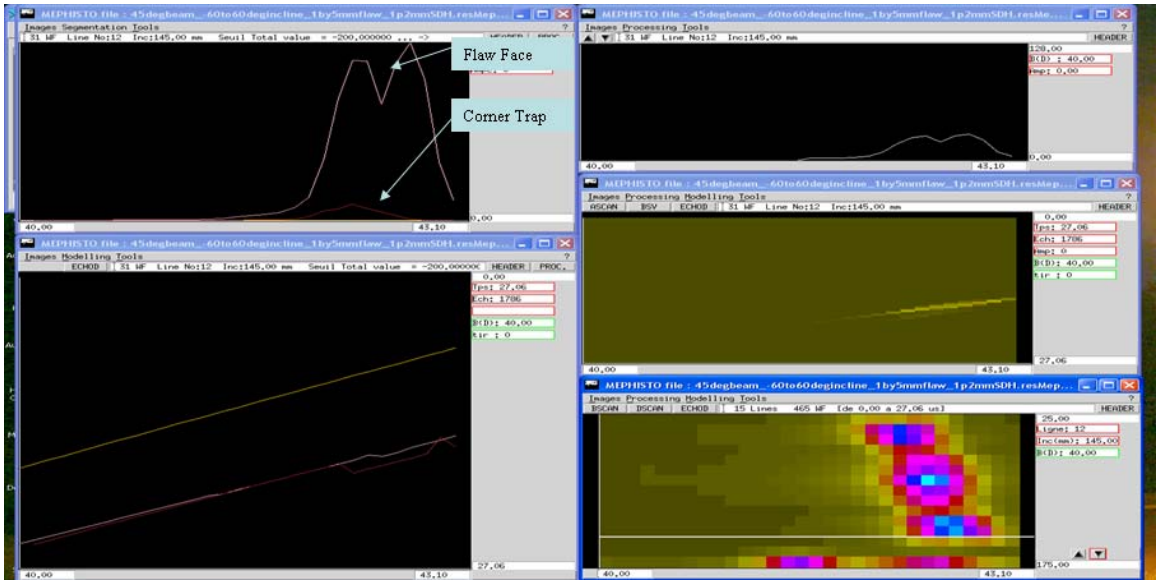

Figure 1.5.2-79. Modal Analysis – Toe Flaw on Saddle, 45-Degree Beam; 60-Degree Flaw Tilt – Geometry 8

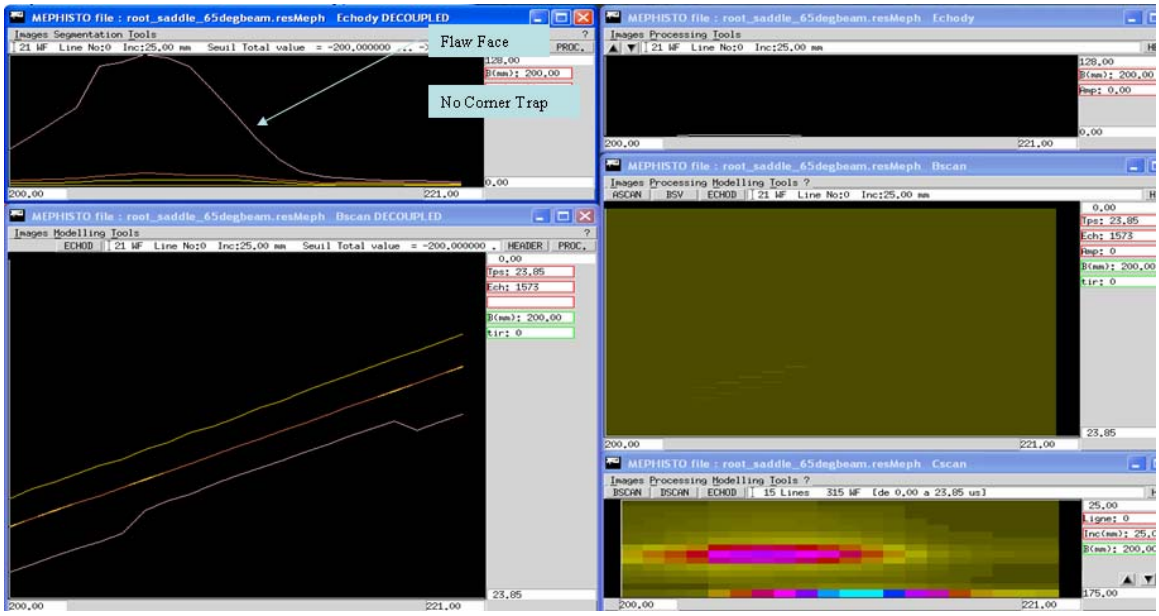

Figure 1.5.2-80. Modal Analysis – Root Flaw on Saddle, 45-Degree Beam; -60-Degree Flaw Tilt – Geometry 8

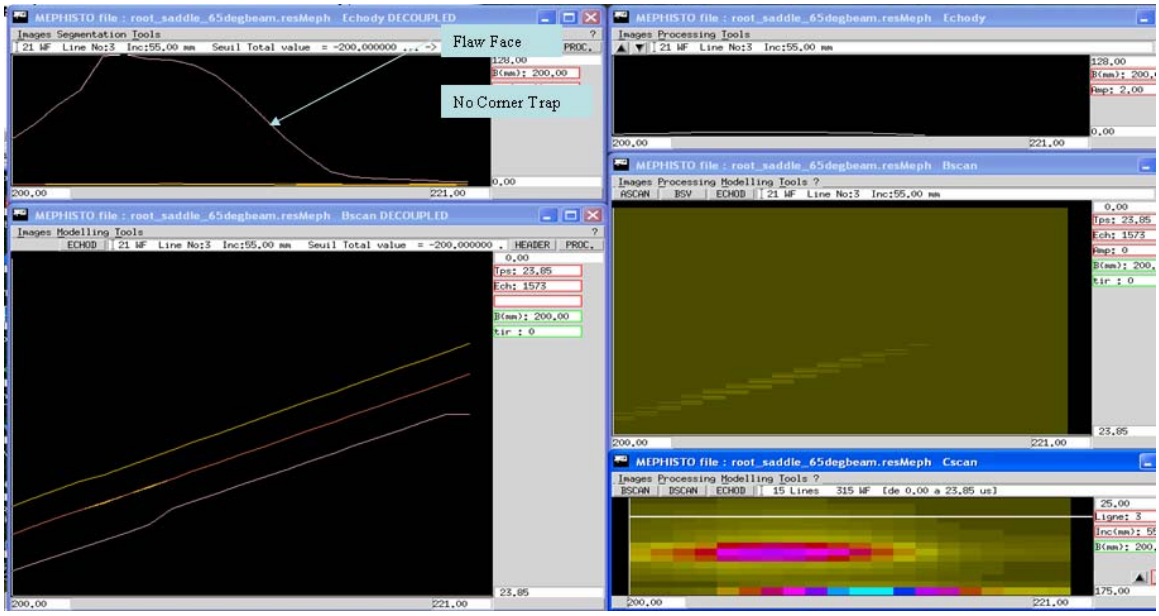

Figure 1.5.2-81. Modal Analysis – Root Flaw on Saddle, 45-Degree Beam; -30-Degree Flaw Tilt – Geometry 8

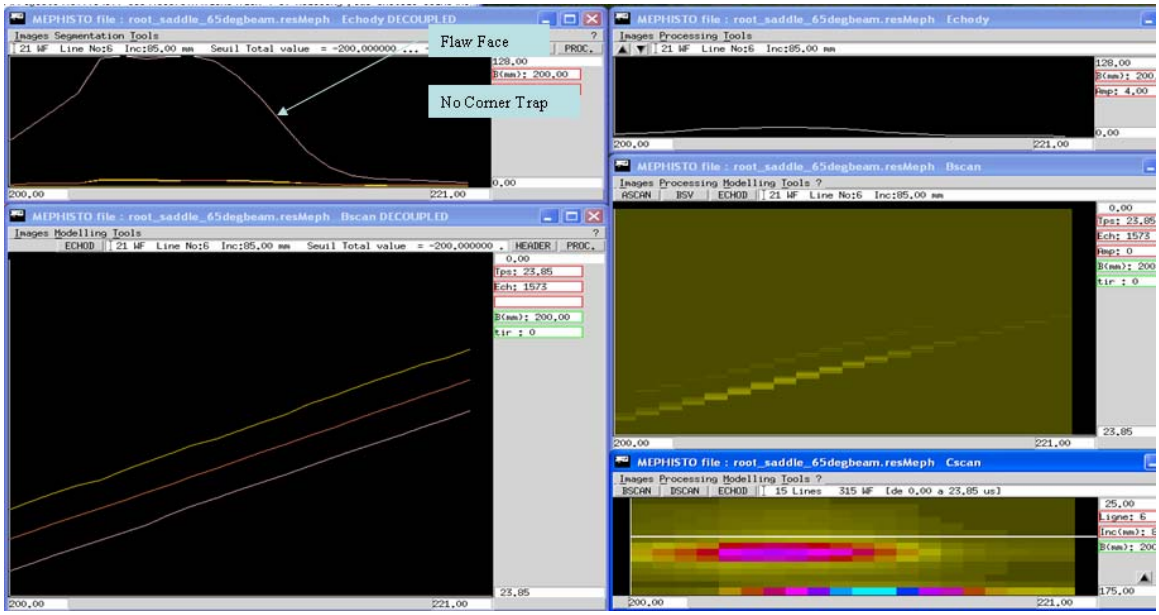

Figure 1.5.2-82. Modal Analysis – Root Flaw on Saddle, 45-Degree Beam; 0-Degree Flaw Tilt – Geometry 8

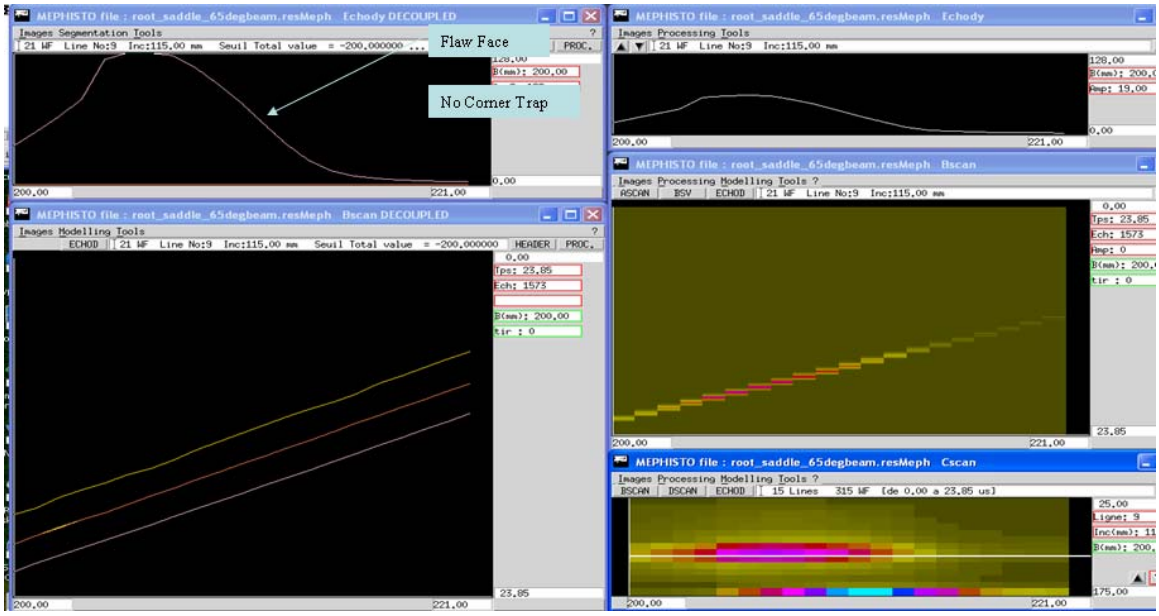

Figure 1.5.2-83. **Modal Analysis – Root Flaw on Saddle, 45-Degree Beam; 30-Degree Flaw Tilt – Geometry 8**

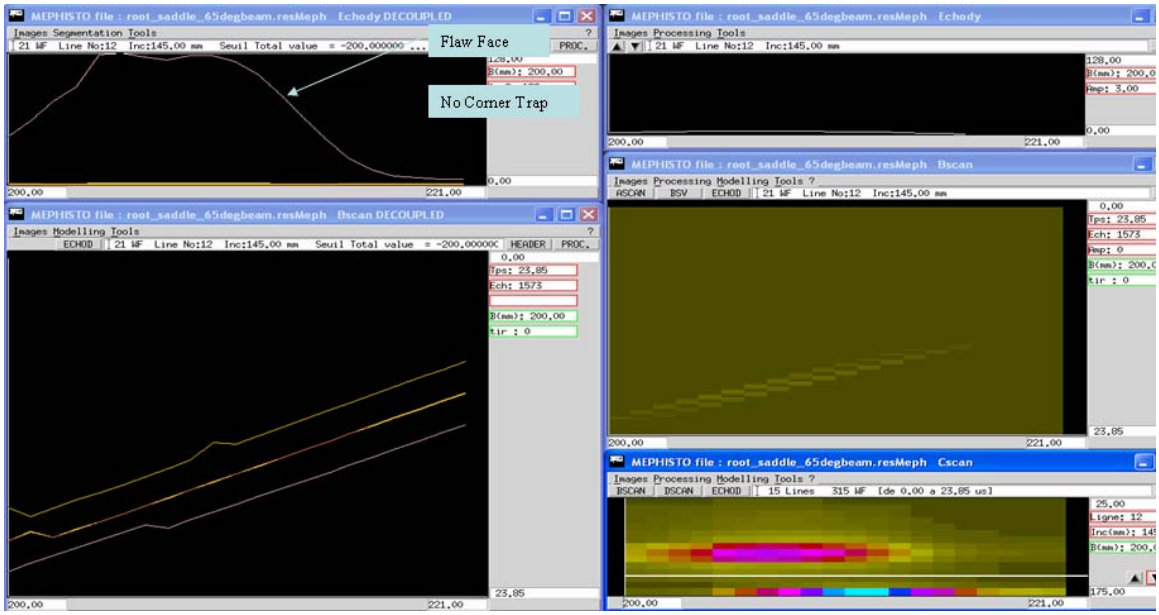

Figure 1.5.2-84. **Modal Analysis – Root Flaw on Saddle, 45-Degree Beam; 60-Degree Flaw Tilt – Geometry 8**

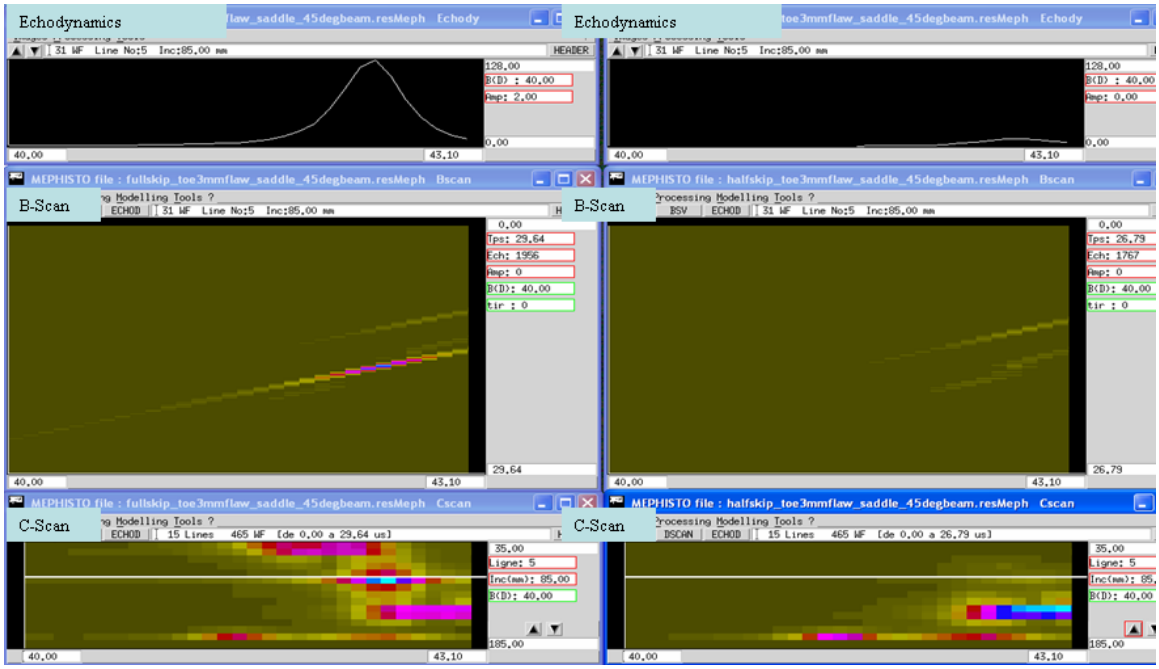

Figure 1.5.2-85. **Interaction Calculations Capture – 3-mm Crack Height at Saddle Position, 45-Degree Beam (Toe Crack – Left, Root Crack – Right) – Geometry 8**

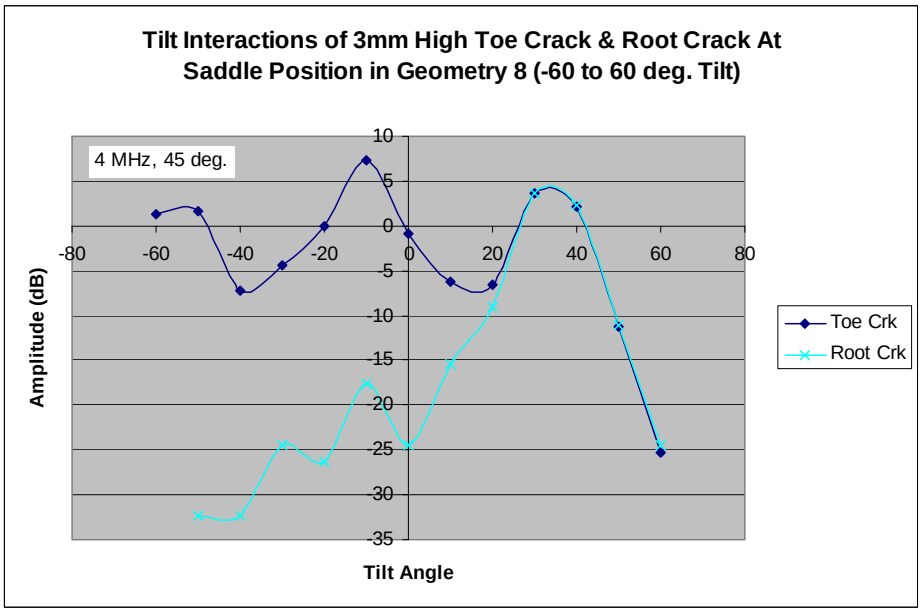

Figure 1.5.2-86 **(dB) Interaction Calculations Plot – 3-mm High Toe and Root Cracks at Saddle Position; Geometry 8; 4-MHz, 45-Degree Beam**

Conclusions

Lower beam angles such in the range of 45 to 55 degrees often did not detect root cracks because of the probe contacting the weld surface.

Corner trap reflections comprised a significant portion of the reflected signal. In cases where a corner trap was not available, such as a root crack, the reflected signal was made up of only reflected signals from the crack face. Without the corner trap condition, the simulations show that root cracks would be much more difficult to detect than toe cracks.

Crack tilt was a major factor in the signal amplitude response. Since crack tilt is somewhat unpredictable, the use of multiple angles should be considered for improving detection of cracks at the weld toe and root.